IOS

DEACON LABORATORY

WAVES AND WAVE SPECTRA RECORDED AT TWO SITES OFF HOLDERNESS 1986 – 1987

BY

S. BACON & D.J.T. CARTER

REPORT NO. 260

1988

Natural Environment Research Council

INSTITUTE OF OCEANOGRAPHIC SCIENCES DEACON LABORATORY

INSTITUTE OF OCEANOGRAPHIC SCIENCES

DEACON LABORATORY

Wormley, Godalming,
Surrey, GU8 5UB, U.K.

Telephone: 0428 79 4141
Telex: 858833 OCEANS G
Telefax: 0428 79 3066

Director: Dr. C.P. Summerhayes

Natural Environment Research Council

INSTITUTE OF OCEANOGRAPHIC SCIENCES

DEACON LABORATORY

REPORT No. 260

Waves and wave spectra recorded at two sites off Holderness 1986 - 1987

S. Bacon & D.J.T. Carter

1988

DOCUMENT DATA SHEET

AUTHOR	BACON, S. & CARTER, D.J.T.	*PUBLICATION DATE* 1988
TITLE	Waves and wave spectra recorded at two sites off Holderness 1986 - 1987.	
REFERENCE	Institute of Oceanographic Sciences Deacon Laboratory, Report, No.260, 88pp.	

ABSTRACT

Measurements were made routinely with two Waverider buoys off Holderness on the Humberside coast over 1986 and 1987, one nearshore on site for four months, the other offshore on site for thirteen months. This report provides information detailing the location, the instrumentation and the data return. Obtained from the wave records are estimates of significant wave height, H_S, and zero-up-crossing period, T_Z. Histograms from these values are presented indicating the probability distributions of H_S and T_Z appropriate to the operational period of each site. Each observed H_S distribution is fitted to a Fisher-Tippett Type 1 probability distribution which is then extrapolated to obtain an estimate of the fifty-year return value of H_S. Observed joint probability distributions of (H_S, T_Z) are presented. For months when data are available from both sites, comparisons between sites are presented of H_S and of T_Z. Some spectral data, representing stormy and quiescent examples of conditions, are presented. Variations of spectral density with time in the high frequency spectral tail are investigated, for which tidal current induced Doppler shifting is adduced as the cause. The variation in spectra of waves propagating onshore and offshore are investigated by comparing nearshore and offshore spectra.

ISSUING ORGANISATION

Institute of Oceonographic Sciences
Deacon Laboratory
Wormley, Godalming
Surrey GU8 5UB. UK.

TELEPHONE 0428 79 4141

TELEX 858833 OCEANS G

TELEFAX 0428 79 3066

KEYWORDS

SIGNIFICANT WAVE HEIGHT
WAVERIDER BUOYS
WAVE SPECTRA
HOLDERNESS

CONTRACT

PROJECT

PRICE £23.00

CONTENTS

	Page
INTRODUCTION	7
LOCATION	7
MEASUREMENT AND RECORDING SYSTEMS	8
MAINTENANCE AND CALIBRATION	8
WAVE DATA COVERAGE AND PRESENTATION	9
DEFINITIONS	10
ANALYSIS OF WAVE CLIMATE DATA	11
PRESENTATION OF WAVE SPECTRAL DATA	15
ANALYSIS OF TIME-MODULATION OF HIGH-FREQUENCY SPECTRAL DENSITIES	16
Spectral analysis of modulation	16
Investigation of modulation assuming Doppler shifting	18
Spectral analysis of time series of T_z records	19
ANALYSIS OF SPECTRA DURING TIMES OF STRONG ONSHORE AND OFFSHORE WINDS	21
Onshore waves	22
Offshore waves	24
CONCLUDING REMARKS	26
ACKNOWLEDGEMENTS	27
REFERENCES	28
APPENDICES	
Frequency logging of wave data	29
Methods of spectral analysis and computation of wave parameters	30
Details of methods used for calculating 50-year return values	34
Distribution of the ratio of spectral components	37

1. INTRODUCTION

Wave measurements were recorded routinely off Holderness using two Waverider buoys, one Nearshore, on site from March to June 1986, and one Offshore, on site from March 1986 to March 1987. This report describes the derivation of frequency spectra and, from these, estimates of significant wave height, H_s, and zero-up-crossing period, T_z. The wave climate as derived from H_s and T_z data is described. Some of the spectral data are presented, and intensity variations in the high frequency spectral tail are investigated. The changes in spectra of waves propagating onshore and offshore are examined by comparing Nearshore and Offshore spectra.

2. LOCATION

The sites at which the wave measurements were taken are shown on the maps in Figure 1. The table below gives the mooring site details, with bearing and distance referred to Hornsea on the Humberside coast.

	Latitude	Longitude	Bearing	Distance (n.m.)	Water Depth (Chart datum, metres)
Nearshore Buoy	53°55'05"N	00°03'32"W	E	3.7	12
Offshore Buoy	53°55'56"N	00°01'24"E	E by N	6.6	17

Tidal heights above Chart Datum reach a maximum of 5.5-6.0 m, with a mean height of the order of 3.0 m.

The receiving site for the buoy radio was at Hornsea Coastguard Station.

The site is open to the North Sea from N through E to SSE. The sea floor slopes gently downwards from the coast; there are no off-lying banks in the immediate vicinity.

Hourly measurements of 10-minute mean wind speed and direction were recorded by the Meteorological Office at Spurn Head.

3. MEASUREMENT AND RECORDING SYSTEMS

Wave measurements were made using standard Waverider buoys moored as described by Humphery (1982). This instrument senses the vertical acceleration of the buoy by means of a stabilized accelerometer and uses analogue double integrators to reconstitute the surface elevation. This information is transmitted ashore via a high-frequency radio link employing a frequency-modulated subcarrier.

At Hornsea, the buoy's transmissions were received and a counting arrangement (described in Appendix 1) was used to decode the wave information. In this way a measure of surface elevation was obtained at 0.5 second intervals in the form of a digital count which was recorded on magnetic tape. The time between starts of successive records was 1.5 hours, and the length of each record was 34 minutes.

4. MAINTENANCE AND CALIBRATION

The buoys were maintained on site by Hydraulic Research Ltd. and the shore station by IOS; special visits were made either when data reception stopped or when data quality fell below acceptable standards. A local coastguard was responsible for tape and/or cartridge changes, and for reporting any malfunctions.

The buoys were calibrated before deployment and after recovery by Hydraulics Research Ltd. staff at Wallingford. The buoys were subjected to circular motion in the vertical plane through attachment to a rotating arm of variable frequency (0.05 Hz to 0.5 Hz) with amplitude 0.9 m (equivalent to 1.8 m 'crest-to-trough'). Calibration is effected by comparing the recorded crest to trough height with 1.8 m at each frequency. Buoy sensitivity has been found to be within ±2%, and the decoding technique (described in Appendix 1) has reduced

reduced variations in sensitivity due to the shore station equipment to a negligible value. The overall sensitivity of the system is therefore stable to within ±2%.

5. WAVE DATA COVERAGE AND PRESENTATION

The tables below give the percentage data return by month, the total data return, and the data return per season. The seasons are defined as follows:

Spring - March to May
Summer - June to August
Autumn - September to November
Winter - December to February

MONTHLY DATA RETURNS (%)

Year					**1986**						**1987**		
Month	**3**	**4**	**5**	**6**	**7**	**8**	**9**	**10**	**11**	**12**	**1**	**2**	**3**
Nearshore Buoy	72.2	94.0	99.6	51.7									
Offshore Buoy	83.7	95.2	99.6	84.4	97.8	14.3	23.8	61.1	91.3	76.6	28.0	97.8	82.3

TOTAL DATA RETURN

	Actual Total	**Possible Total**	**Actual %**
Nearshore Buoy	1551	1952	79.5
Offshore Buoy	4848	6636	73.2

SEASONAL DATA RETURN

		Actual Total	Possible Total	Actual %
Nearshore Buoy	Spring	1303	1472	88.5
Offshore Buoy	Spring	1775	1968	90.2
	Summer	961	1472	65.3
	Autumn	827	1456	56.8
	Winter	985	1440	68.4

Figures 2-5 present as time series all Nearshore and Offshore records of significant wave height (H_s) and zero-up-crossing period (T_z) over the recording period, where each vertical bar above the time axis represents a valid record whose height is proportional to the value of H_s or T_z for that record. Missing or invalid records are represented as short vertical bars below the time axis.

Two major breakdowns of receiving site hardware occurred, affecting the data return of the Offshore buoy. The first resulted in the gap covering most of July and August 1986; the second resulted in the gap during January 1987. No difficulties were experienced with the buoy data transmission system; data return quality was affected by problems with the shore-based reception and recording systems. Some data may have been lost in high sea states due to line of transmission interruption.

6. DEFINITIONS

The n^{th} moment of a continuous spectrum is

$$m_n = \int_0^\infty f_n \, S(f) df$$

where S(f) is the spectral density at frequency f(Hz). Values of significant wave height, H_s, and zero-up-crossing wave period, T_z, presented in this report have been derived from the spectral moments using the following definitions:

$H_S = 4\sqrt{m_0}$

$T_Z = \sqrt{(m_0/m_2)}$

Significant steepness, S_S, is defined by

$$S_S = \frac{2\pi H_S}{gT_Z^2}$$

The fifty-year return value of H_S, $H_S(50)$, is defined as the value of H_S which is exceeded on average once in fifty years.

7. ANALYSIS OF WAVE CLIMATE

The maximum value of H_S recorded at the Nearshore site occurred on the 10th April 1986 at 0600 hours with H_S = 4.21 m and associated T_Z = 7.47 s; the maximum Offshore H_S occurred on the 7th April 1986 at 2230 hours with H_S = 4.09 m and associated T_Z = 6.48 s.

The mean and maximum values of H_S recorded during each individual month are given in the table below. Figures in parentheses indicate values for a month with less than 50% valid records.

Nearshore Buoy

Year	Month	Mean H_S	Maximum H_S
1986	3	0.69	2.90
	4	1.06	4.21
	5	0.58	1.52
	6	0.74	2.49

Offshore Buoy

Year	Month	Mean H_S	Maximum H_S
1986	3	0.76	3.12
	4	1.09	4.09
	5	0.65	1.62
	6	0.80	2.76
	7	0.51	1.14
	8	(0.72)	(1.58)
	9	(0.62)	(1.35)
	10	0.58	1.87
	11	1.04	3.00
	12	1.15	2.77
1987	1	(1.30)	(2.59)
	2	0.96	2.46
	3	1.51	3.61

Estimates of the probability distributions of H_S are shown in Figs.6 and 7 which present histograms giving the percentage occurrence of H_S over all data for both sites and over each season for the Offshore site, with the H_S values grouped in 0.25 m bins. These histograms are the marginal H_S distributions from the joint H_S:T_Z histograms ('scatterplots') which were constructed allowing for the variation in the number of records per month. Note that the scatterplots used to generate both the marginal H_S and marginal T_Z distributions are not those used to present the joint H_S:T_Z distributions, which are binned in 0.5 m steps. The probability values for each bin and each histogram are set out in Tables 1 and 2.

Estimates of the cumulative H_S non-exceedance probability distributions, presented as ogives, are given in Figs.8 and 9. These were calculated in the same manner as the histograms above, but with H_S values grouped in 0.1 m bins to smooth the curves.

Estimates of the fifty-year return value of H_S, $H_S(50)$, were obtained by fitting a Fisher-Tippett Type I distribution to the observed distributions of H_S and extrapolating to the required probability, as described in Appendix 3. The table below gives a summary of the results; see also Figs.10-12, where the FT-1

distribution is represented by the solid straight line; the data were binned in 0.25 m steps, as above. Fig.12 (FT-1 fit to Offshore Spring data) is included for comparison with the Nearshore FT-1 fit. Note that the data interval of $1\frac{1}{2}$ hours was used to calculate the return value probability; using the more usual 3-hour interval would have given return values about 5-6% lower.

Site	Period	$H_S(50)$ (m)	location parameter (m)	scale parameter (m)
Offshore	All data	5.99	0.64	0.43
	Spring	6.46	0.67	0.52
	Summer	4.19	0.49	0.33
	Autumn	4.15	0.57	0.32
	Winter	5.29	0.92	0.39
Nearshore	Spring	5.66	0.51	0.46

The $H_S(50)$ for all the offshore data is 0.5 m less than that for just the spring data. The implication is that were a structure to be erected in the vicinity of the Offshore buoy site, it would experience worse conditions were it to be stationed there for fifty springs than if it were stationed for fifty full years! This apparent difficulty is believed to stem from the shortness of the data series, which provides an inadequate sample of the wave climate. A further effect of climate variability is seen below in relation to the joint H_S:T_Z histograms.

The Nearshore data are poorly fitted by the FT-1 distribution. (The Log-Normal distribution was also tried, but was not found to give an improved fit, and is not shown.) It is possible that they stem from two different distributions, represented by lower and upper sections, dividing about H_S = 3 m. The Nearshore and Offshore cumulative spring H_S probability distributions are different below and quite similar above this value. This would not seem unreasonable, as many of the spring H_S measurements above 3 m derive from the April 1986 storm, which was generated by North-Easterly winds, and since waves do not change greatly in propagating onshore (see section 10), both Nearshore and Offshore sites would have similar measurements from this period. Differences in

the H_S distribution above 3 m arise primarily from the different effects of gaps in the data (the height of the April 1986 storm is excised from the Offshore records by such a gap), and by the contribution of high seas to the March 1987 Offshore record. This latter is further mentioned below.

The maximum recorded value of zero-up-crossing period T_Z occurred at the Nearshore site on 10 April 1986 at 0900 hours with T_Z = 7.63 sec and associated H_S = 3.79 m; the Offshore maximum T_Z occurred on 29th March 1987 at 1930 hours with T_Z = 8.97 sec and associated H_S = 2.68 m.

Figure 13 shows the joint probability distribution (or scatterplot) of H_S and T_Z for the Nearshore buoy; figure 14 shows the seasonal and total scatterplots for the Offshore buoy. Included in these figures are lines of significant steepness of 1/7, 1/10, 1/15 and 1/20. When computing the scatterplots, allowance was made for the variation in the number of valid records per month throughout the year by computing a scatterplot for each calendar month, then combining the resulting monthly scatterplots (suitably weighted for different numbers of days per month) into plots representing the whole year and the seasons.

It is interesting to note the difference between the Nearshore and Offshore spring scatterplots; the latter includes a quantity of probability ascribed to waves of $T_Z > 6.5$ s which is not seen on the Nearshore scatterplot. This probability derives from waves generated by storms in March 1987, after the Nearshore buoy had been removed, and is indicative of the difficulty of deriving reliable wave statistics from just one year of measurements.

Comparisons were effected between records taken simultaneously at both Nearshore and Offshore sites; figs.15 and 16 show plots of Nearshore vs. Offshore values of H_S and T_Z respectively. These plots also include the least-squares best straight-line fit; of the H_S plots, the lowest slope (0.805) is seen in March 1986, and the highest (0.907) in April 1986, the former containing a period of sustained strong offshore winds, the latter sustained strong onshore winds. The matter is discussed further in section 10.

8. PRESENTATION OF WAVE SPECTRAL DATA

Appendix 2 describes the methods of spectral analysis by means of which the recorded samples of wave height are processed into spectra.

The examples of spectra chosen for presentation are given as contoured time series, plotted in 'variance-preserving' format in which, instead of plotting contours of spectral density against axes of time and frequency, contours of spectral density times frequency are plotted against axes of time and log frequency; i.e. f is replaced by f' = lnf and S(f) is replaced by S'(f') = f S(f) so that S(f)df = S'(f')df'. This format increased the graphed area around the spectral peak frequencies and swell frequencies (0.1-0.2 Hz), while the area of the otherwise over-extensive low energy tail is decreased; further, the volume under any portion of the surface plotted, S(f)dfdt or S'(f')df'dt has the same significance in either format, being the variance of the spectrum in df multiplied by dt.

The plotted contours are arranged in three quasi-logarithmically spaced intensity bands (low, medium and high), as below:

	fS(f)
LOW INTENSITY	0.01
(Broken Line)	0.033
	0.067
MEDIUM INTENSITY	0.1
(Full Line)	0.25
	0.5
	0.75
HIGH INTENSITY	1.0
(Bold Line)	1.5
	2.0
	2.5
	3.0
	3.5

The values were chosen by trial and error, providing clarity over sequences of spectra representing sea states ranging from quiescent to stormy.

Six examples of contoured time-series of spectra are presented here: see Figs.17-22. All cover nine days of spectra. The first two are from March 1986 Nearshore and Offshore sites during a period of strong offshore winds; the second two are for April 1986 Nearshore and Offshore sites, during a period of strong onshore winds (this period included the highest H_S storm observed at Holderness); the fifth is a further example of a storm with strong offshore winds, from March 1987 Offshore site; the sixth is an example of a quiescent period, from July 1986 Offshore site.

9. ANALYSIS OF TIME-MODULATION OF HIGH-FREQUENCY SPECTRAL DENSITIES

Inspection of the contoured spectra (Figs.17-22) reveals modulation with time of the spectral densities of the high-frequency tail at an approximately semidiurnal frequency.

In 9.1 we derive the spectrum of the modulation at high frequencies, with significant coherence at the two sites of the 12.5 hour component of modulation. In 9.2 we show, using a simple model, that current speeds required to produce the modulations by Doppler shifting are not unreasonable, although the differences in speeds at the two sites suggest that wave refraction and wave-current interactions could also be producing modulations.

9.1 Spectral analysis of modulation

The observed approximately semidiurnal modulation on the high-frequency tail was spectrally analysed to confirm that the frequency was tidal. The spectral densities of each sample spectrum were averaged from 0.4 Hz to 0.5 Hz; the time series of nine days (conforming with the contoured spectra) of these high-frequency mean spectral densities was then spectrally analysed, using NAG G13CAF FFT routine. See Figs.23a (April 1986, Nearshore) and 24a (April 1986,

Offshore), which show the resulting spectra. Energy at frequencies less than about 0.05 cycles per 1.5 hours (or of period > 30 hours) is due to 'weather' events. The two remaining peaks are of frequencies approximately 0.12 and 0.24 cycles per 1.5 hours (periods 12.5 and 6.25 hours approx.).

To determine whether the 6.25 hour peak was a side lobe of the 12.5 hour peak, a sinusoid of period 12.42 hours, equivalent to the M2 tidal period, was fitted to the data and then removed; this had no effect on the 6.25 hour peak, nor was the whole of the 12.5 hour peak removed. Therefore, four sinusoids were fitted to and removed from the spectrum; these sinusoids were of periods 12.42, 12.00, 6.21 and 6.00 hours, being M2 and S2 tidal periods, and half of each period respectively. The amplitudes and relative phases of these components are given below; see Figs.23b and 24b also, which show the spectra after removal of these four components.

SPECTRAL DENSITIES AT TIDAL PERIODS

Component period (hours)	Nearshore		Offshore	
	Amplitude	Phase (deg.)	Amplitude	Phase (deg.)
12.42	0.613E-02	-26.4	0.693E-02	-7.8
12.00	0.365E-02	29.3	0.412E-02	42.0
6.21	0.386E-02	138.4	0.221E-02	128.2
6.00	0.195E-02	-16.1	0.092E-02	-29.5

The higher frequency components are considerably more intense at the shallower water Nearshore site than the Offshore site.

To investigate further the relationship between spectral densities at the two sites, the cross-spectrum of the time series of spectral densities at both sites at one frequency (0.41 Hz) was found, using NAG G13CCF FFT routine. See Fig.25, which shows coherence, gain and phase as a function of frequency (cycles per 1.5 hours) where the coherence, gain and phase (at each frequency) are defined as below:

$$\text{Coherence:} \quad \gamma^2 = \frac{C_{12}^2 + Q_{12}^2}{C_{11}C_{22}}$$

$$\text{Gain} = \frac{C_{22}}{C_{11}} \gamma^2$$

$$\text{Phase} = \tan^{-1}(Q_{12}/C_{12})$$

where C_{12} and Q_{12} are the co- and quadrature spectral densities respectively, and C_{11} and C_{22} are autospectral densities. Most significantly, there is a well defined peak in the coherence at 0.12 cycles/1.5 hours (i.e. period 12.5 hours). This indicates strongly that there is a linear relationship between the spectral densities at 0.41 Hz at the two sites; i.e., they both contain a significant time-varying component of period (approximately) 12.5 hours. However, no such peak is seen around 0.24 cycles/1.5 hours. This information is not inconsistent with the foregoing; the posited M2/S2 nearshore and offshore tidal components are of comparable magnitude; however, the offshore 'half-period' components are significantly smaller than the nearshore. This difference is reflected in the gain, which shows a peak around 0.225 cycles/1.5 hours (period 6.5 hours).

Over the width of the 0.12 cycles/1.5 hours peak, the phase of the offshore spectral densities relative to the nearshore varies by as much as ±45°. This is not inconsistent with the phase differences calculated between the posited M2 and S2 tidal components at the individual sites (55° Nearshore and 50° Offshore).

The foregoing is believed to substantiate the tidal nature of the modulation of the high frequency spectral densities. The approximately semidiurnal signals are likely to have been generated by the effect of the tidal currents alternately opposing and following the wave propagation. The source of the 'half-period' signals could either be M4 and S4 tidal currents, or an effect of the response of the wave spectrum to semidiurnal tidal current magnitude, irrespective of direction, or to lack of symmetry in the response to the semidiurnal tide.

9.2 Investigation of Modulation Assuming Doppler Shifting

In this section, angular frequency ω (rad s^{-1}) is used for convenience and in accordance with the usual convention rather than f(Hz).

The wave energy in a band $d\omega$ around frequency ω of a spectrum, $S(\omega)d\omega$ will appear, in the presence of a current, to be shifted to an apparent frequency ω_a such that, assuming no transfer of energy between the wave spectrum and the current,

$$S(\omega)d\omega = S_a(\omega_a)d\omega_a \tag{9.1}$$

where subscript a represents apparent.

In the presence of a current $\underline{u}$, a frequency ω is observed as ω_a in accordance with

$$\omega_a = \omega + \underline{k}.\underline{u}$$

where $\underline{k}$ is wave number. Assuming parallel waves and current and the deep-water dispersion relationship (applicable at the Holderness sites for high frequencies), this becomes

$$\omega_a = \omega + \omega^2 u/g$$

This is quadratic in ω with roots

$$\omega = \frac{g}{2u}\{-1 \pm (1 + \frac{4u\omega_a}{g})^{\frac{1}{2}}\}$$

Further, and taking the positive square root

$$\frac{d\omega}{d\omega_a} = (1 + \frac{4u\omega_a}{g})^{-\frac{1}{2}}$$

Applying this to (9.1)

$$S_a(\omega_a) = \left(1 \pm \frac{4u\omega_a}{g}\right)^{-\frac{1}{2}} S(\omega) \qquad (9.2)$$

Eqn.9.2 provides a means of determining current u from the apparent spectrum $S_a(\omega_a)$, if the intrinsic spectral density $S(\omega)$ is known:

$$u = \frac{g}{4\omega_a}\left[\left\{\frac{S(\omega)}{S_a(\omega_a)}\right\}^2 - 1\right] \qquad (9.3)$$

This was approached by selecting a section of the high frequency spectrum in which the intrinsic spectral density could be seen to be approximately constant; i.e. where a contour mean remained constant, and about which value the magnitude of the tidal-induced oscillations was roughly constant. Nearshore site, day 97 to day 100, 1986, at 0.38 Hz, was chosen for this purpose. An estimate of the intrinsic spectral density was found by assuming the time-averaged current to be zero (not strictly true in the presence of some wind-driven current), so that, from (9.3)

$$S(\omega) = \left(\overline{[S_a(\omega_a)]^{-2}}\right)^{-\frac{1}{2}} \qquad (9.4)$$

where the bar signifies an average over time. A time series of current values was generated, to which was fitted a function of the form

$$u(t) = \alpha + \beta \sin \omega_T t + \gamma \cos \omega_T t$$

where ω_T is the M2 tidal frequency. The spectral time series, and resulting current time series with superimposed sinusoid, are shown in Fig.26, also given in which are spectral time series and current values for day 97 to day 98, 1986, 0.38 Hz Offshore site. The shorter time series was used to exclude a gap in the data.

The Nearshore computed current is much more spikey than the Offshore; the former seems to include a 'half-period' signal. The fitted current amplitude is considerably greater Offshore (0.73 m/s) than Nearshore (0.39 m/s); these

figures, although unreliable, tend to support the assumption of the presence of a considerable horizontal current shear perpendicular to the coast, as suggested below in section 10.1.

9.3 Spectral Analysis of Time Series of T_Z Records

Sixteen days of T_Z records from both Offshore and Nearshore sites for May 1986 were spectrally analysed (With G13CAF) to determine the period(s) of the seemingly regular fluctuations in T_Z, which have an amplitude of about 5-10% of T_Z. See Figs.27 and 28, which show the spectra of the time series. Peaks are seen at about 0.12 cycles per 1.5 hours (covering, as previously mentioned, M2 and S2 tidal periods); also, small peaks are seen around 0.24 cycles per 1.5 hours. The dependence of T_Z on m_2, the 2nd spectral moment, renders T_Z sensitive to the high-frequency spectral tail, so that the previously mentioned Doppler shifting is seen to affect T_Z significantly, even though only the 'low-energy' part of the spectrum is affected.

10. ANALYSIS OF SPECTRA DURING TIMES OF STRONG ONSHORE AND OFFSHORE WINDS

The changes in spectra of waves propagating shorewards and of waves created by offshore winds are the result of different processes. Onshore waves, particularly the low frequency components, are affected by shoaling, refraction, bottom friction, and eventually by breaking. Spectra of waves being propagated away from the coast, generated by offshore winds, vary with fetch (assuming that the wind is not so light or the fetch so large that the waves are fully developed).

The difference in spectra at two sites, at different fetches from the shore, can be described by calculating the ratio of spectral energies at the two sites as a function of frequency. Figs.29 and 30 show these ratios for measurements from the two Waveriders off Holderness, at 6.9 and 12.2 km from the shore, during nine days from day 79, 1986, and from day 95, 1986. During the former period, there was a strong wind from the NNE, (i.e. towards the coast at about 45° to the bottom contours), reaching 36 knots for a time. During the

second period, the wind was consistently blowing offshore, reaching up to 40 knots. Simple models are proposed for the energy ratios in these two situations and the results compared with the observations shown in Figs.29 and 30.

10.1 Onshore Waves

Assuming only that shoaling and refraction are important, and ignoring any loss of energy by bottom friction or breaking and any gain in energy by reflections and by wind input, then it may readily be shown (see, for example, Sarpkaya and Isaacson, 1981) that the frequency spectrum S(f) at a site in a water depth d is given, for long-crested waves, by

$$S(f) = S_o(f).K_s^2.K_r^2$$

where $S_o(f)$ is the deep water spectrum and the shoaling and refraction coefficients are given by

$$K_s^2 = 2\cosh^2(kd)/(2kd + \sinh(2kd))$$

and

$$K_r^2 = |\cos\theta_o|/\sqrt{[1 - \sin^2\theta_o \tanh(kd)]}$$

where θ_o is the angle of propagation in deep water and k is the wave number in water depth d given by the dispersion relationship

$$gk\tanh(kd) = (2\pi f)^2$$

where f is the frequency in Hz.

If the deep water waves are short-crested with a directional spectrum $S_o(f,\theta) = S_o(f)G_o(\theta_o-\alpha_o)$, where α_o is the dominant direction of propagation, then it follows that

$$S(f) = S_o(f).K_s^2\int G_o(\theta_o-\alpha_o).K_r^2.d\theta_o \qquad (10.1)$$

We restrict θ_o to $|\theta_o| \leq \pi/2$, so only rays propagating shorewards are considered, and the directional spreading function in deep water, G_o, is truncated so that there is no energy propagated offshore. A commonly accepted form for G_o is

$$G_o(\theta_o - \alpha_o) = \{\cos^{2n}[(\theta_o - \alpha_o)/2]\}/Q \qquad |\theta_o - \alpha_o| \leq \pi$$

where Q is a normalising constant so that $\int G_o d\theta_o = 1$. We shall use

$$G_o(\theta_o - \alpha_o) = \{\cos^{2n}[(\theta_o - \alpha_o)/2]\}/Q' \qquad |\theta o| \leq \pi/2$$

with a revised normalising constant, Q', and with n = 10 and $\alpha_o = 45°$.

The ratio R(f) of the spectral energies $S_1(f)$ and $S_2(f)$ at depths d_1 and d_2 is readily obtained from (10.1), and is seen not to depend upon $S_o(f)$. The mean values of d_1 and d_2 at the Holderness sites are 15 m and 20 m, with a tidal range of about ±3 m. The results of solving for R for these ranges of d_1 and d_2 are shown in Fig.31. The general shape of R agrees with the observations, as in Fig.29, but there are two marked differences:

(a) the trough around 0.16 Hz is considerably deeper in the observations,
(b) at high frequencies, the observed ratios are significantly less than 1, at around 0.9.

The reason for (a) is probably that the model assumes no energy loss. It might also be caused in part by irregularities in the bottom contours.

The reason for (b) cannot be bottom friction, since these high frequency components are in relatively deep water (unless they are 'tied' components of steep low frequency waves). It is probably the differences in surface currents at the two sites, as suggested by the results in section 9.2. Such differences could cause refraction, particularly of the higher frequency wave energy components, and would vary the effect of wave-current interaction at the two sites, with increased transfer to higher frequencies with increasing current speed (see for example Longuet-Higgins and Stewart, 1960).

The ratios of energies in frequency bands (smoothed over n frequencies) were calculated by averaging the ratios from individual measurements. Appendix 4 demonstrates for the Holderness data with n = 15 that this method of calculation biases the ratios approximately 7% high, assuming for the case of waves propagating onshore that S_1/S_2 is constant. This does not affect the foregoing discussion.

10.2 Offshore Waves

Given the wind speed, U, blowing directly offshore over a specified fetch, X, then the significant wave height, H_s, and spectral peak period, T_p, can be estimated using the relationships given in section 4 of Hasselmann et al. (1976) for fetch-limited waves:

$$H_s = 0.0162X^{0.5}U$$

$$T_p = 0.566X^{0.3}U^{0.4}$$

where H_s, T_p, X, and U are in m, s, km, and ms^{-1}.

The JONSWAP spectrum is given, using the same units, by

$$S(f) = \frac{1}{4.88} H_s^2 T_p^{-4} f^{-5} \exp[-1.25/(T_p f)^4] \gamma^q$$

where $q = \exp[-(T_p f - 1)^2/2\sigma^2]$

with $\sigma = 0.07$ for $T_p f \leq 1$

and $\sigma = 0.09$ for $T_p f > 1$

and γ is the peakedness parameter, usually given the mean value from the JONSWAP measurements of 3.3.

So the ratio of the two spectral energies at fetches X1 and X2 is given by

$$R(f) = \frac{S_1(f)}{S_2(f)} = Q \frac{\exp[-1.25(T_{p1} f)^{-4}] \gamma^{q1}}{\exp[-1.25(T_{p2} f)^{-4}] \gamma^{q2}} \qquad (7)$$

where $Q = (X_2/X_1)0.2$

For comparisons with observations, the mean of the function R(f), with $\gamma = 3.3$, was calculated for a range of wind speeds, weighted by the distribution of observed winds at Spurn Head during the nine days from day 79, 1986, which is given in the table below. The result is shown in Fig.32.

Distribution of Wind Speeds at Spurn Head from Day 79 to Day 87, 1986

Wind Speed (m/s)	% Occurrence
0-2	0.0
2-4	1.4
4-6	7.9
6-8	13.5
8-10	32.1
10-12	17.2
12-14	9.3
14-16	12.1
16-18	3.3
18-20	2.3
20-22	0.9

The observations (Fig.30) clearly include low frequency energy propagating shorewards; but at the higher frequencies, >0.2 Hz, there is reasonable agreement between theory and observations, except that at the highest observed frequencies, around 0.4-0.5 Hz, there is relatively more energy at the shorter fetch than predicted. (Since S_1/S_2 varies during these measurements, it is not possible to estimate any bias in the estimated ratios.)

Now, from (10.2), putting $\tau = T_{p1}/T_{p2} = (X_1/X_2)^{0.3}$ and $x = T_{p1}f$

gives

$$R(x) = Q \exp[-1.25x^{-4}(1-\tau^4)].\exp[\ln\gamma\{e^{-(x-1)^2/2\sigma_1^2}-e^{-(x/\tau-1)^2/2\sigma_2^2}\}]$$

where $\sigma_1 = 0.07 \quad x \leq 1$

$= 0.09 \quad x > 1$

and $\sigma_2 = 0.07 \quad x/\tau \leq 1$

$= 0.09 \quad x/\tau > 1$

The maximum value of R is derivable from this equation (except when $\gamma = 1$) in terms of x, so is only a function of X_1/X_2 and γ, and is independent of U.

Fig.33 shows the result of plotting observed and theoretical distributions of R against x ($=T_{p1}f$), where T_{p1} was estimated from the observed spectral peak.

Data between 1630 hours, day 79 and 1330 hours, day 80 were used, this period being one of consistent wind direction (between 260° and 280°), which avoided any difficulty of cross-sea generation. The wind speed was 20 ±4 m/s.

The theoretical curves represent, from lowest to highest, γ = 2, 3, 4 and 5. The data peak lies between γ = 3 and 4, and the shape of the leading edge of the data peak matches well the predictions; the trailing edge, however is ~25% too high. The minima of data and prediction lie at $T_{p1}f$ ~0.8; data at $T_{p1}f$ less than this stem from swell energy propagating in from the north. It is interesting that γ appears to be remarkably close to the JONSWAP value of 3.3.

11. CONCLUDING REMARKS

The presence of two buoys on site made possible useful comparisons between the two data sets, particularly with regard to examining the different effects resulting when waves propagate onshore and offshore. However, much more would have been possible had on-site wind data and surface current measurements been available, in which case non-linear wave-current interactions, refraction and wave growth could have been studied.

The difficulty of producing climate statistics based on short data sets was evidenced by differences between the Nearshore and Offshore spring data as seen in the joint H_s:T_z distributions and the resulting fitted cumulative H_s

probability distributions (with associated fifty-year return values). Persistence statistics have not been produced, partly for this reason, but also because of presence of gaps in the data.

Spectral data exist for most records for which there are H_s and T_z values. Although only a few examples have been presented, the data can be obtained from IOSDL.

12. ACKNOWLEDGEMENTS

Thanks are due to the UK Ministry of Agriculture, Fisheries and Food who provided the funding for the collection of the data and the production of this report, and also to the Meteorological Office, which kindly provided the Spurn Head wind data.

13. REFERENCES

HASSELMANN, K., ROSS, D.B., MULLER, P. & SELL, W. 1976 A parametric wave prediction model.
Journal of Physical Oceanography, 6, 200-228.

HUMPHERY, J.D. 1982 Operational experiences with Waverider buoys and their moorings.
Institute of Oceanographic Sciences, Report, No. 145, 33pp.

LONGUET-HIGGINS, M.S. & STEWART, R.W. 1960 Changes in the form of short gravity waves on steady non-uniform currents.
Journal of Fluid Mechanics, 10, 529-549.

SARPKAYA, T. & ISAACSON, M. 1981 Mechanics of wave forces on offshore structures.
New York: Van Nostrand Reinhold Co., 651pp.

APPENDIX 1

FREQUENCY LOGGING OF WAVE DATA

The Waverider buoy employs a 259 Hz frequency modulated (FM) subcarrier to encode wave height information and has a nominal calibration so that an upward motion of the buoy of 1 metre displacement results in an increase in subcarrier frequency by 1.86 Hz. In the standard receiving system supplied by Datawell the wave height information is extracted from the signal by monitoring the V.C.O. (voltage control oscillator) voltage in a phase locked loop demodulator. In the IOS system however a different approach is used. The 259 Hz FM signal is applied to a phase locked loop which multiplies the subcarrier frequency by a factor of 128 and also serves to filter out any extraneous noise. The phase locked loop output is subtracted from a signal with a fixed frequency of 128 x 290 Hz. This gives a signal whose frequency depends upon wave height and for which (290-259) x 128 Hz corresponds to zero wave height. The frequency of this signal is counted over a period of one half second, so that for zero wave height a count of 1984 is obtained. In the presence of waves the count will change by -1.86 x 64 counts per metre of upward displacement.

The counting scheme described above determines the frequency response of the detector system which has the form:

$$\frac{\sin x}{x}$$

where $x = \pi f t$, t is the time period over which the frequency is counted (0.5 seconds); and f is the sea wave frequency. For high frequencies (above 1 Hz) the response function should be slightly modified to take account of the frequency response inherent in the phase locked loop.

This system has two advantages over the standard analogue logging system: first, the receiver and demodulator do not require regular calibration. Second, the system frequency response serves as a precisely defined low pass anti-alias filter.

APPENDIX 2

METHODS OF SPECTRAL ANALYSIS AND COMPUTATION OF WAVE PARAMETERS

The wave data described in this report are derived from time-series containing 4096 values of sea-surface elevation sampled at 0.5 second intervals producing 34 minute records. The spectrum produced from the time series is considered to be representative of the 1.5-hour period of which it is a sample. An outline of the method of spectral analysis is given below.

The Fast Fourier Transform

Using the Fourier theorem, the elevation of the sea surface above its mean at time t is given by

$$h(t) = \sum_{i=1}^{\infty} \{a_i \cos(\frac{2\pi it}{T}) + b_i \sin(\frac{2\pi it}{T})\}$$

where

$$a_i = \frac{2}{T} \int_0^T h(t) \sin(\frac{2\pi it}{T}) dt$$

$$b_i = \frac{2}{T} \int_0^T h(t) \sin(\frac{2\pi it}{T}) dt$$

and T is the record length.

The Fast Fourier Transform, based on the above relationships, is used to compute the pairs of coefficients (a_i, b_i) at the fundamental frequency

$$f_0 = \frac{1}{T}$$

and at integral multiples of this frequency up to the Nyquist frequency

$$f_{max} = \frac{1}{2\Delta T}$$

where ΔT is the sampling interval.

The sample estimate of the spectrum at the i^{th} frequency, Φ_i, is then computed as

$$\Phi_i = \frac{1}{2f_0}(a_i^2 + b_i^2)$$

Tapering of the Data

Variance of the wave record which is not located at one of the harmonic frequencies appears in the spectral estimates not only at the harmonic adjacent to the true frequency but in a band of harmonics. This leakage leads to biased estimates in that on balance a small proportion of the variance which should appear in the neighbourhood of the spectral peak leaks towards higher and lower frequencies. The effect can be reduced by tapering the ends of the time-series data smoothly to zero before performing the Fast Fourier Transform; a cosine taper applied to 12.5% of the record at each end has been used on the data described in this report. (This leads to a small increase in the sampling errors of the spectral estimates.)

Smoothing the Spectral Estimates

The spectral estimates Φ_i have a standard error of 100%. This may be reduced by taking the average of consecutive spectral estimates, and assigning to it the mid-frequency of the band of estimates used. The smoothed spectral estimates, S_j have been averaged in blocks of 15:

$$S_j = \frac{1}{15}\sum_{i=15j-14}^{15j} \Phi_i$$

and

$$f_j = (15j - 7)f_0$$

Application to the Wave Data

The fundamental frequency used is

$$f_0 = \frac{1}{2048} = 0.4833 \times 10^{-3} \text{ Hz}$$

and the maximum frequency is

$$f_{max} = \frac{1}{2 \times 0.5} = 1.0 \text{ Hz}$$

Smoothed estimates are at the following frequencies

$$f_1 = 3.91 \times 10^{-3} \text{ Hz}$$

to

$$f_{max} = 0.993 \text{ Hz}$$

with

$$\Delta f = 7.324 \times 10^{-3} \text{ Hz}$$

The normalised standard error of the smoothed spectral estimates is 26%, although the tapering process increases these by a small amount.

Computation of Spectral Moments

The nth moment of a continuous spectrum is

$$m_n = \int_0^\infty f^n \, S(f) df$$

where S(f) is the spectral density at frequency f. The unsmoothed spectral estimates Φ_i are used to compute the spectral moments:

$$m_n = \frac{1}{T} \sum_{i=i_L}^{i_u} f_i^n \, \Phi_i$$

where i_L = 83, corresponding to = 0.0405 Hz, and i_u = 1302, corresponding to 0.6357 Hz.

APPENDIX 3

DETAILS OF METHODS USED FOR CALCULATION 50-YEAR RETURN VALUES

H_S is used as a measure of the "sea-state", (i.e., the intensity of wave activity) and it is sampled every 1.5 hours. It is assumed that a set of H_S data for one year, or an integral number of years, is representative of the wave climate.

For each binned data value of H_S, the probability that this value will not be exceeded is calculated; this probability is then plotted against H_S. The axes are scaled according to an appropriate distribution, so that data with a perfect fit would appear as a straight line on the diagram. In practice, the class of functions known as extreme-value distributions are often found to give a close fit to the data. It should be noted that these functions are used only as 'templates' and not strictly as extreme-value distributions. These functions describe independent random data only, which climatic data are not, given 1.5-hourly data records and weather-system time-scales ranging from hours to years, etc.

The formula for the Fisher-Tippett Type 1 distribution, used in this report, is given below:

$$\text{Prob}\ (H_S \leq h) = \exp[-\exp\{-(\frac{h-A}{B})\}], \text{ where } B>0$$

where A is the location parameter and B is the scale parameter.

The best straight line fit to the data is drawn, then extrapolated to some desired probability and the corresponding value of H_S read off as the "design sea-state".

Fitting the Fisher-Tippett Type 1 Distribution by the Method of Moments

The mean and variance of this distribution are $A + \gamma B$ and $\pi^2 B^2/6$ respectively, where γ (Euler's constant) = 0.5772...; so the moments estimators given data x_i, $1 \leq i \leq n$, are given by

$$\tilde{A} = \bar{x} - \gamma \tilde{B}$$

$$\tilde{B} = \sqrt{6}\, s/\pi$$

where

$$\bar{x} = \sum_i x_i/n$$

$$s^2 = \sum_i (x_i - \bar{x})^2/(n - 1)$$

Values of $\bar{x}$ and s^2 may be estimated from grouped data.

Calculation of 50-year Return Value

The 50-year return value of H_S is defined as that value of Hs which is exceeded on average once in 50 years. In each case this has been determined by extrapolating the relevant distribution to the required probability of exceedance which is determined by assuming some frequency of observation (taken in this report to be 1.5-hourly), and by assuming all H_S observations to be independent.

The 50-year return value of H_S, $H_S(50)$ is then given by

$$\text{Prob}\,(H < H_S(50)) = 1 - \frac{1}{50 \times 365.25 \times 16}$$

$$= 0.99999658$$

Fitting to seasonal or monthly data reduces the number of days observation per year from 365.25 to 365.24/4 or 365.25/12 respectively, and reduces the relevant probabilities to 0.9999863 and 0.9999589 respectively.

APPENDIX 4

DISTRIBUTION OF THE RATIO OF SPECTRAL COMPONENTS

Given m pairs of estimates, $E_1(f)$ and $E_2(f)$, from two spectra $S_1(f)$ and $S_2(f)$, then the ratio $S_1(f)/S_2(f)$ may be estimated by

$$\bar{R} = \overline{E_1(f)/E_2(f)}$$

where the bar denotes averaging over the m estimates.

If E_1 and E_2 are histogram values obtained by averaging over n frequencies, then their distributions are χ^2_{2n}, or more correctly, the distribution of $\{2nE/S\}$ is χ^2_{2n}. So the ratio $(E_1/S_1)/(E_2/S_2)$ has an F distribution with (2n,2n) degrees of freedom (Johnson and Kotz, 1970), with mean and variance given by

$$\text{Exp}\{(E_1/S_1)/(E_2/S_2)\} = n/(n - 1) \qquad n > 1$$

and

$$\text{Var}\{(E_1/S_1)/(E_2/S_2)\} = \frac{n(2n - 1)}{(n - 1)^2(n - 2)} \qquad n > 2$$

The mean and variance are infinite if $n \leq 1$ and $n \leq 2$ respectively.

Therefore, assuming that the ratio S_1/S_2 is constant throughout the m measurements:

$$\text{Exp}(\bar{R}) = \frac{n}{n - 1} \cdot \frac{S_1}{S_2} \qquad n > 1 \qquad \text{(A4.1)}$$

and the variance of $\overline{(E_1/S_1)/(E_2/S_2)}$ is the variance of $(E_1/S_1)/(E_2/S_2)$ divided by m, so

$$\mathrm{Var}(\bar{R}) = \frac{n(2n-1)}{m(n-1)^2(n-2)}\left(\frac{S_1}{S_2}\right)^2 \qquad n > 2 \qquad \text{(A4.2)}$$

So, from (A4.1) R is a biased estimate, and for example if n = 15 then

$$\mathrm{Exp}(\bar{R}) \approx 1.07\ \frac{S_1}{S_2}$$

If m = 144 (equivalent to nine days of Holderness data) then

$$\mathrm{Var}(\bar{R}) \approx 0.00119\left(\frac{S_1}{S_2}\right)^2$$

and the standard error of R is given by

$$\mathrm{S.E.}(\bar{R}) \approx 0.0344\ \frac{S_1}{S_2}$$

REFERENCE

JOHNSON, N. L. & KOTZ, S. 1970. Continuous univariate distributions - 2. Houghton Mifflin, Boston, 306pp.

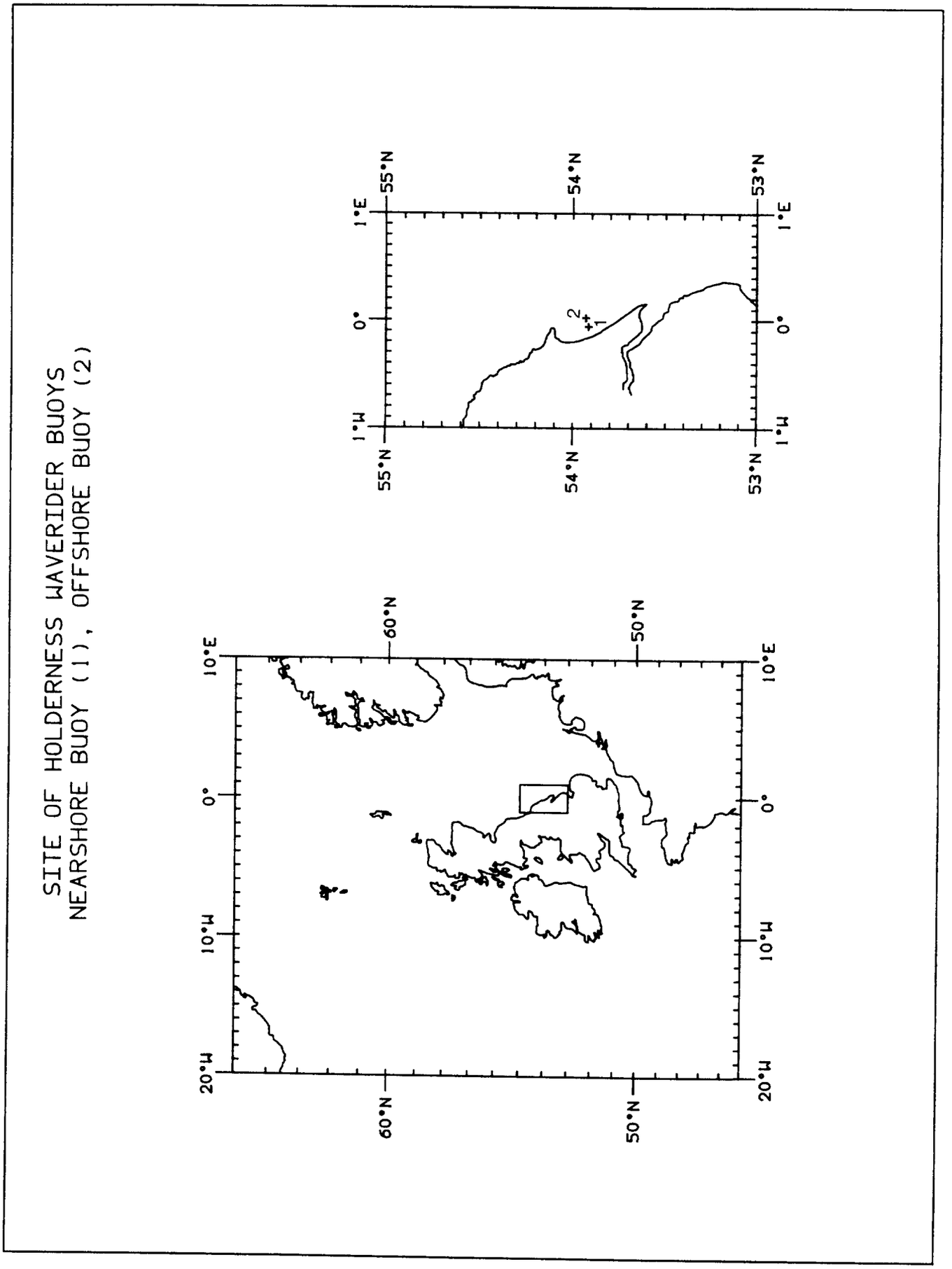
SITE OF HOLDERNESS WAVERIDER BUOYS
NEARSHORE BUOY (1), OFFSHORE BUOY (2)
55°N
54°N
53°N
1°E
0°
1°W
2
1
60°N
50°N
10°E
0°
10°W
20°W

Fig. 1

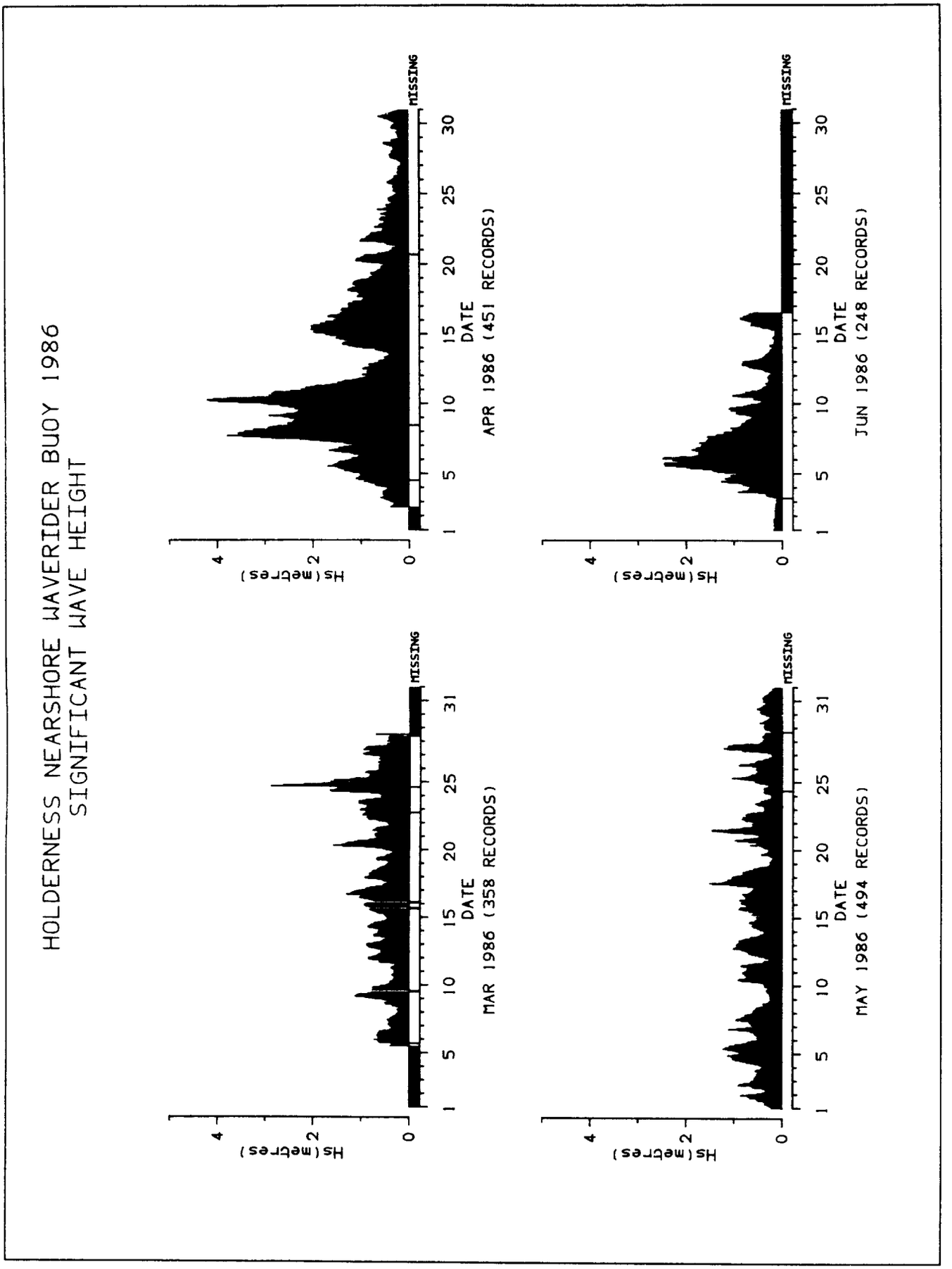
HOLDERNESS NEARSHORE WAVERIDER BUOY 1986
SIGNIFICANT WAVE HEIGHT
Hs (metres)
0
2
4
1
5
10
15
20
25
30
31
DATE
MISSING
APR 1986 (451 RECORDS)
MAR 1986 (358 RECORDS)
JUN 1986 (248 RECORDS)
MAY 1986 (494 RECORDS)

Fig. 2

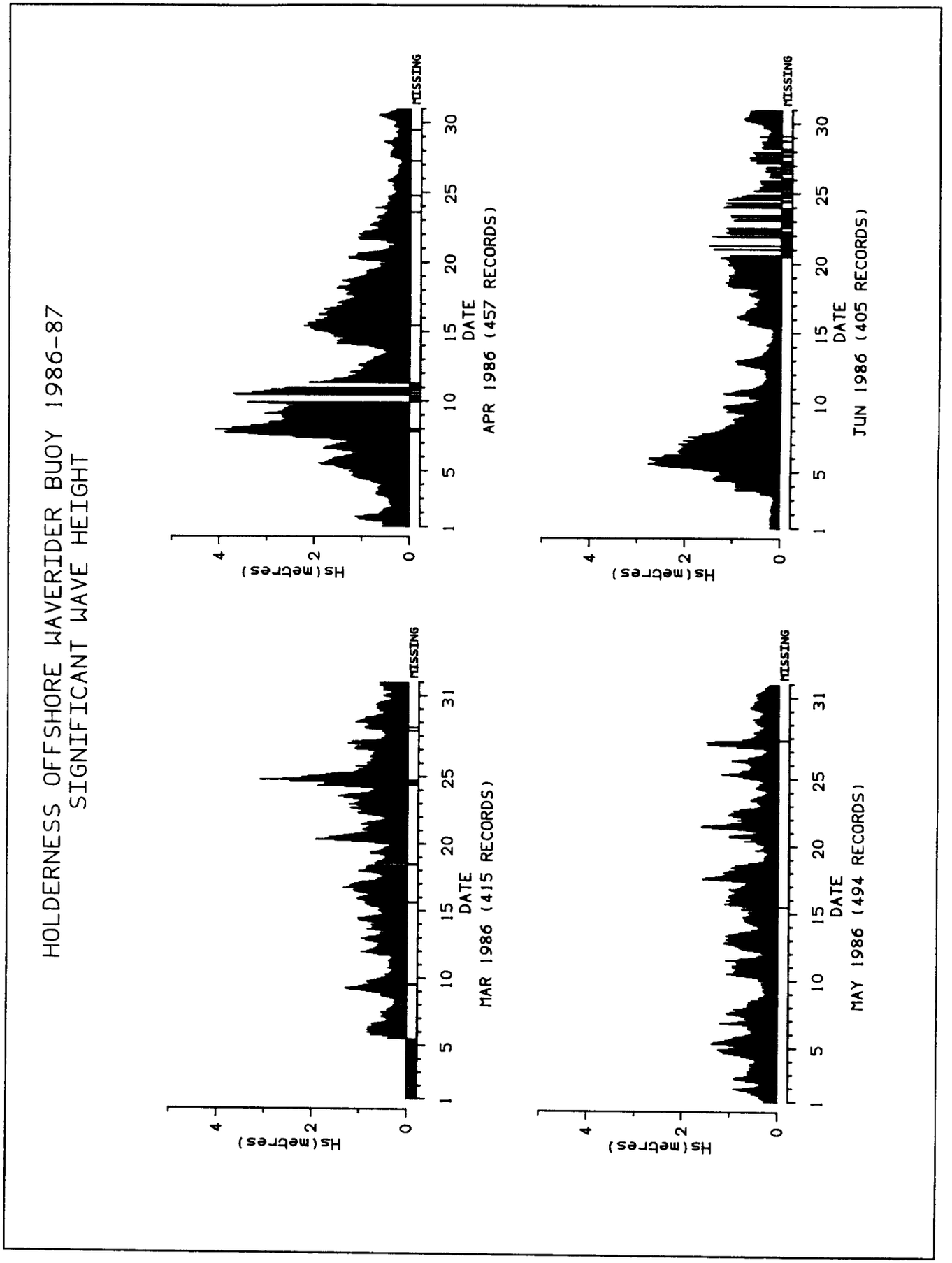
HOLDERNESS OFFSHORE WAVERIDER BUOY 1986-87
SIGNIFICANT WAVE HEIGHT
Hs (metres)
0
2
4
1
5
10
15
20
25
30
31
DATE
MISSING
MAR 1986 (415 RECORDS)
APR 1986 (457 RECORDS)
MAY 1986 (494 RECORDS)
JUN 1986 (405 RECORDS)

Fig. 3a

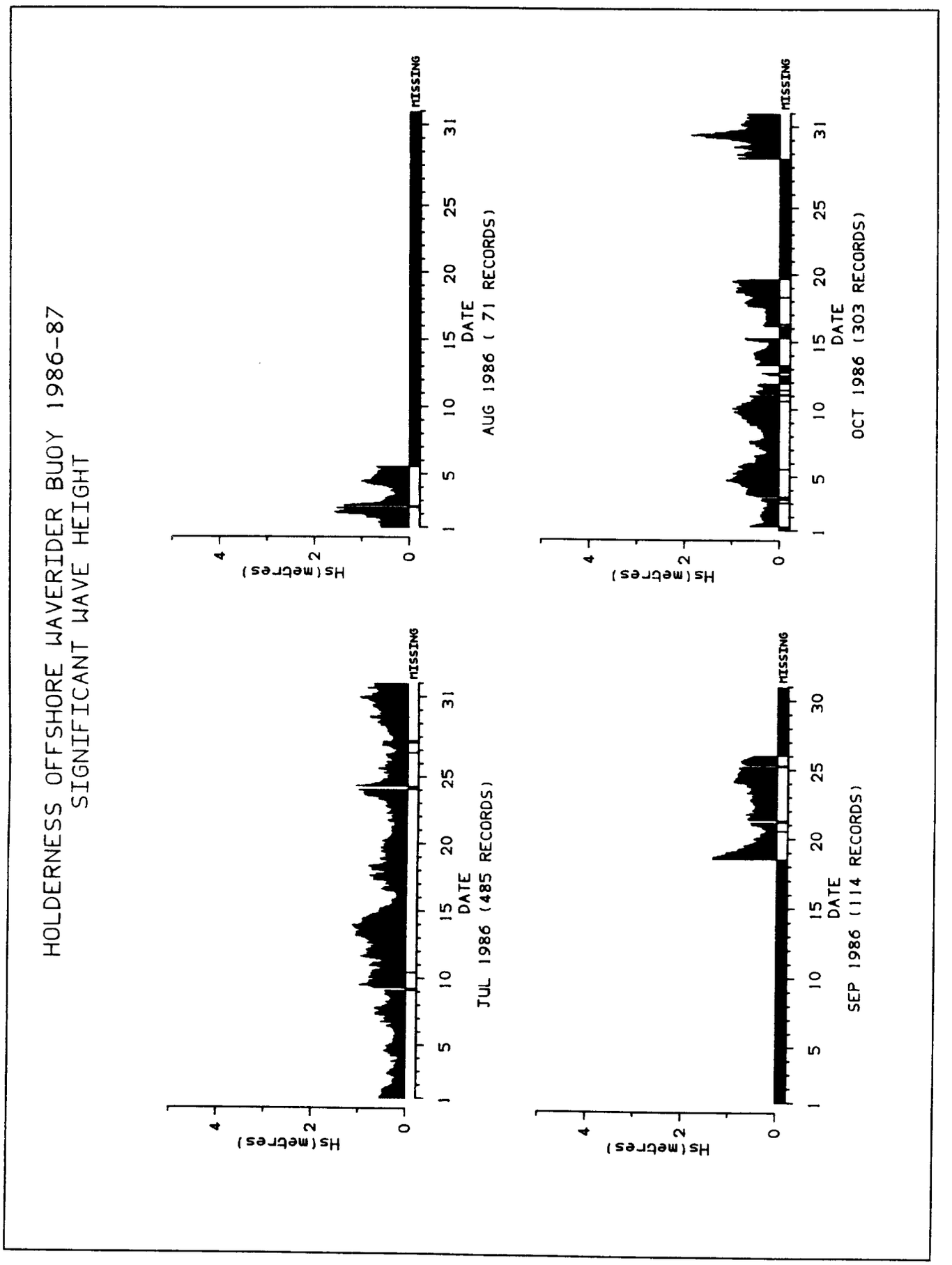
HOLDERNESS OFFSHORE WAVERIDER BUOY 1986-87
SIGNIFICANT WAVE HEIGHT
Hs (metres)
0
2
4
1
5
10
15
20
25
31
30
DATE
MISSING
AUG 1986 (71 RECORDS)
OCT 1986 (303 RECORDS)
JUL 1986 (485 RECORDS)
SEP 1986 (114 RECORDS)

Fig. 3b

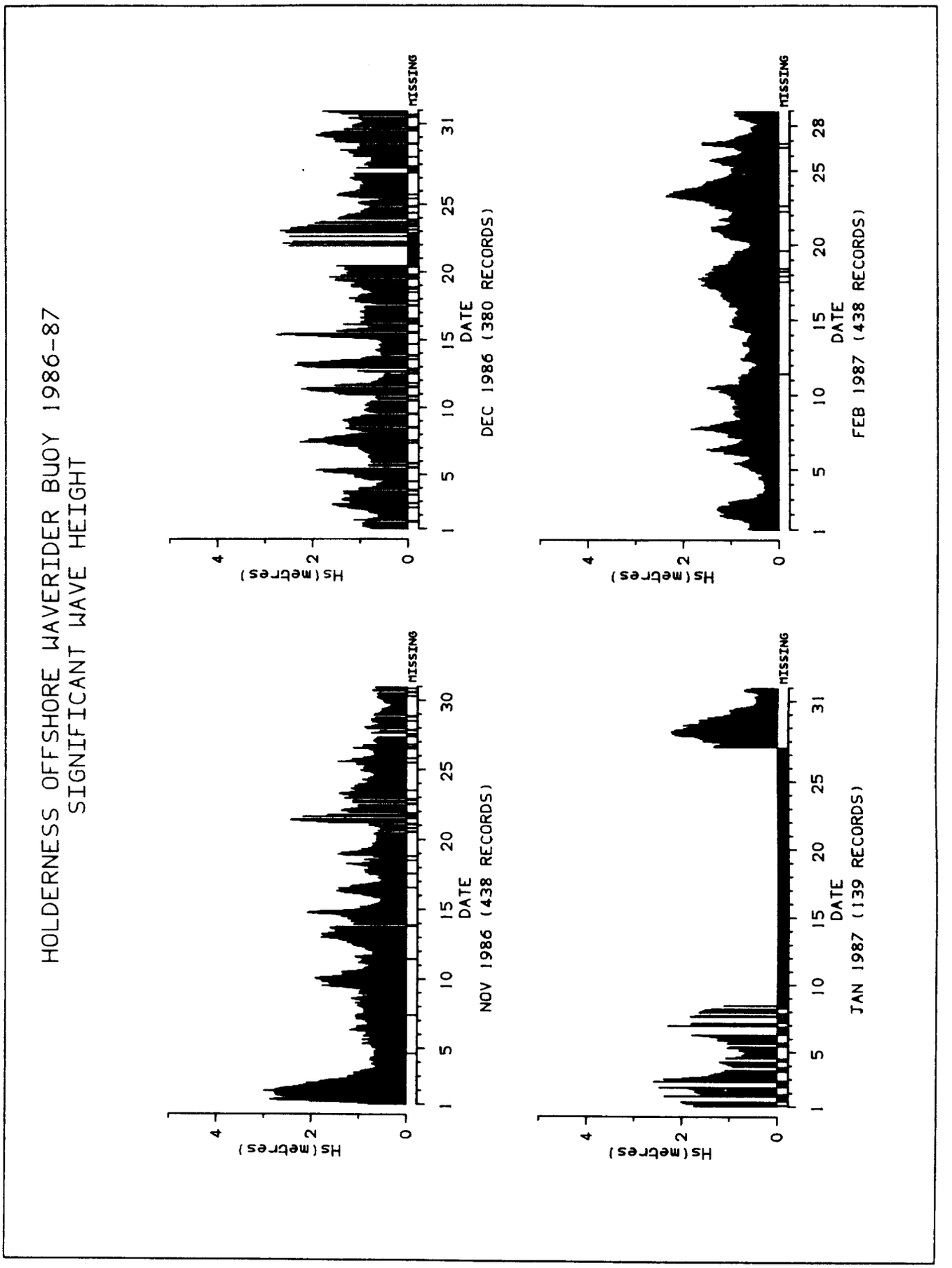
HOLDERNESS OFFSHORE WAVERIDER BUOY 1986-87
SIGNIFICANT WAVE HEIGHT
Hs (metres)
0
2
4
1
5
10
15
20
25
30
31
DATE
MISSING
NOV 1986 (438 RECORDS)
DEC 1986 (380 RECORDS)
JAN 1987 (139 RECORDS)
FEB 1987 (438 RECORDS)
28

Fig. 3c

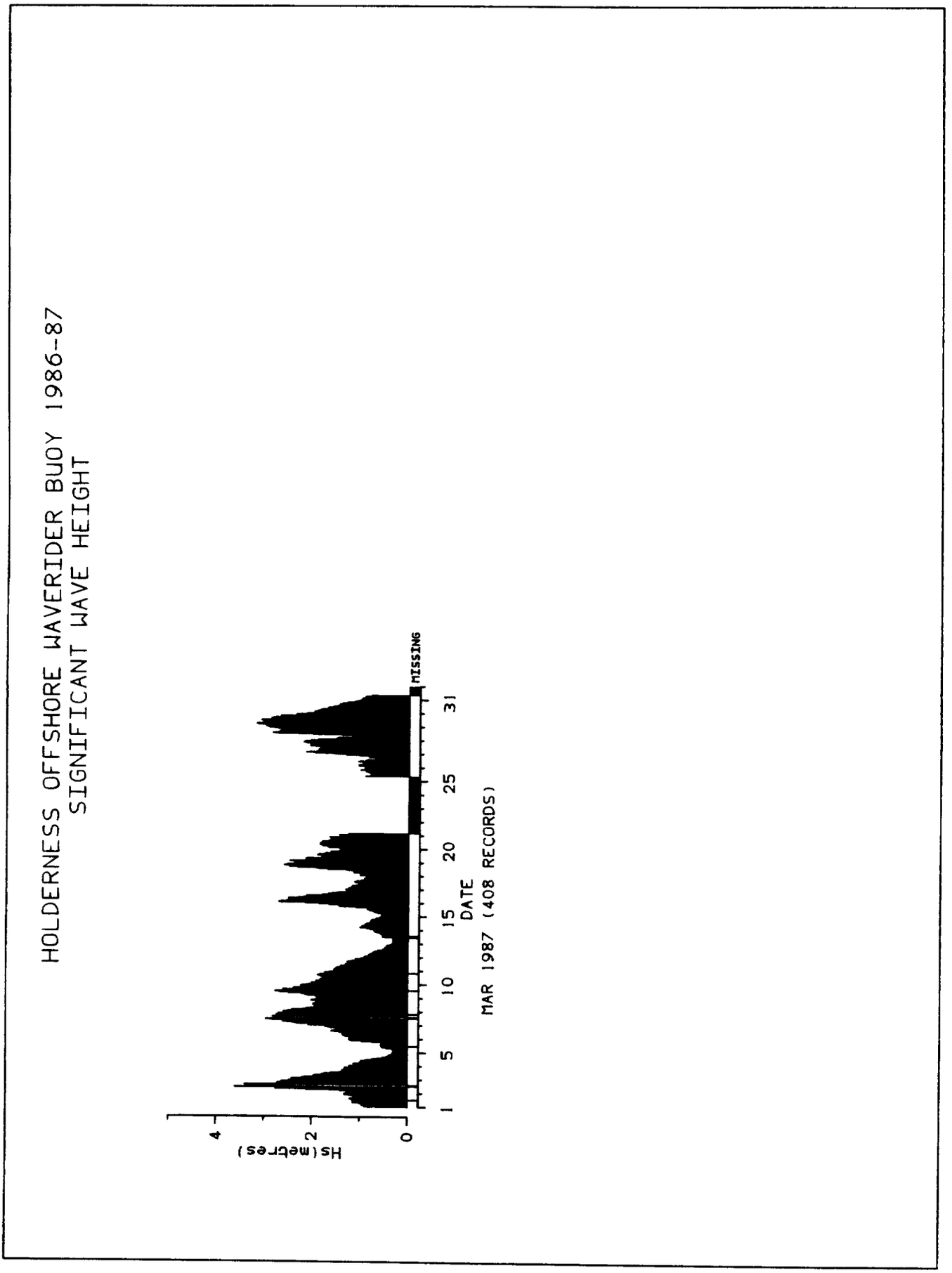
HOLDERNESS OFFSHORE WAVERIDER BUOY 1986-87
SIGNIFICANT WAVE HEIGHT
Hs (metres)
0
2
4
1
5
10
15
20
25
31
DATE
MAR 1987 (408 RECORDS)
MISSING

Fig. 3d

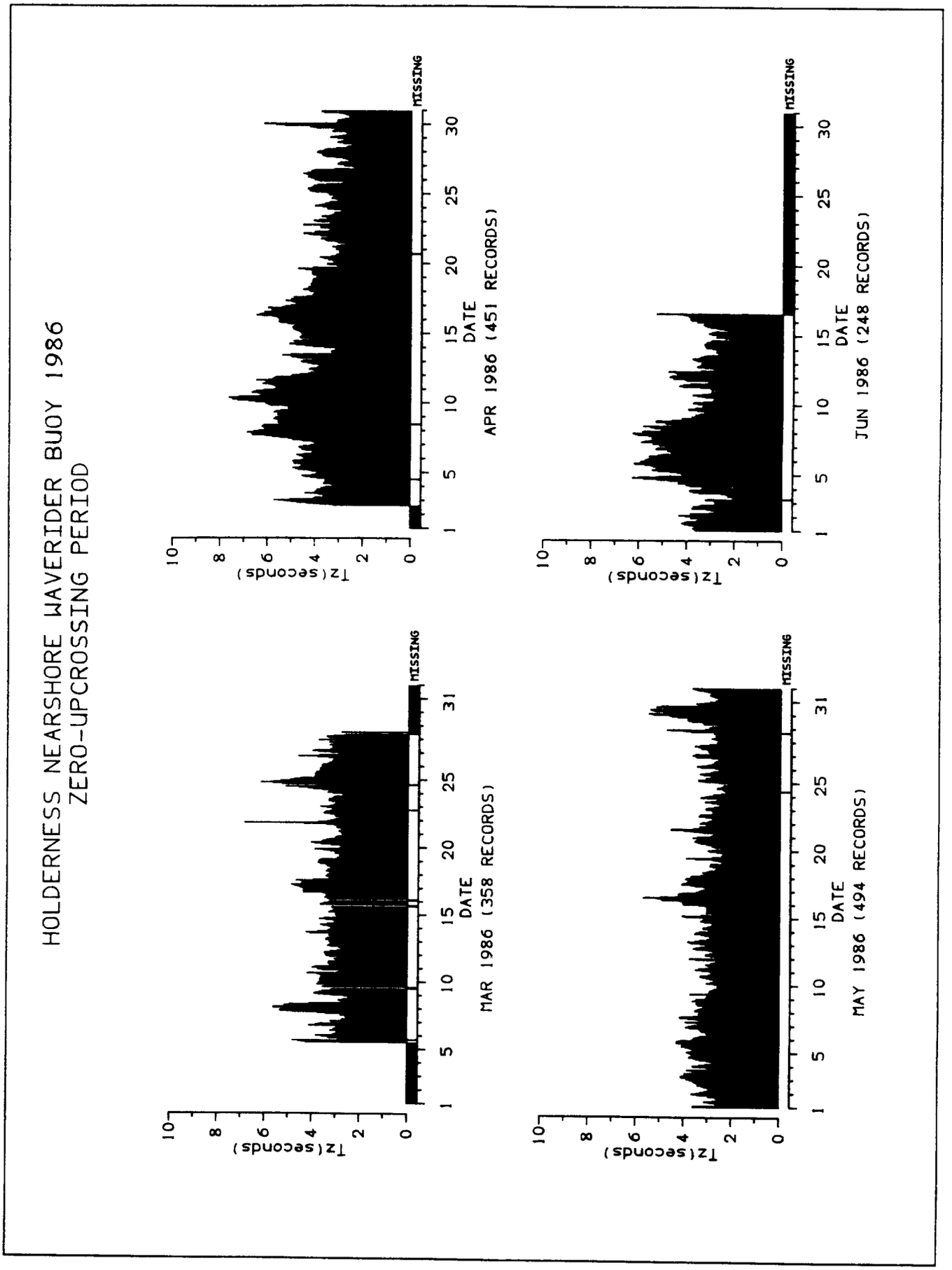
HOLDERNESS NEARSHORE WAVERIDER BUOY 1986
ZERO-UPCROSSING PERIOD
Tz(seconds)
DATE
MISSING
MAR 1986 (358 RECORDS)
APR 1986 (451 RECORDS)
MAY 1986 (494 RECORDS)
JUN 1986 (248 RECORDS)

Fig. 4

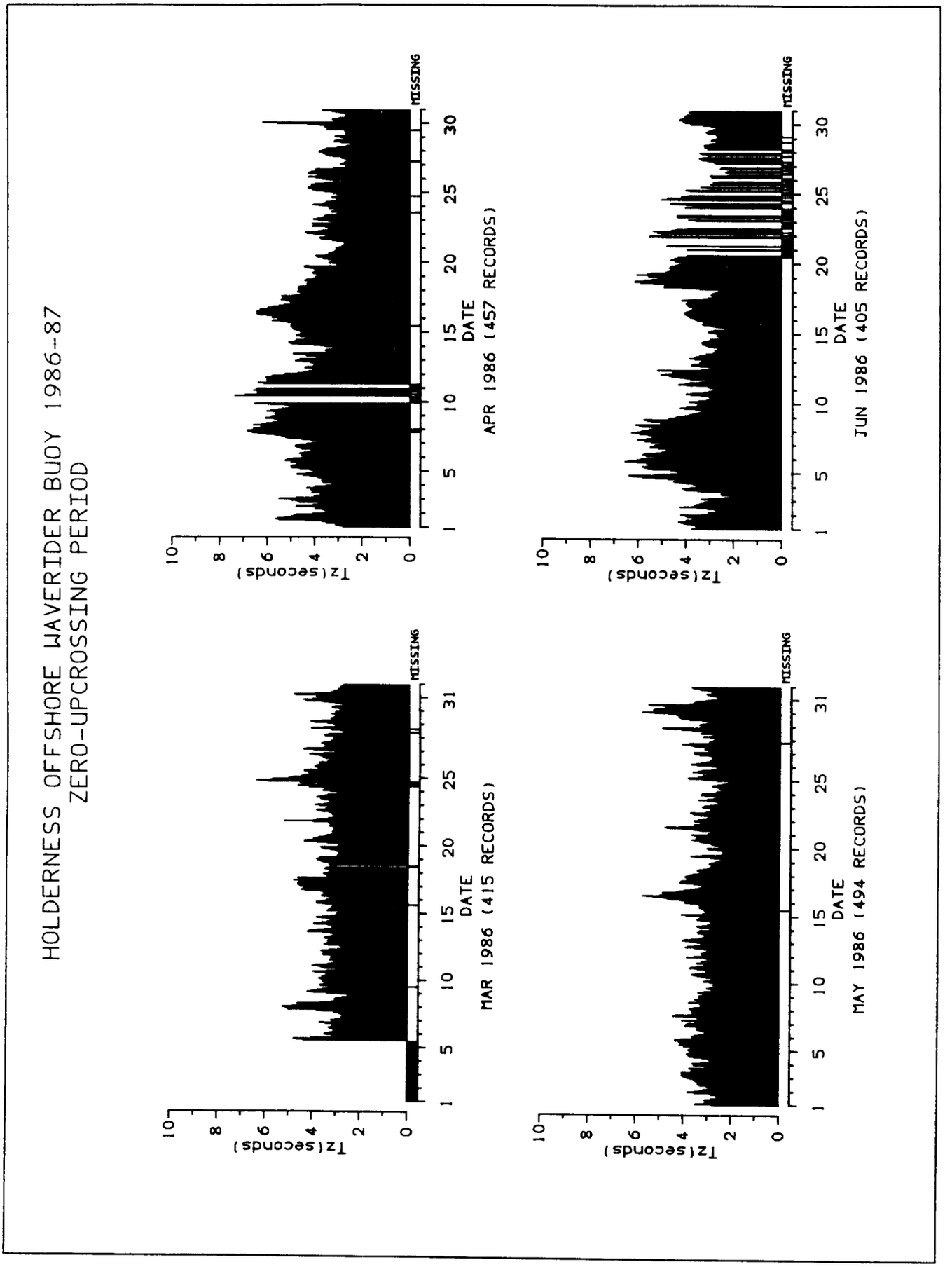
HOLDERNESS OFFSHORE WAVERIDER BUOY 1986-87
ZERO-UPCROSSING PERIOD
Tz(seconds)
DATE
MISSING
MAR 1986 (415 RECORDS)
APR 1986 (457 RECORDS)
MAY 1986 (494 RECORDS)
JUN 1986 (405 RECORDS)

Fig. 5a

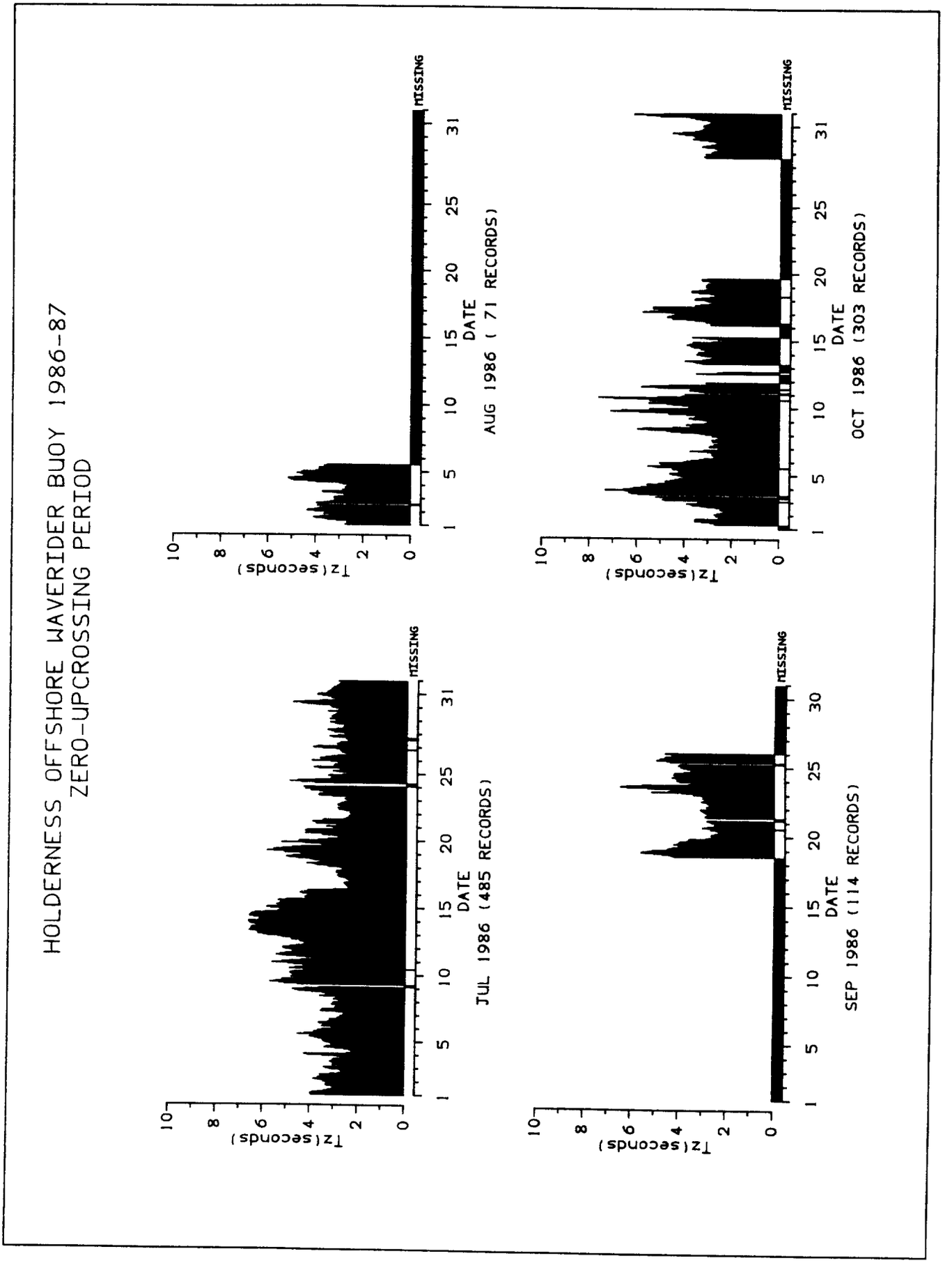
HOLDERNESS OFFSHORE WAVERIDER BUOY 1986-87
ZERO-UPCROSSING PERIOD
Tz (seconds)
DATE
MISSING
JUL 1986 (485 RECORDS)
AUG 1986 (71 RECORDS)
SEP 1986 (114 RECORDS)
OCT 1986 (303 RECORDS)

Fig. 5b

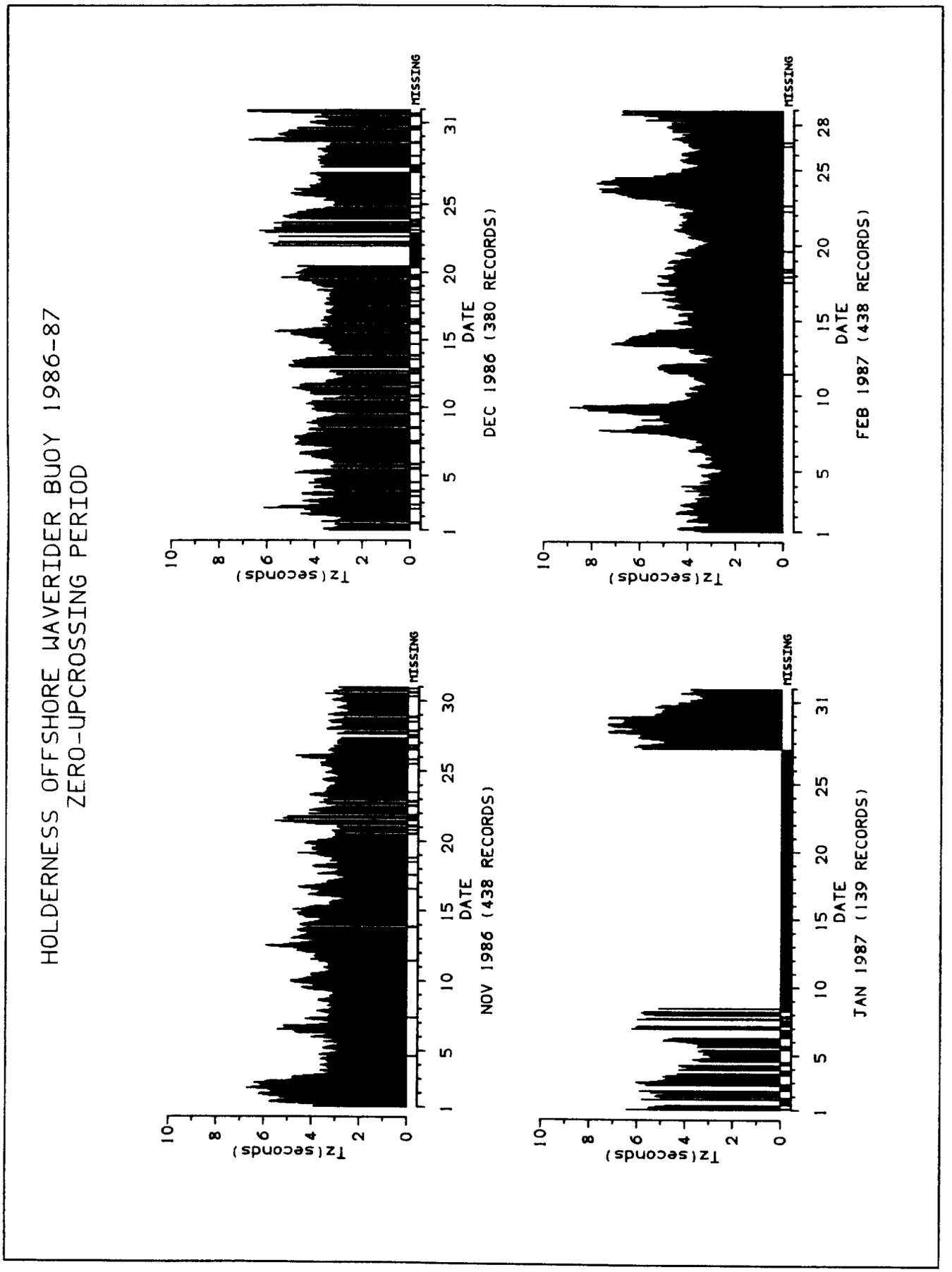
HOLDERNESS OFFSHORE WAVERIDER BUOY 1986-87
ZERO-UPCROSSING PERIOD
Tz (seconds)
DATE
MISSING
NOV 1986 (438 RECORDS)
DEC 1986 (380 RECORDS)
JAN 1987 (139 RECORDS)
FEB 1987 (438 RECORDS)

Fig. 5c

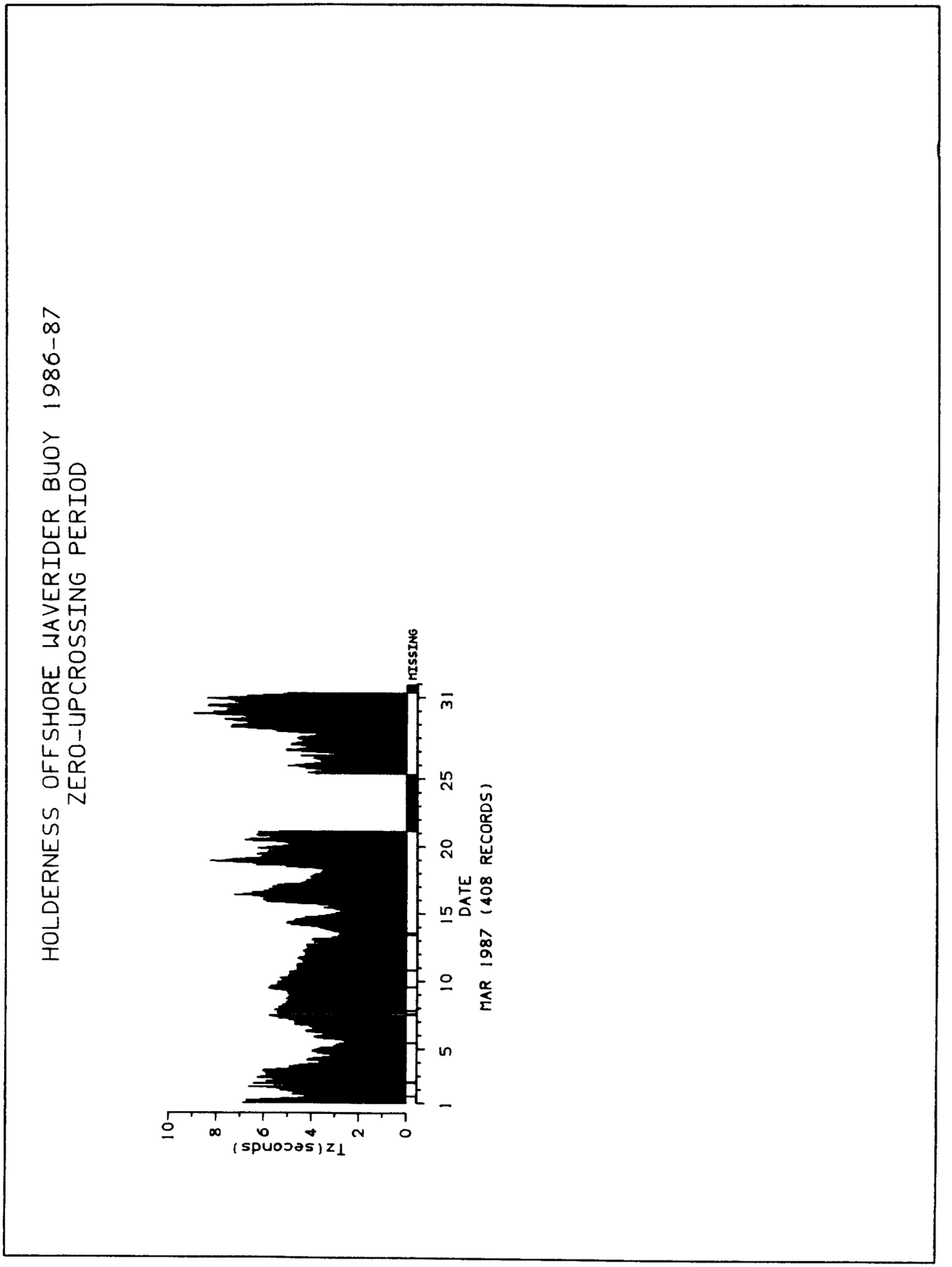
HOLDERNESS OFFSHORE WAVERIDER BUOY 1986-87
ZERO-UPCROSSING PERIOD
Tz(seconds)
0
2
4
6
8
10
1
5
10
15
20
25
31
DATE
MAR 1987 (408 RECORDS)
MISSING

Fig. 5d

HOLDERNESS NEARSHORE WAVERIDER BUOY 1986
Percentage Occurrence Histograms for Hs and Tz
SPRING

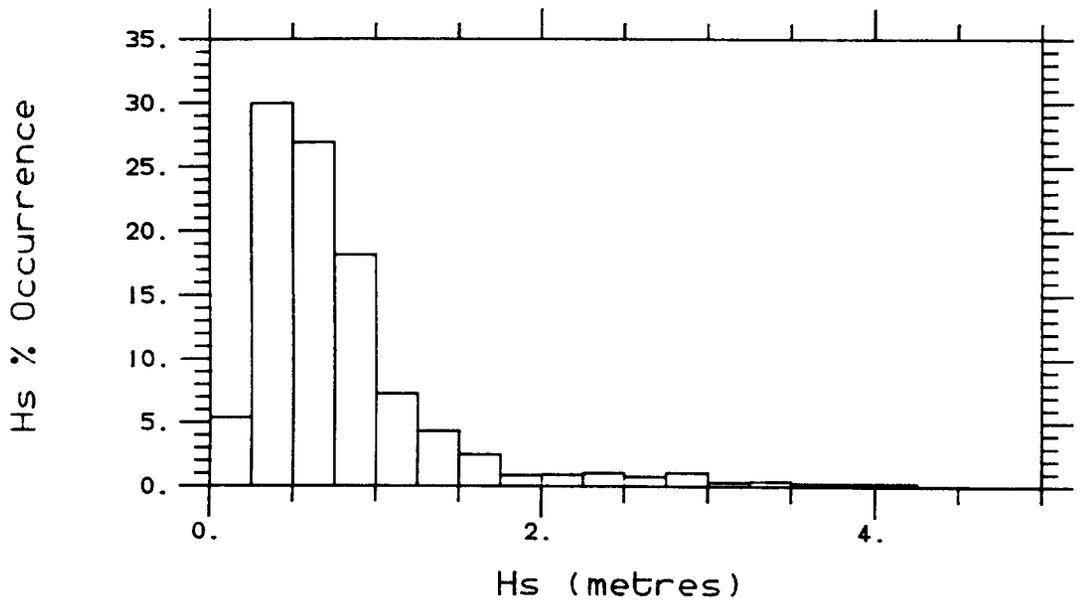

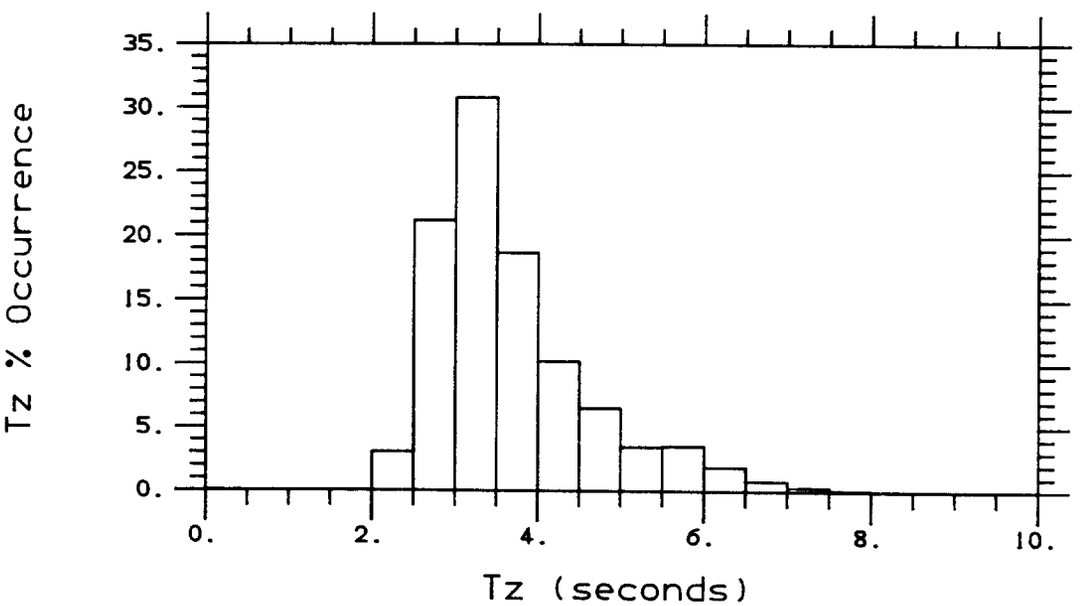

Fig. 6

HOLDERNESS OFFSHORE WAVERIDER BUOY 1986-87
Percentage Occurrence Histograms for Hs and Tz
ALL DATA

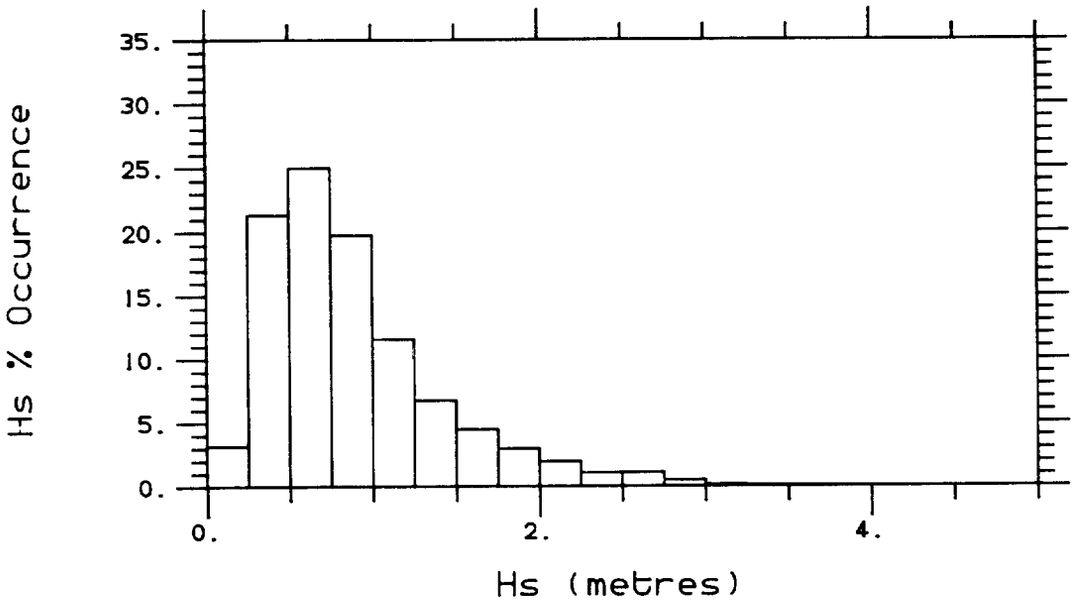

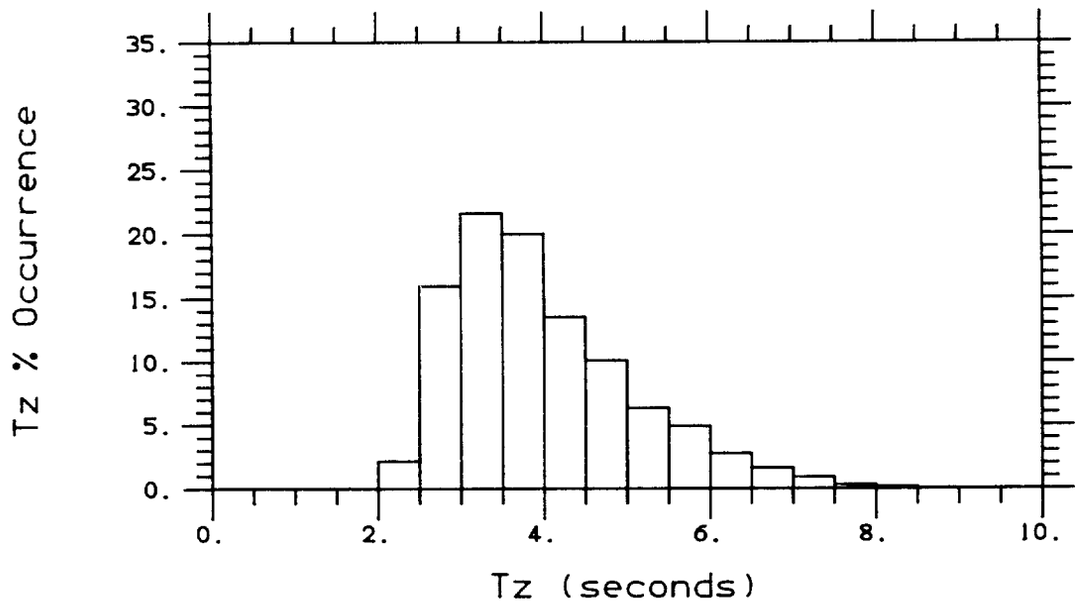

Fig. 7a

HOLDERNESS OFFSHORE WAVERIDER BUOY 1986-87
Percentage Occurrence Histograms for Hs and Tz
SPRING

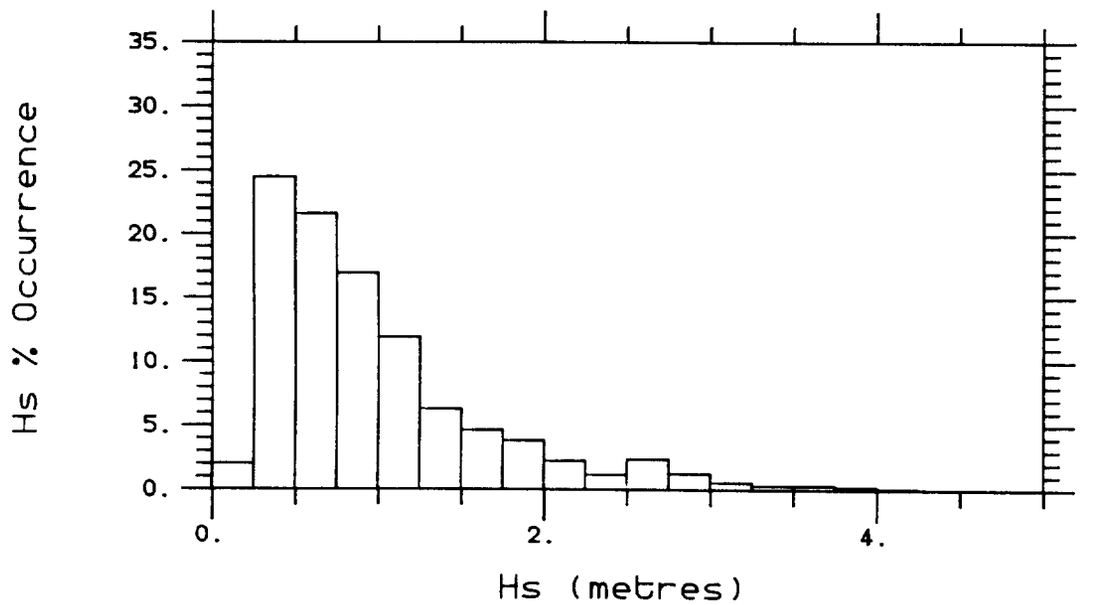

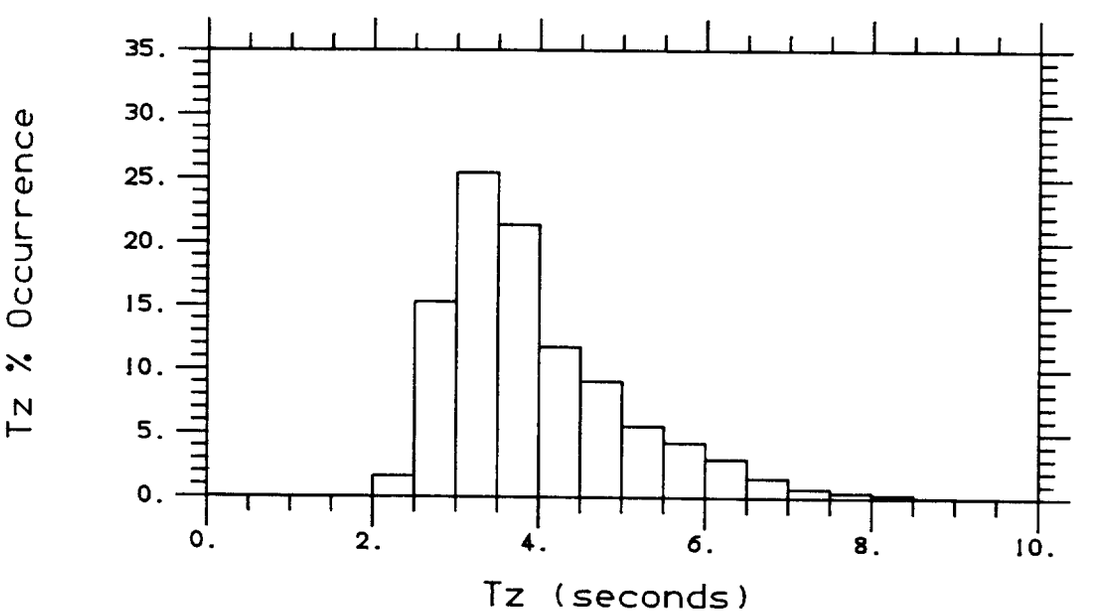

Fig. 7b

HOLDERNESS OFFSHORE WAVERIDER BUOY 1986-87
Percentage Occurrence Histograms for Hs and Tz
SUMMER

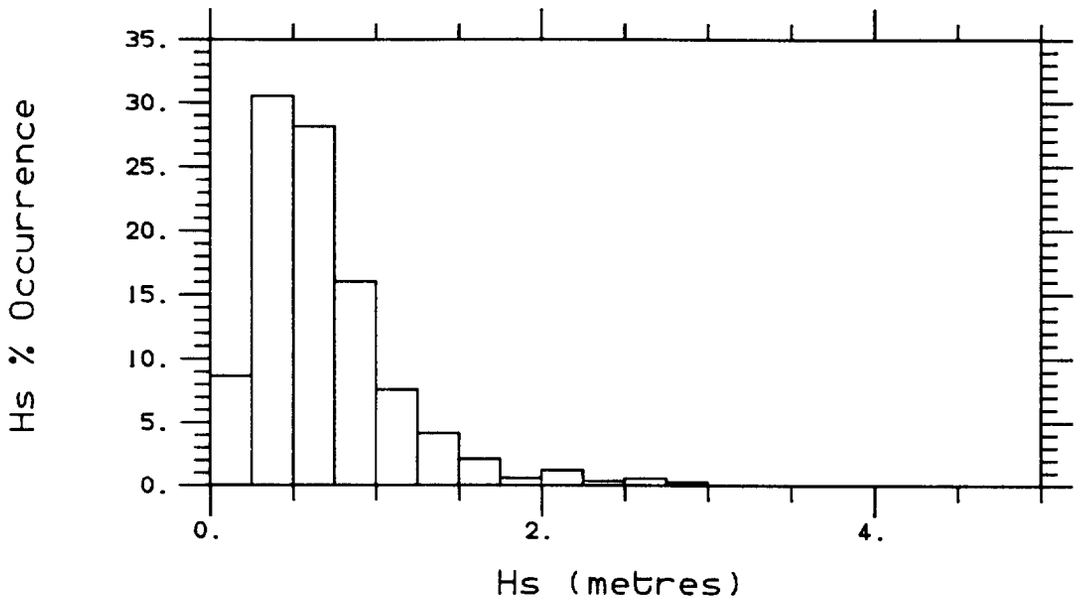

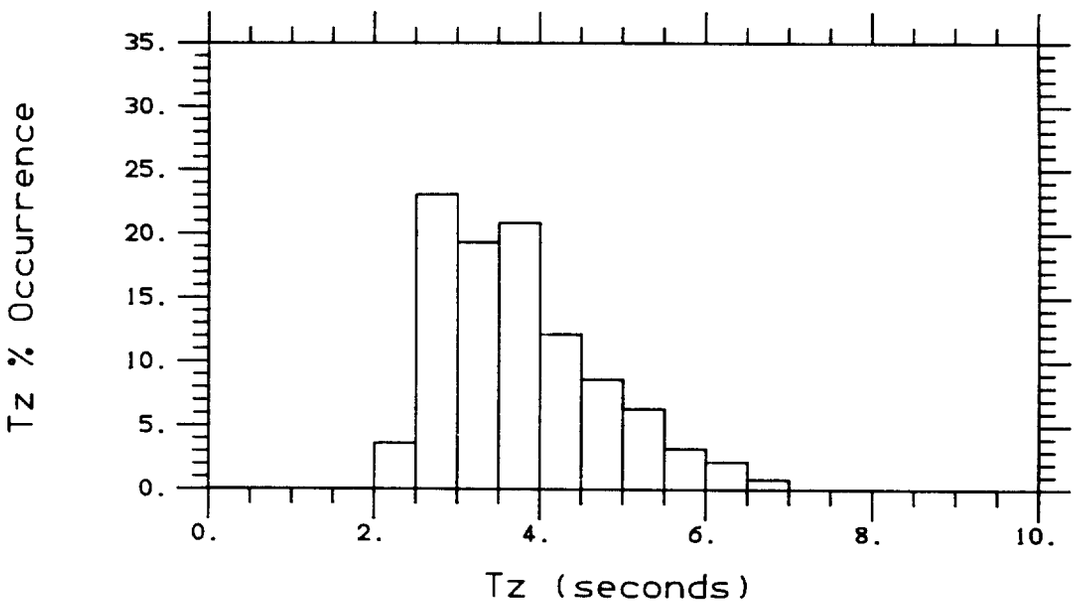

Fig. 7c

HOLDERNESS OFFSHORE WAVERIDER BUOY 1986-87
Percentage Occurrence Histograms for Hs and Tz
AUTUMN

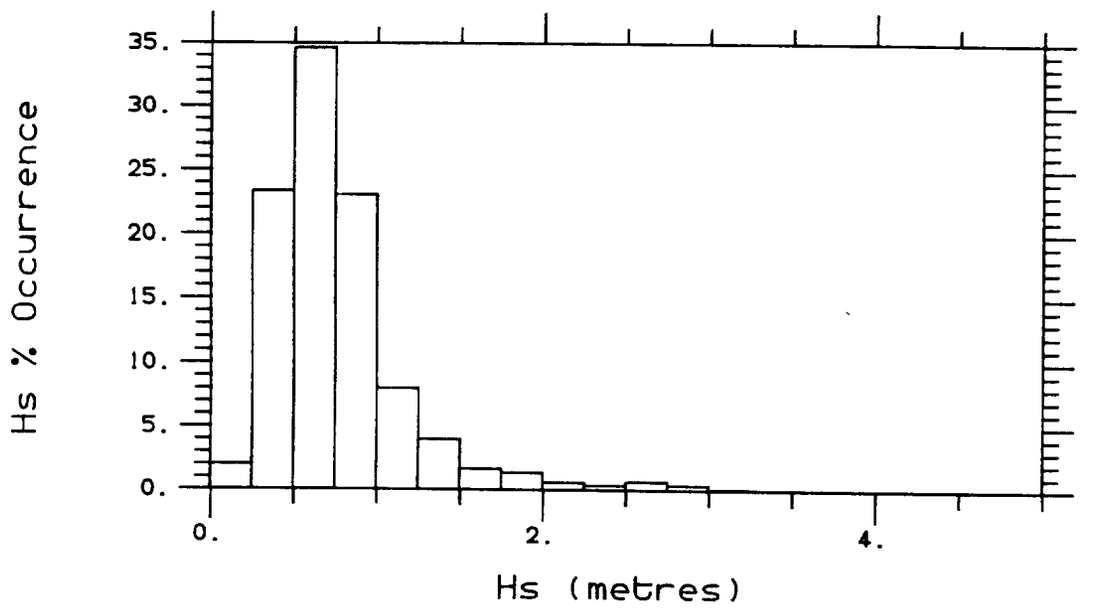

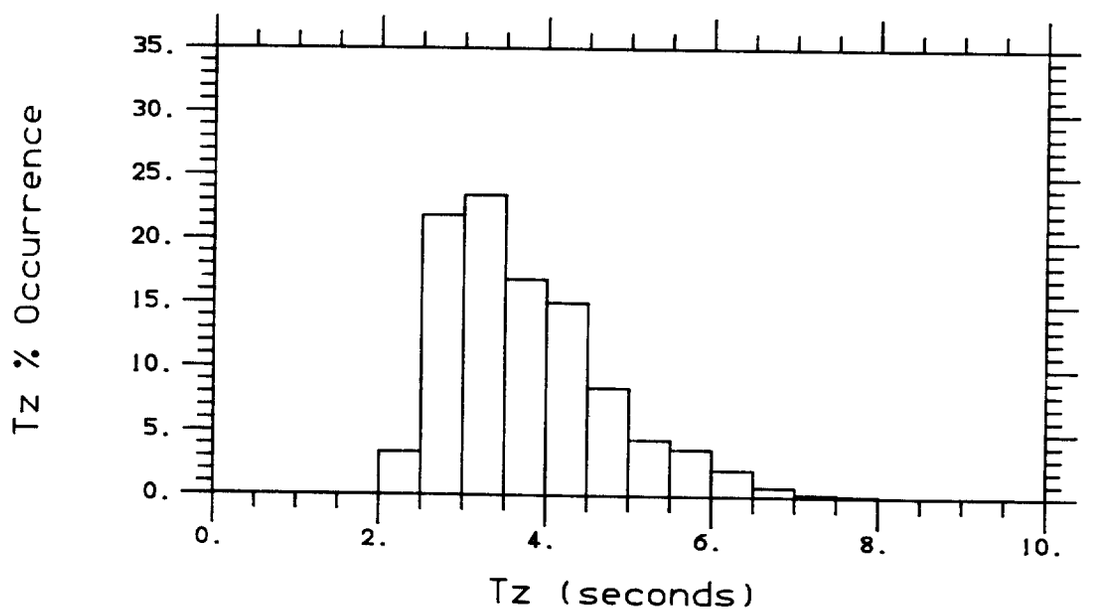

Fig. 7d

HOLDERNESS OFFSHORE WAVERIDER BUOY 1986-87
Percentage Occurrence Histograms for Hs and Tz
WINTER

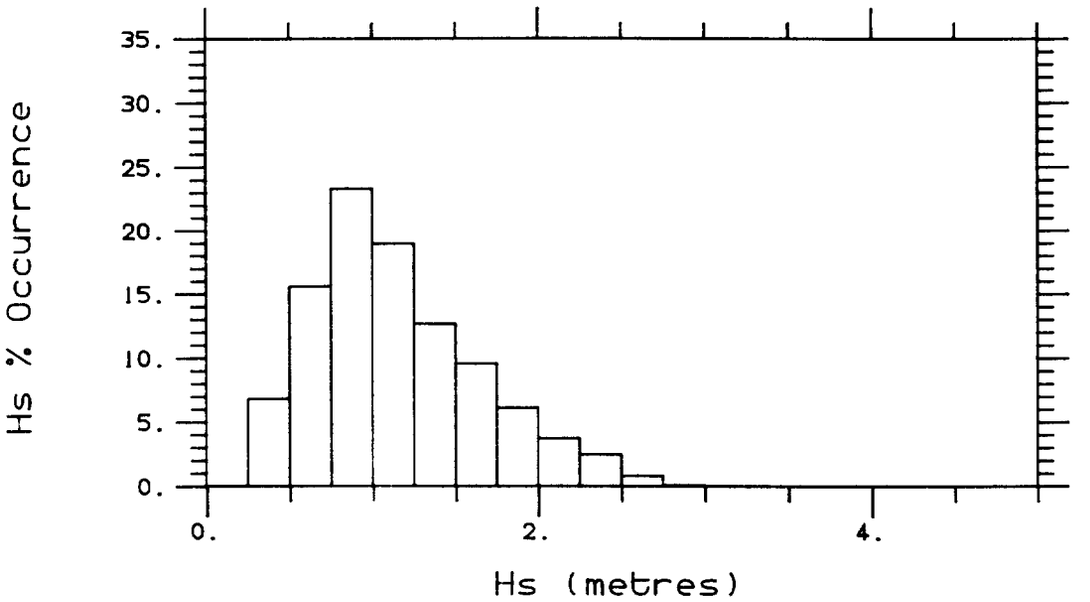

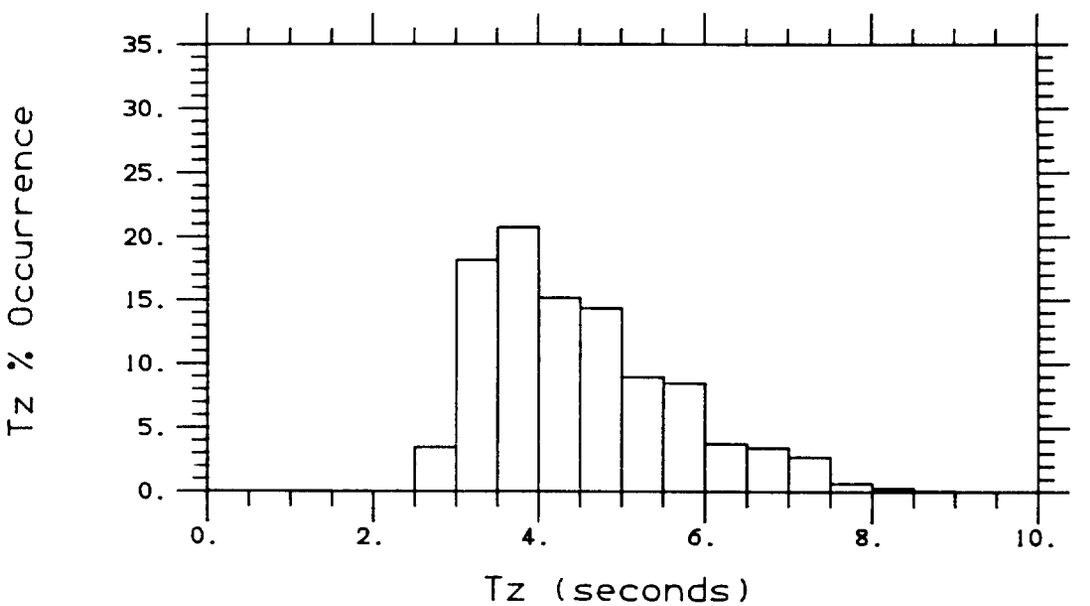

Fig. 7e

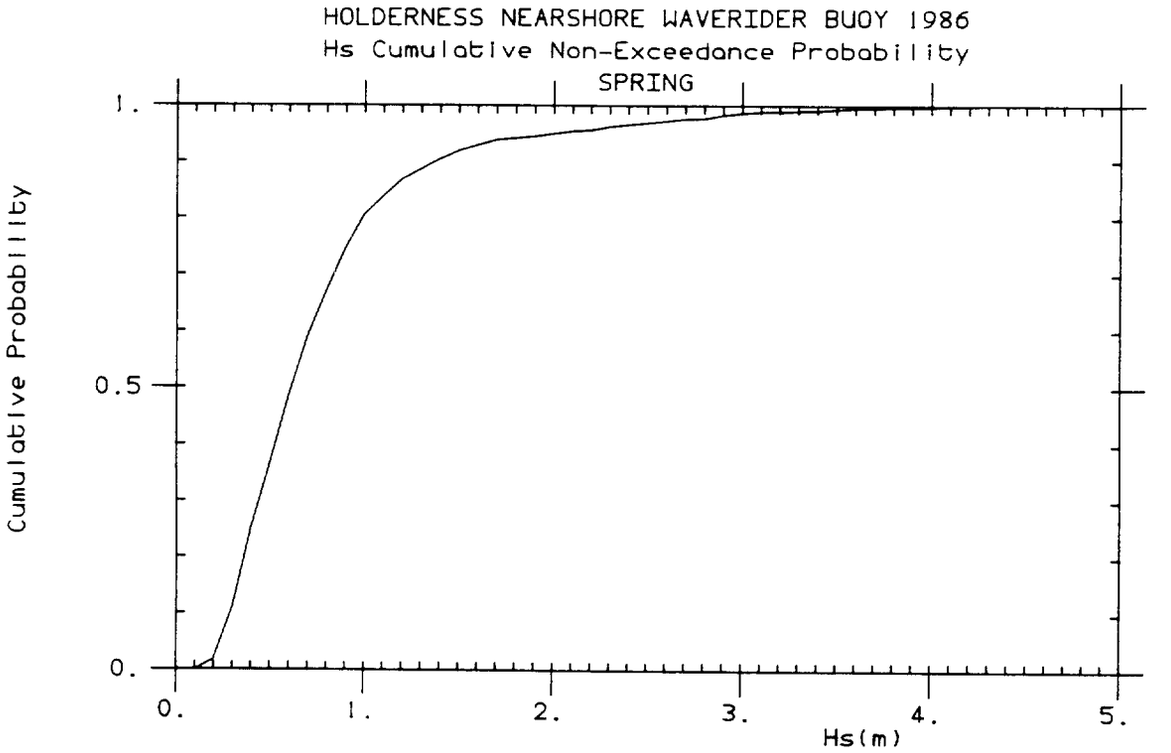
HOLDERNESS NEARSHORE WAVERIDER BUOY 1986
Hs Cumulative Non-Exceedance Probability
SPRING
Cumulative Probability
1.
0.5
0.
0.
1.
2.
3.
4.
5.
Hs(m)

Fig. 8

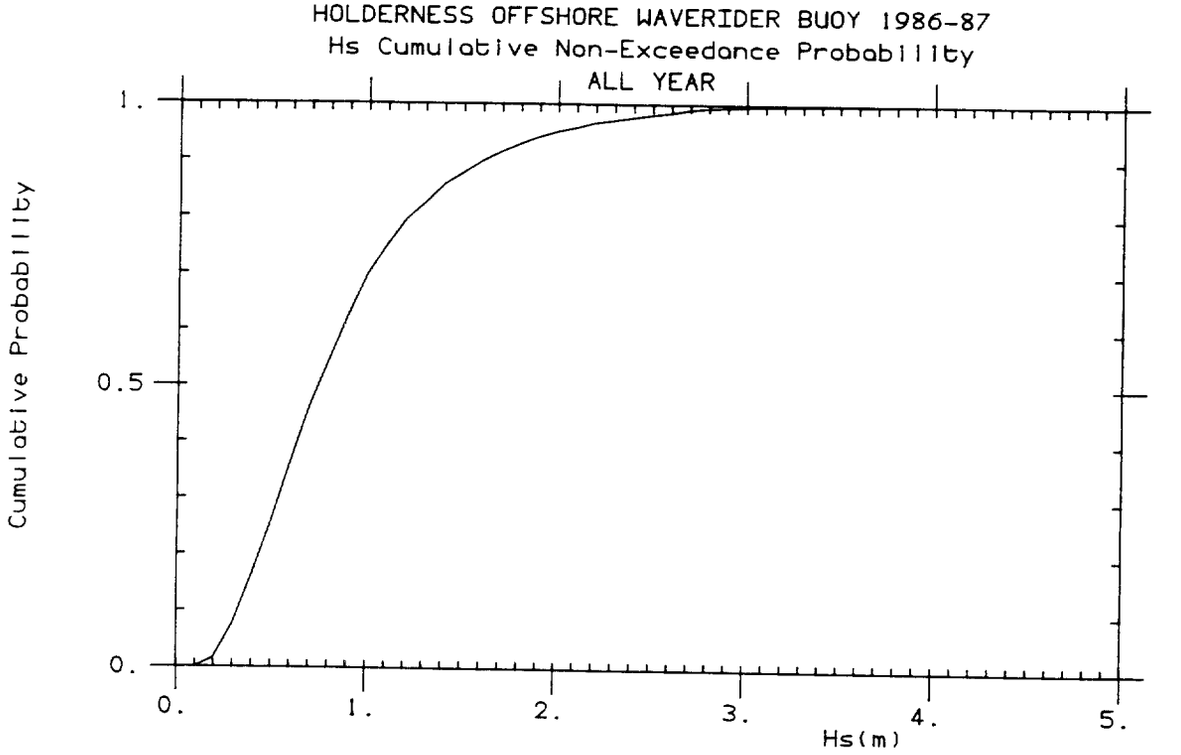
HOLDERNESS OFFSHORE WAVERIDER BUOY 1986-87
Hs Cumulative Non-Exceedance Probability
ALL YEAR
Cumulative Probability
1.
0.5
0.
0.
1.
2.
3.
4.
5.
Hs(m)

Fig. 9a

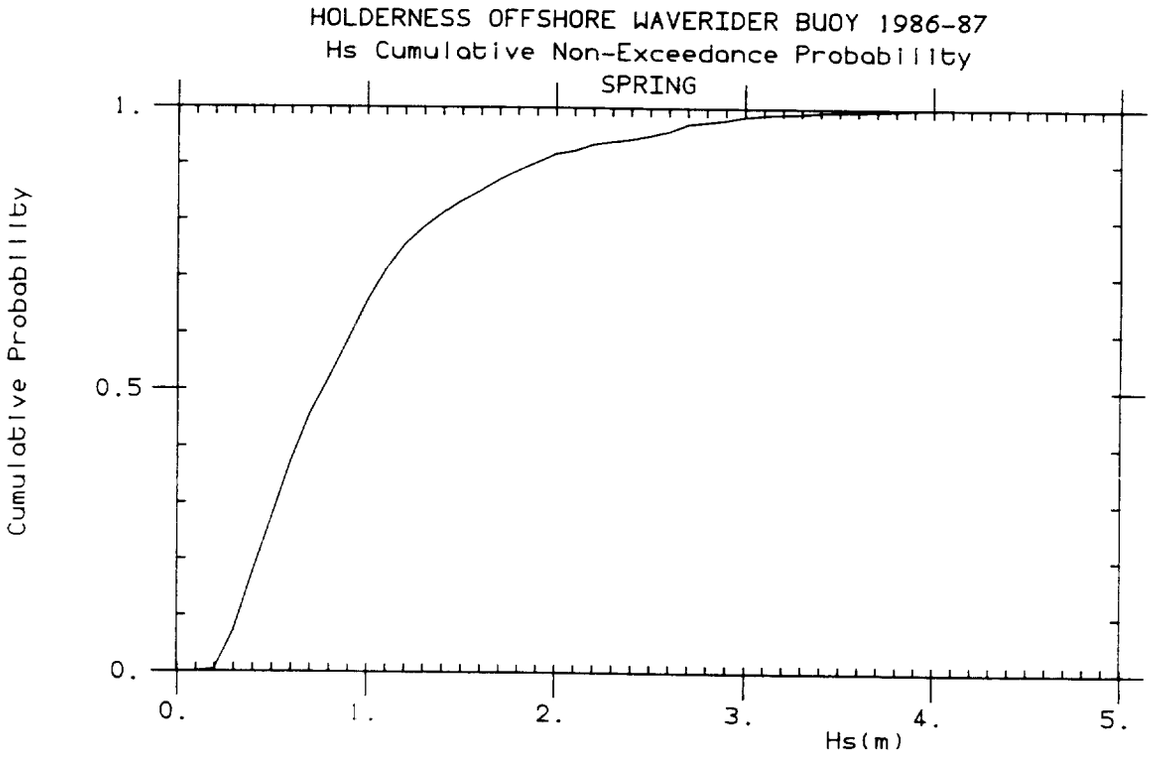
HOLDERNESS OFFSHORE WAVERIDER BUOY 1986-87
Hs Cumulative Non-Exceedance Probability
SPRING
Cumulative Probability
1.
0.5
0.
0.
1.
2.
3.
4.
5.
Hs(m)

Fig. 9b

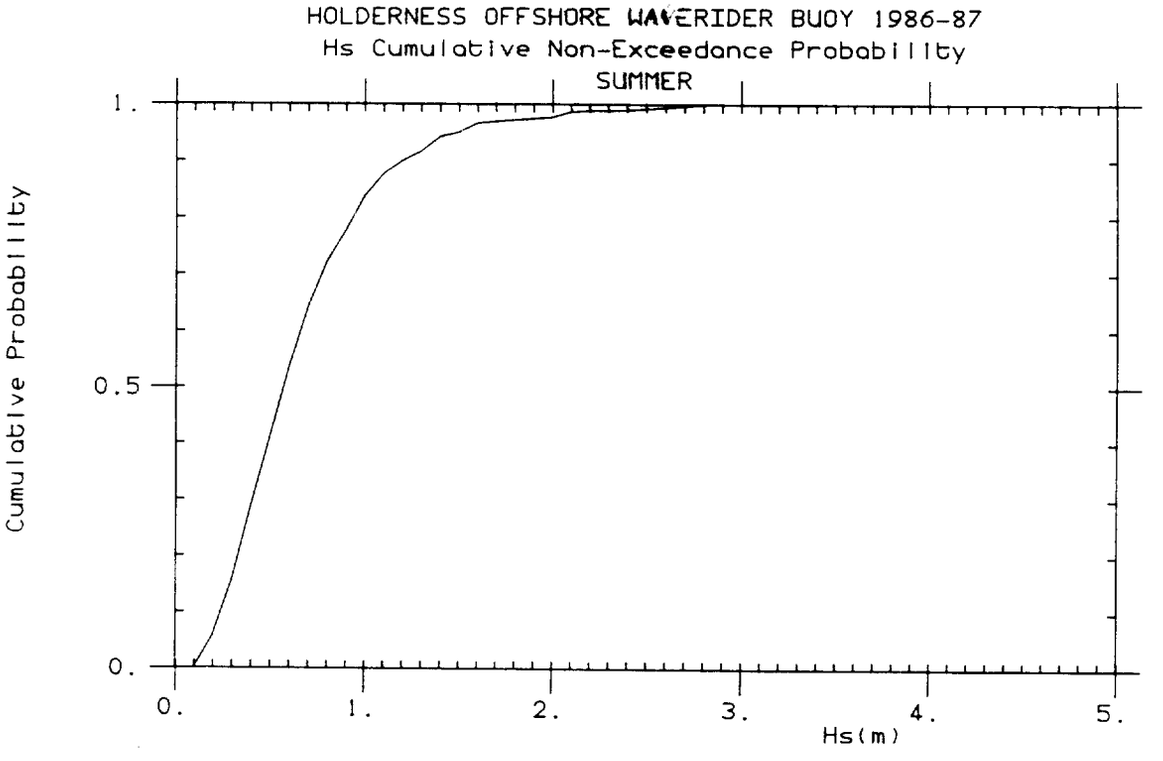
HOLDERNESS OFFSHORE WAVERIDER BUOY 1986-87
Hs Cumulative Non-Exceedance Probability
SUMMER
Cumulative Probability
1.
0.5
0.
0.
1.
2.
3.
4.
5.
Hs(m)

Fig. 9c

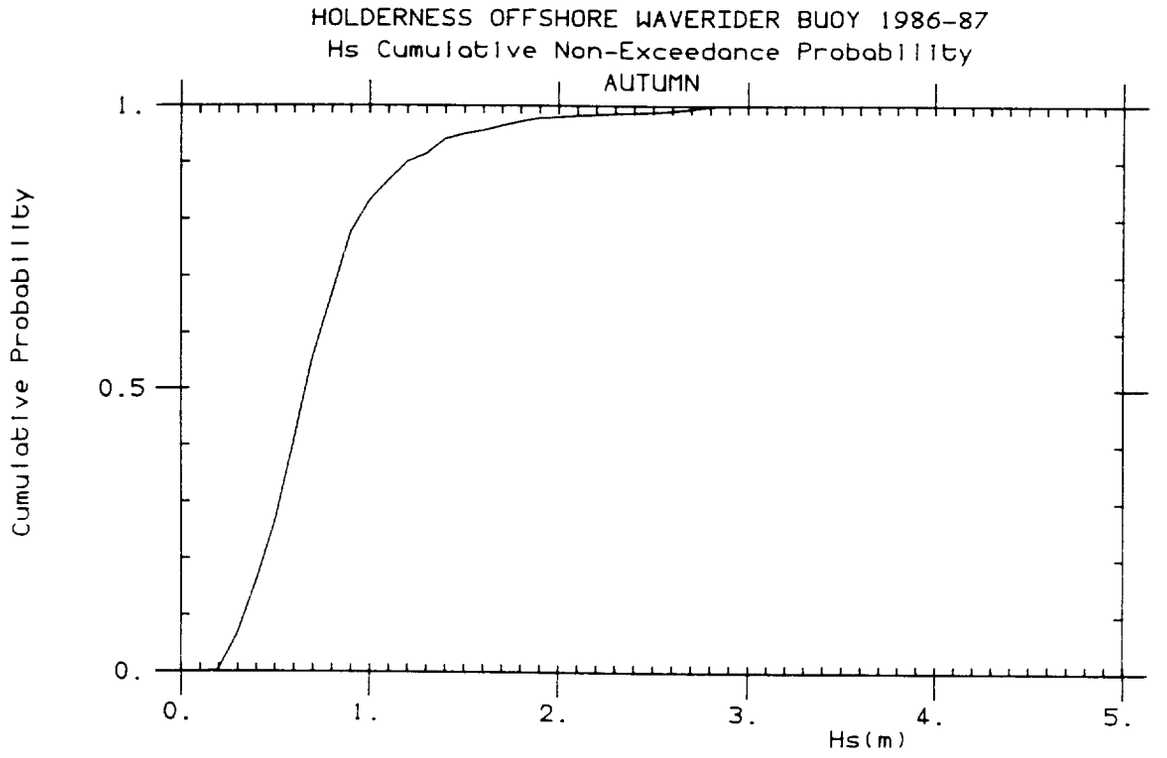
HOLDERNESS OFFSHORE WAVERIDER BUOY 1986-87
Hs Cumulative Non-Exceedance Probability
AUTUMN
Cumulative Probability
1.
0.5
0.
0.
1.
2.
3.
4.
5.
Hs(m)

Fig. 9d

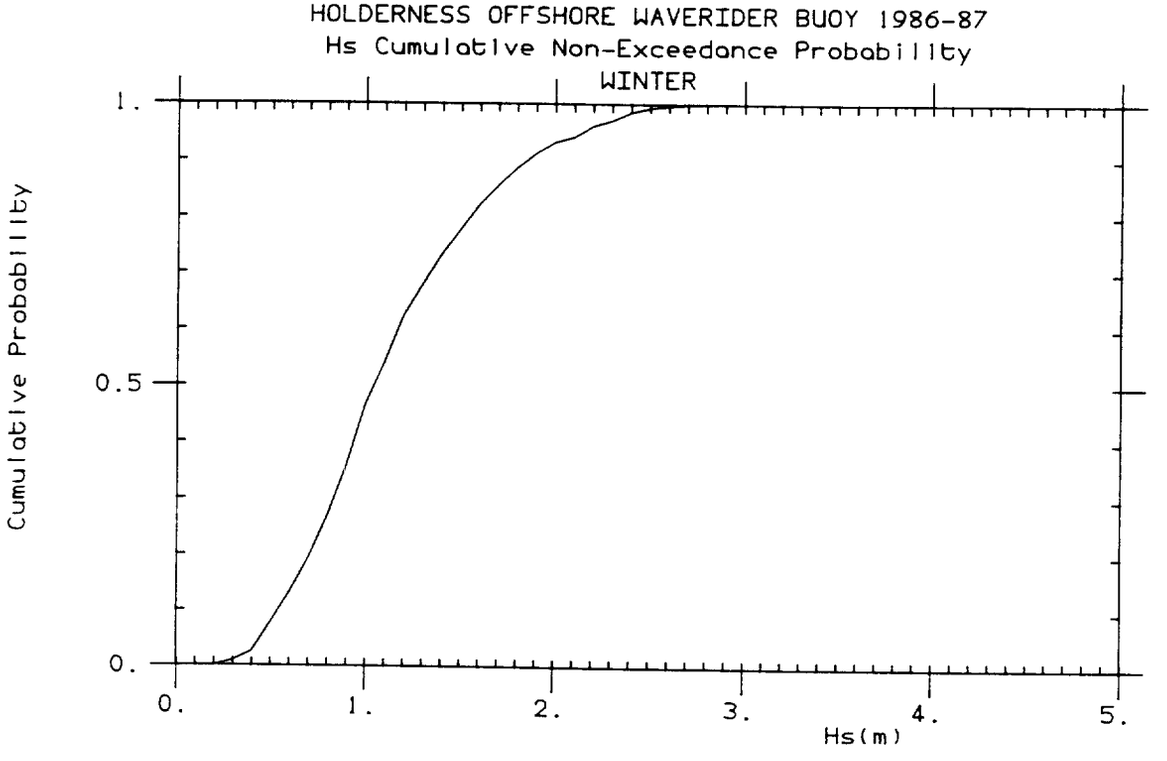
HOLDERNESS OFFSHORE WAVERIDER BUOY 1986-87
Hs Cumulative Non-Exceedance Probability
WINTER
Cumulative Probability
1.
0.5
0.
0.
1.
2.
3.
4.
5.
Hs(m)

Fig. 9e

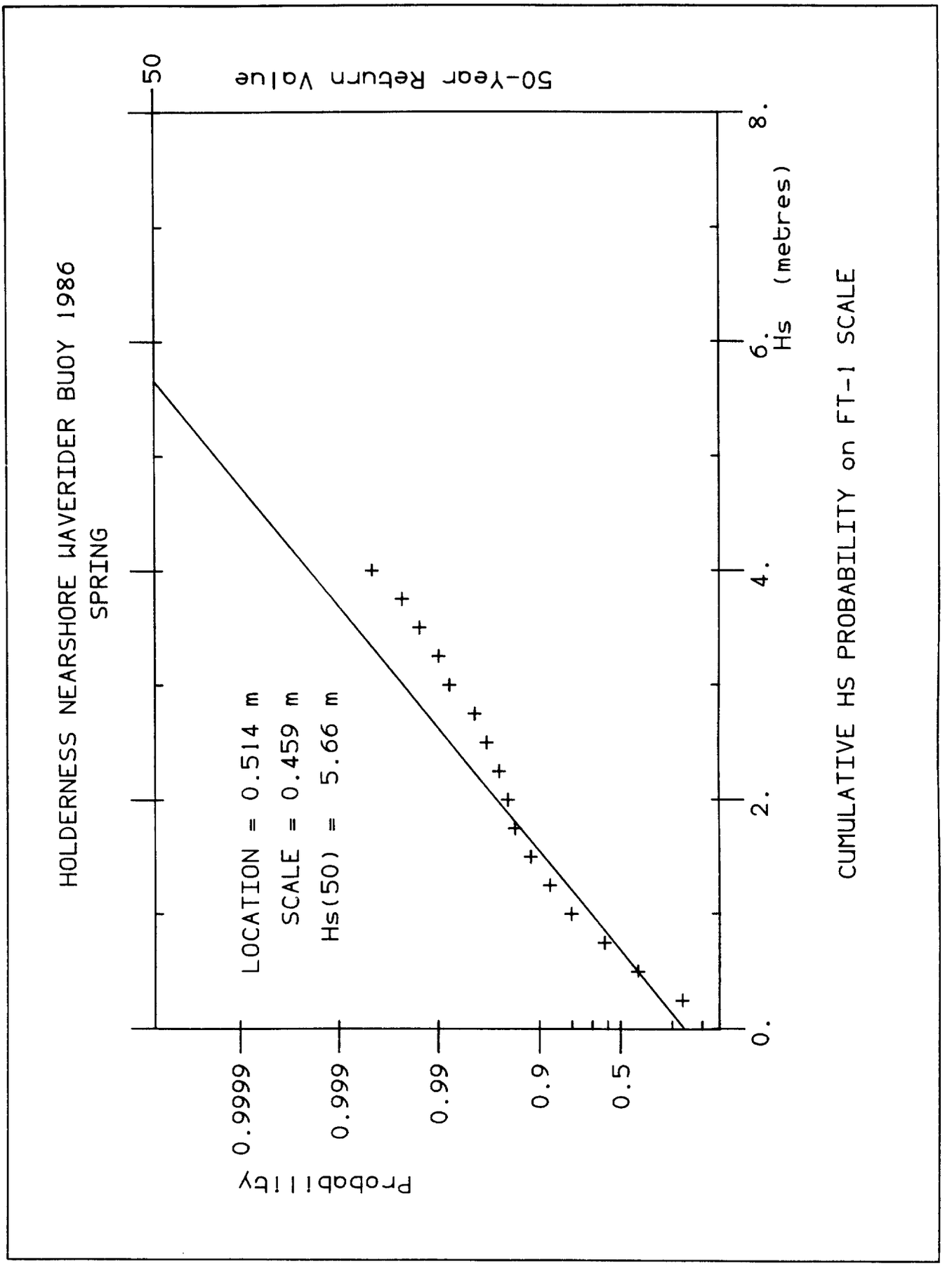
HOLDERNESS NEARSHORE WAVERIDER BUOY 1986
SPRING
CUMULATIVE HS PROBABILITY on FT-1 SCALE
LOCATION = 0.514 m
SCALE = 0.459 m
Hs(50) = 5.66 m
50-Year Return Value
50
Probability
0.9999
0.999
0.99
0.9
0.5
0.
2.
4.
6.
8.
Hs (metres)

Fig. 10

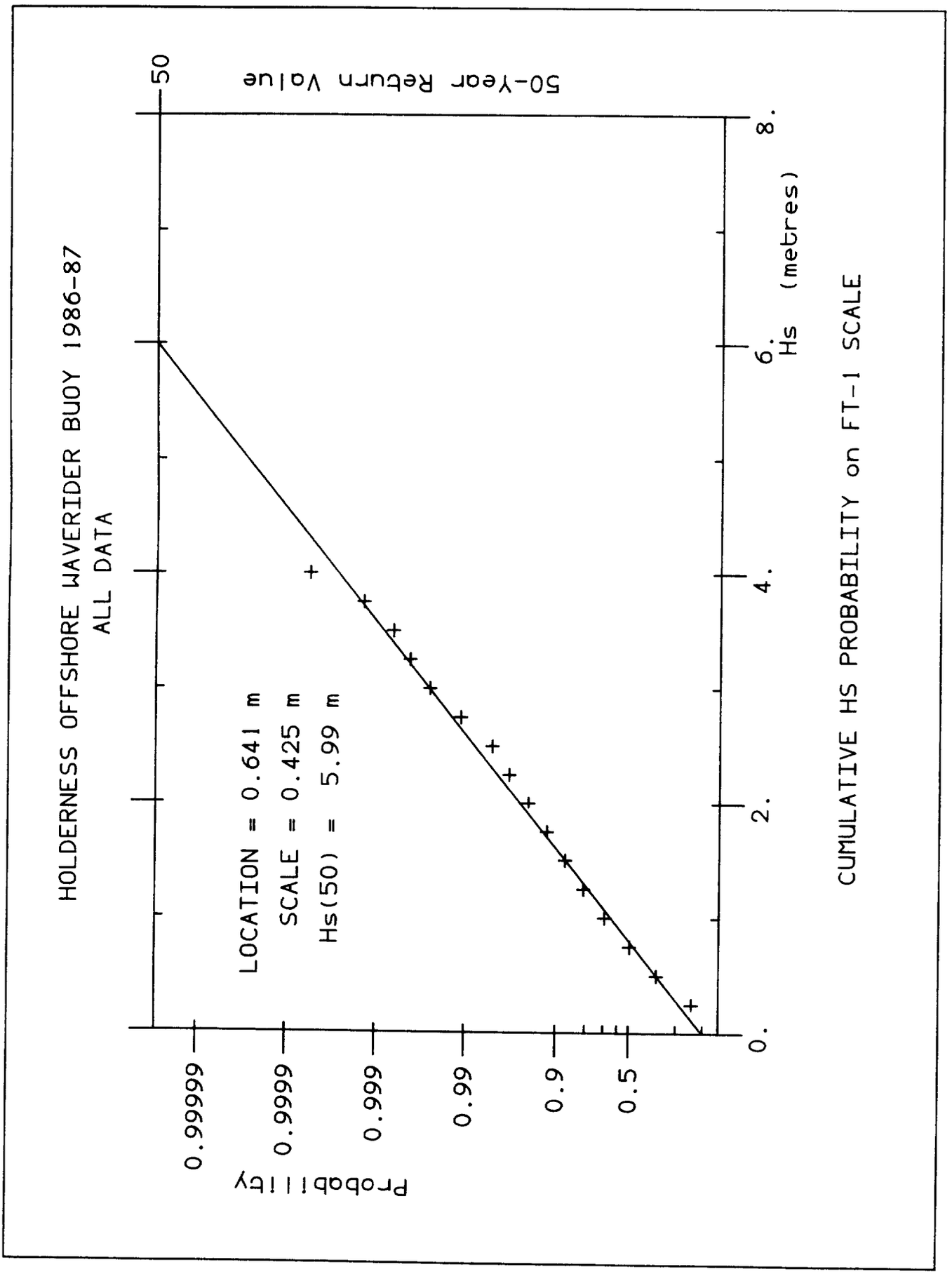
HOLDERNESS OFFSHORE WAVERIDER BUOY 1986-87
ALL DATA
LOCATION = 0.641 m
SCALE = 0.425 m
Hs(50) = 5.99 m
50-Year Return Value
50
Probability
0.99999
0.9999
0.999
0.99
0.9
0.5
0.
2.
4.
6.
8.
Hs (metres)
CUMULATIVE HS PROBABILITY on FT-1 SCALE

Fig. 11

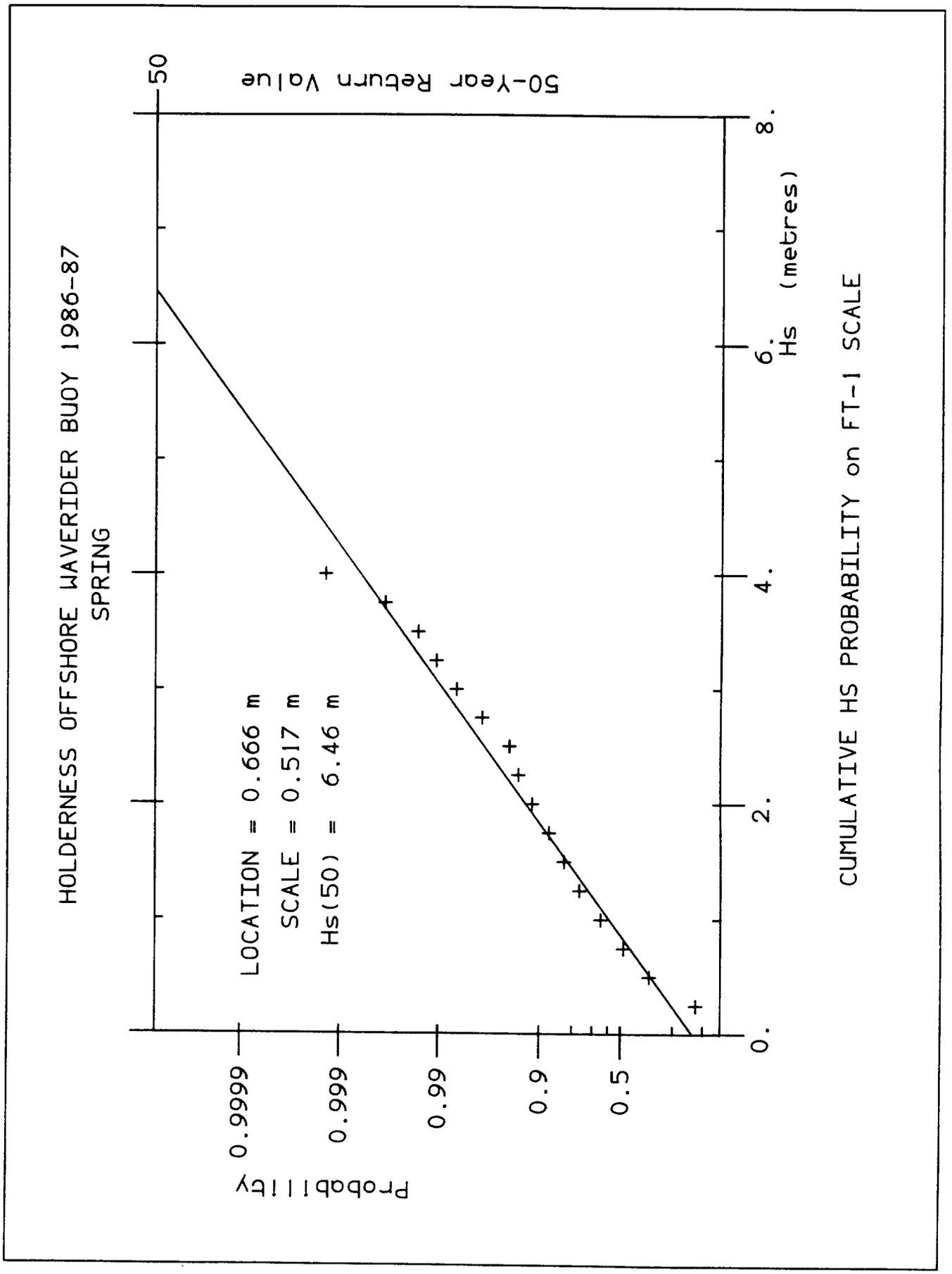
HOLDERNESS OFFSHORE WAVERIDER BUOY 1986-87
SPRING
LOCATION = 0.666 m
SCALE = 0.517 m
Hs(50) = 6.46 m
50-Year Reburn Value
50
Probability
0.9999
0.999
0.99
0.9
0.5
0.
2.
4.
6.
8.
Hs (metres)
CUMULATIVE HS PROBABILITY on FT-1 SCALE

Fig. 12

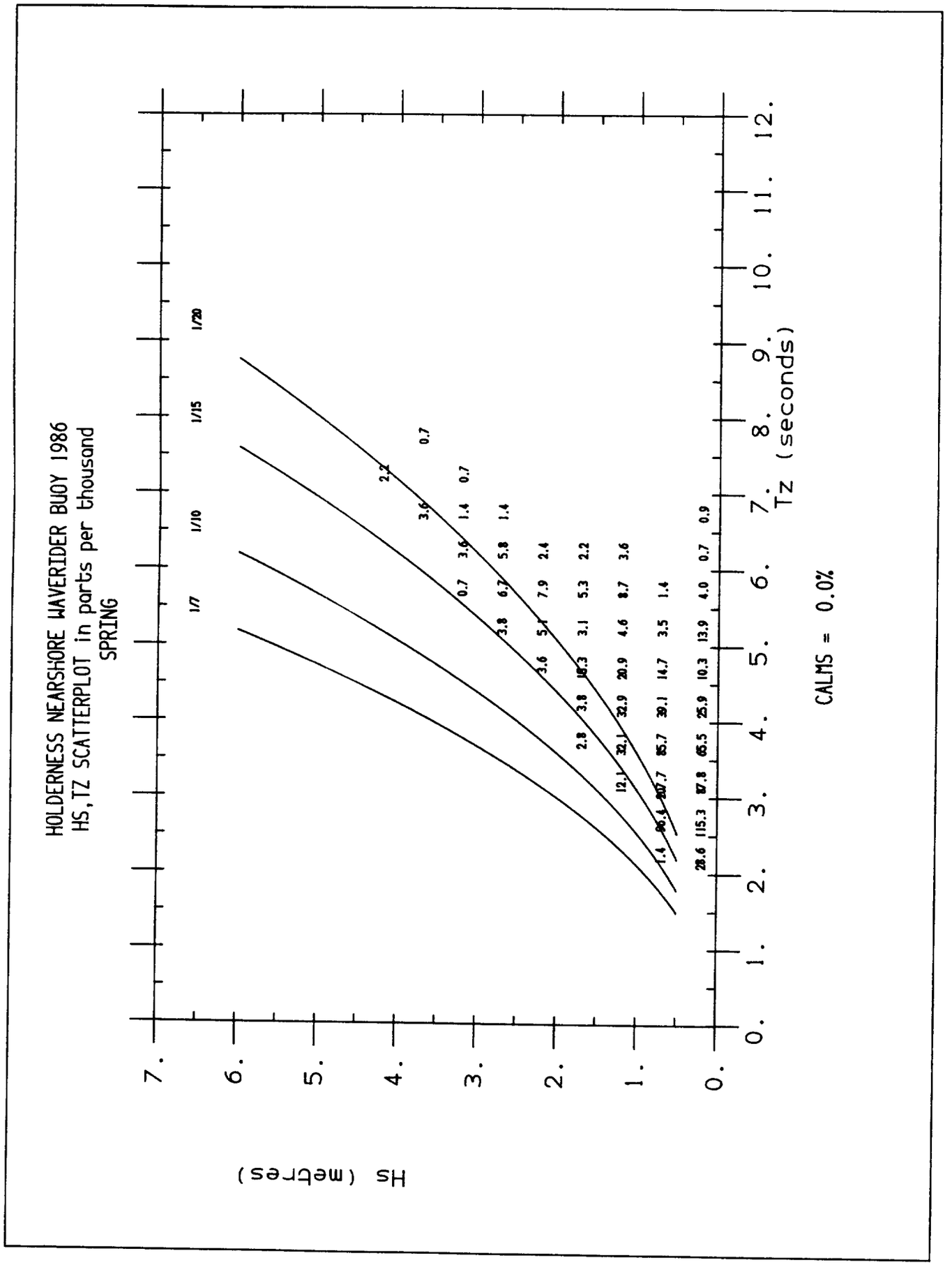
HOLDERNESS NEARSHORE WAVERIDER BUOY 1986
HS,TZ SCATTERPLOT in parts per thousand
SPRING
1/7
1/10
1/15
1/20
Hs (metres)
Tz (seconds)
0. 1. 2. 3. 4. 5. 6. 7. 8. 9. 10. 11. 12.
0. 1. 2. 3. 4. 5. 6. 7.
CALMS = 0.0%

Fig. 13

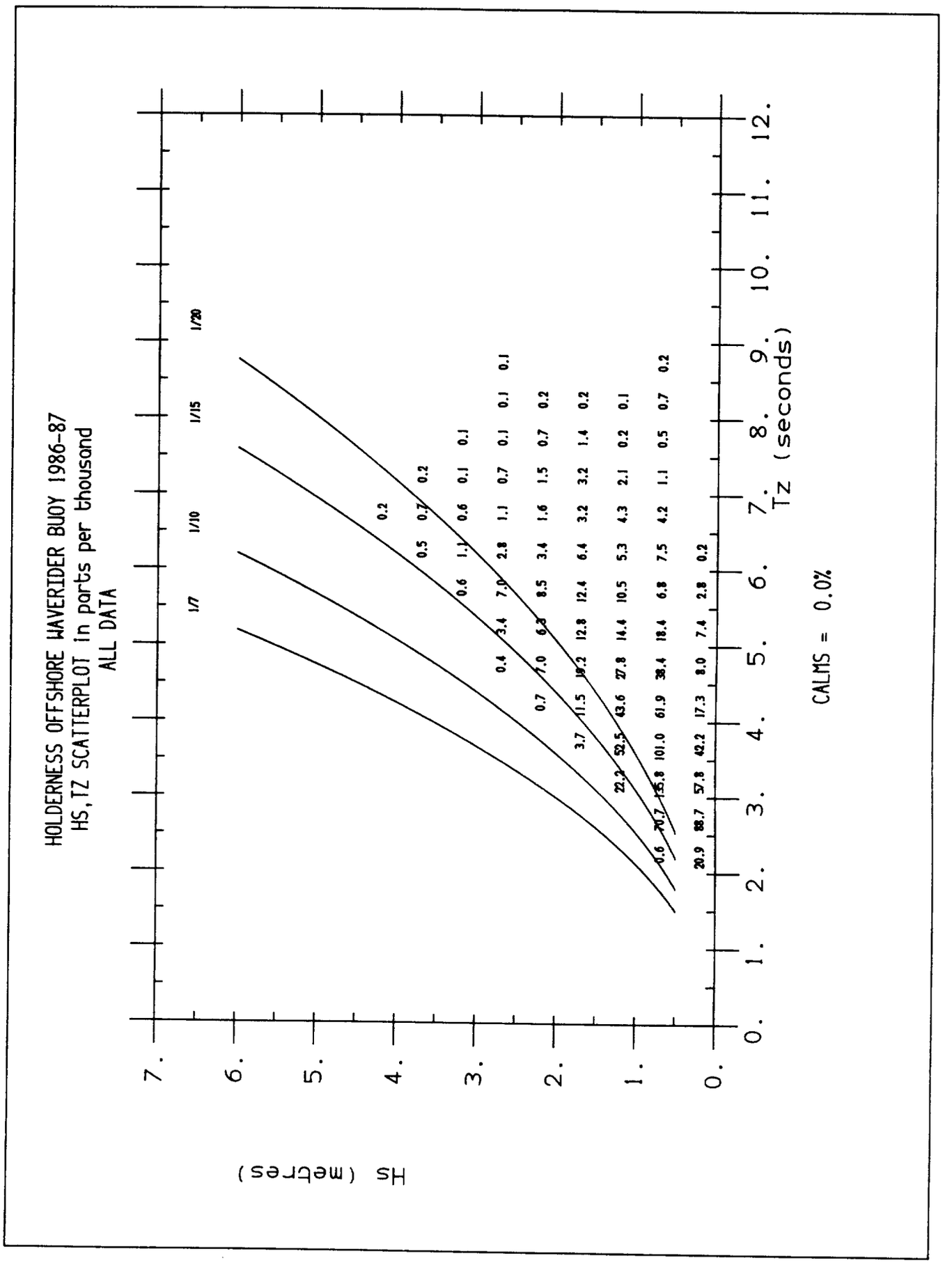
HOLDERNESS OFFSHORE WAVERIDER BUOY 1986-87
HS,TZ SCATTERPLOT in parts per thousand
ALL DATA
Hs (metres)
Tz (seconds)
CALMS = 0.0%
1/7
1/10
1/15
1/20

Fig. 14a

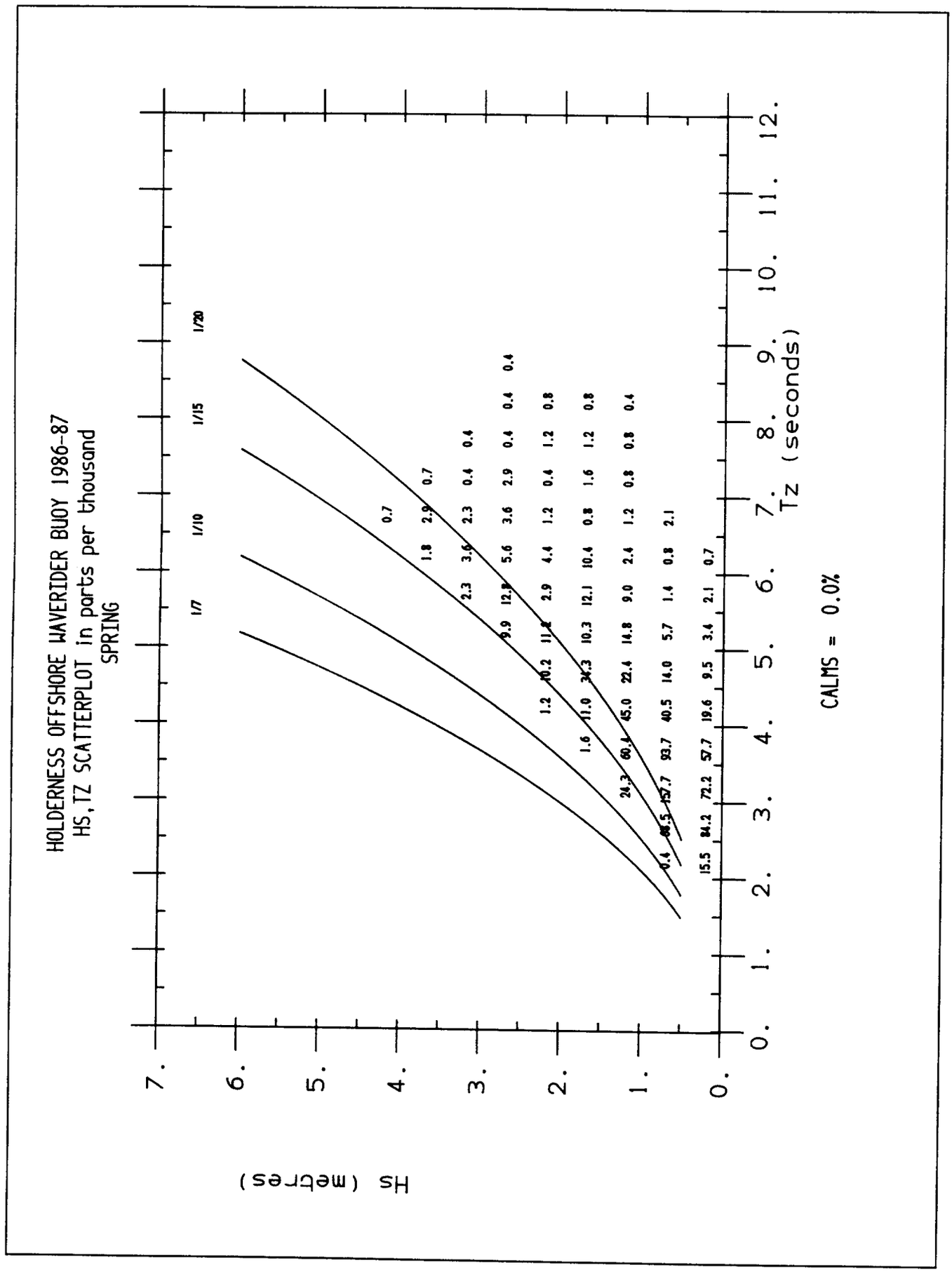
HOLDERNESS OFFSHORE WAVERIDER BUOY 1986-87
HS,TZ SCATTERPLOT in parts per thousand
SPRING
1/7
1/10
1/15
1/20
Hs (metres)
Tz (seconds)
CALMS = 0.0%

Fig. 14b

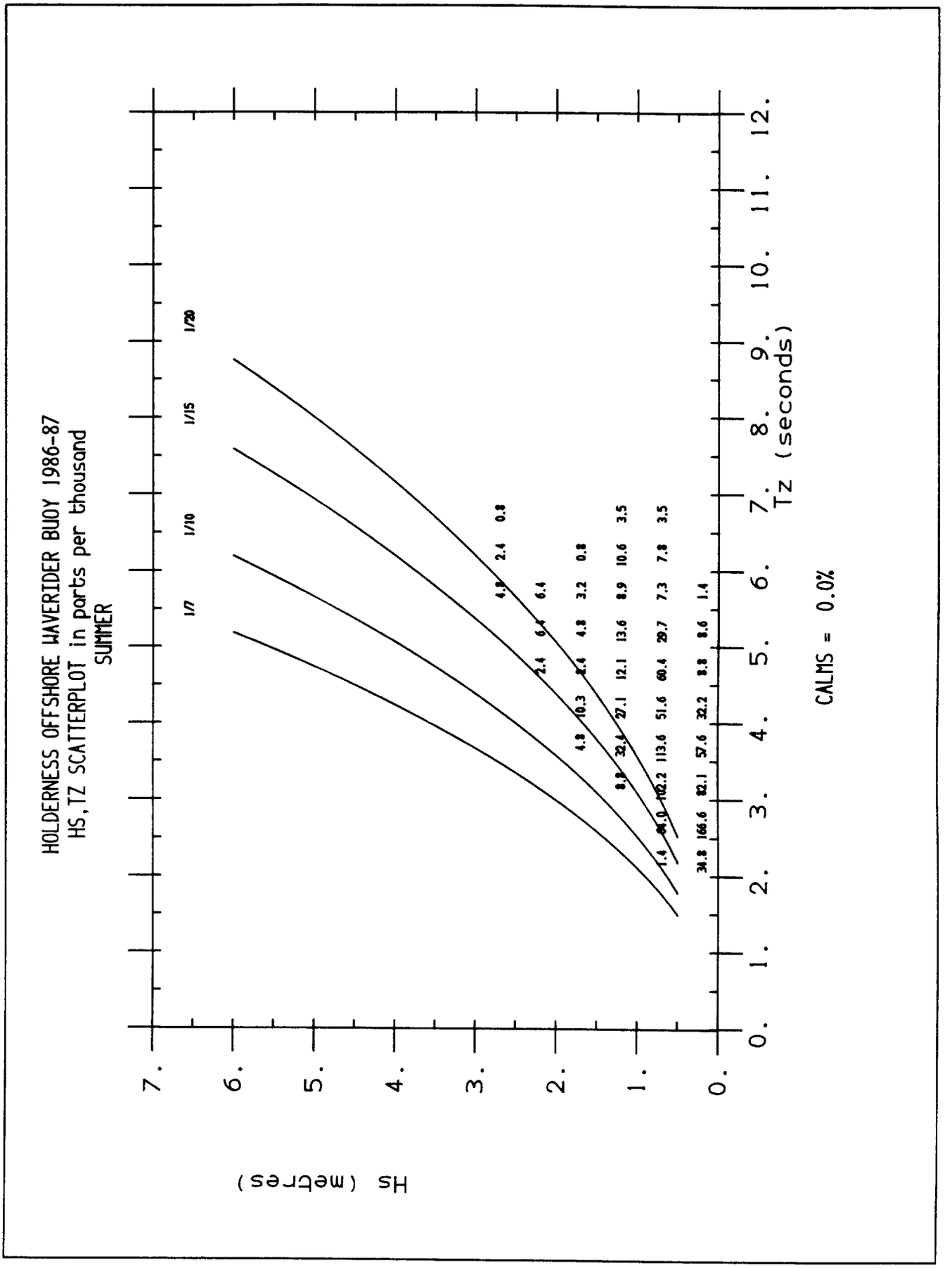
HOLDERNESS OFFSHORE WAVERIDER BUOY 1986-87
HS,TZ SCATTERPLOT in parts per thousand
SUMMER
1/7
1/10
1/15
1/20
Hs (metres)
Tz (seconds)
CALMS = 0.0%

Fig. 14c

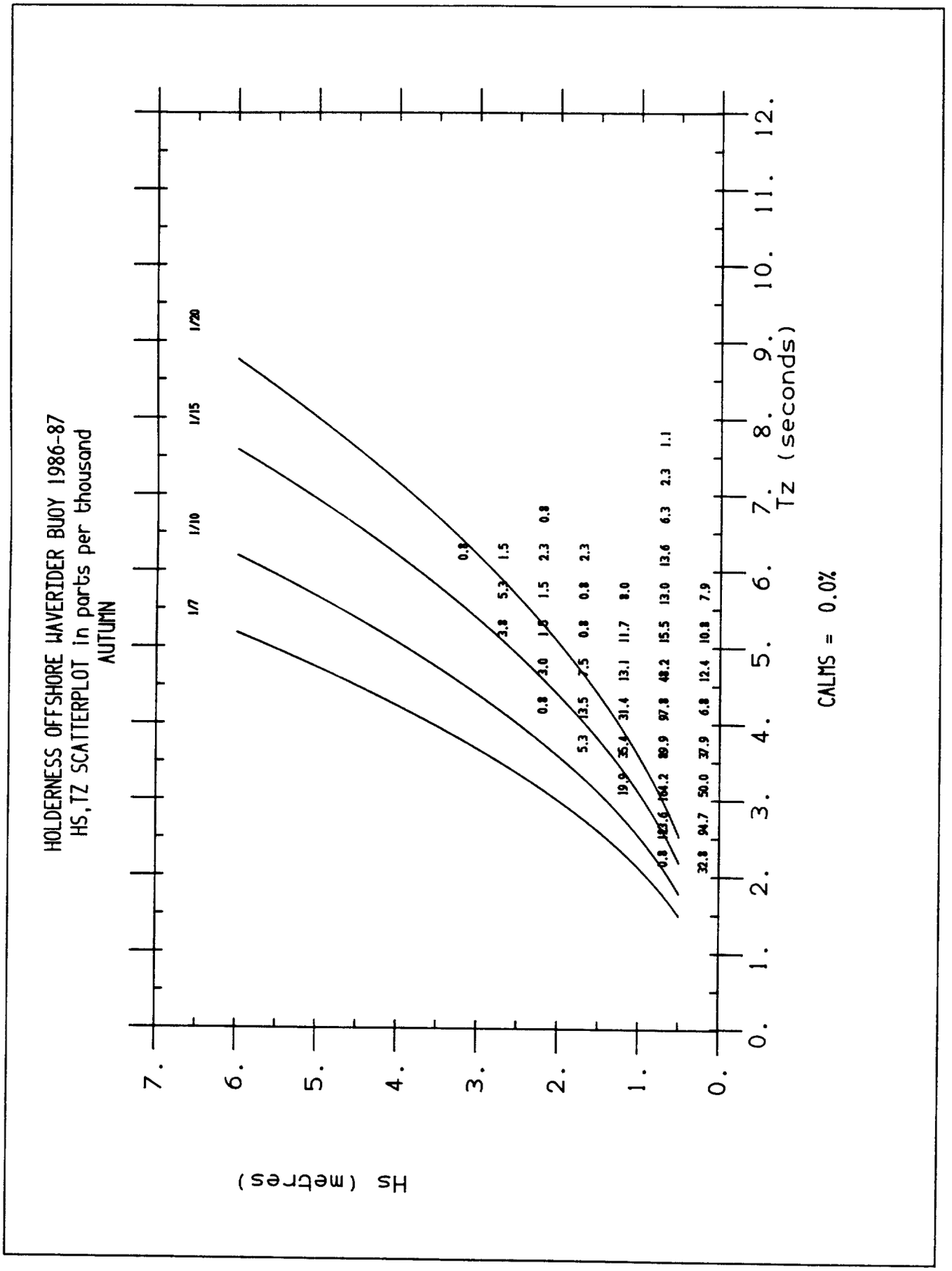
HOLDERNESS OFFSHORE WAVERIDER BUOY 1986-87
HS,TZ SCATTERPLOT in parts per thousand
AUTUMN
1/7
1/10
1/15
1/20
Hs (metres)
Tz (seconds)
0. 1. 2. 3. 4. 5. 6. 7. 8. 9. 10. 11. 12.
0. 1. 2. 3. 4. 5. 6. 7.
CALMS = 0.0%

Fig. 14d

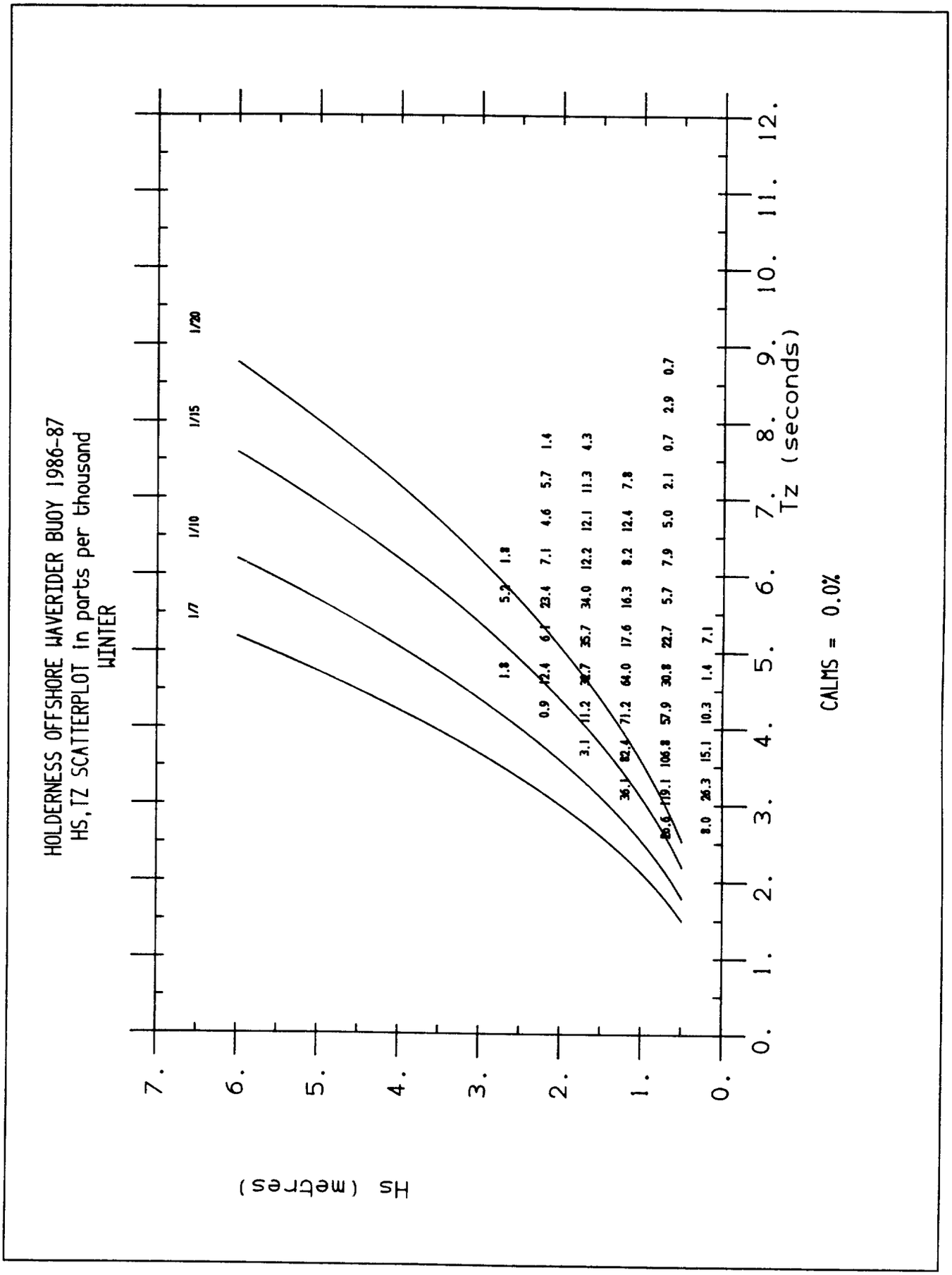
HOLDERNESS OFFSHORE WAVERIDER BUOY 1986-87
HS,TZ SCATTERPLOT in parts per thousand
WINTER
1/7
1/10
1/15
1/20
Hs (metres)
Tz (seconds)
0. 1. 2. 3. 4. 5. 6. 7. 8. 9. 10. 11. 12.
7. 6. 5. 4. 3. 2. 1. 0.
CALMS = 0.0%

Fig. 14e

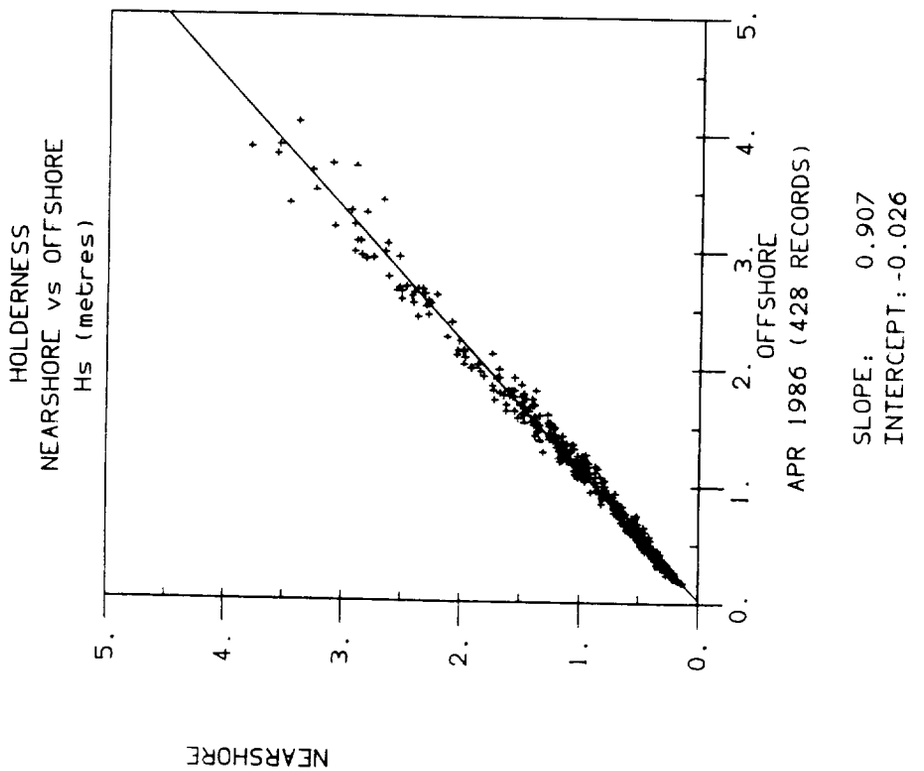

Fig. 15a

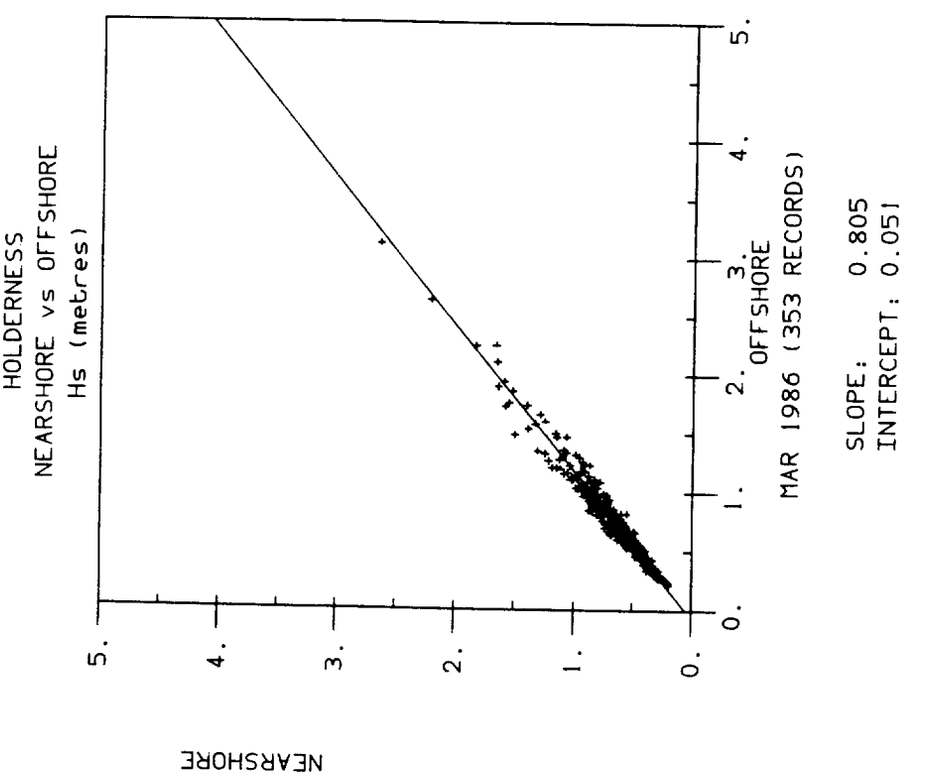

Fig. 15b

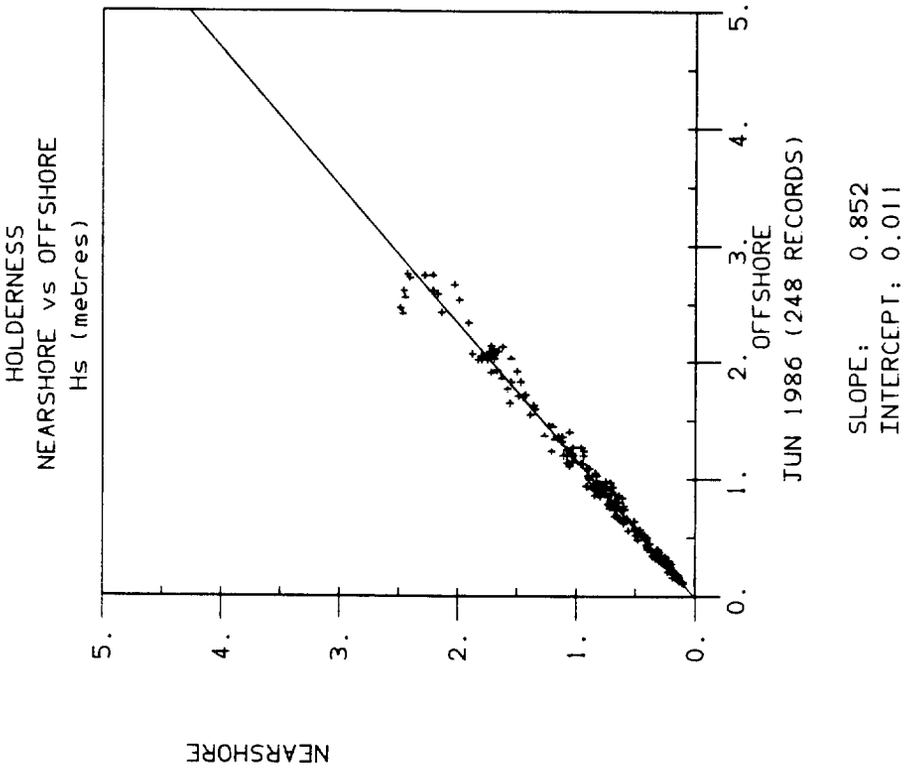

Fig. 15c

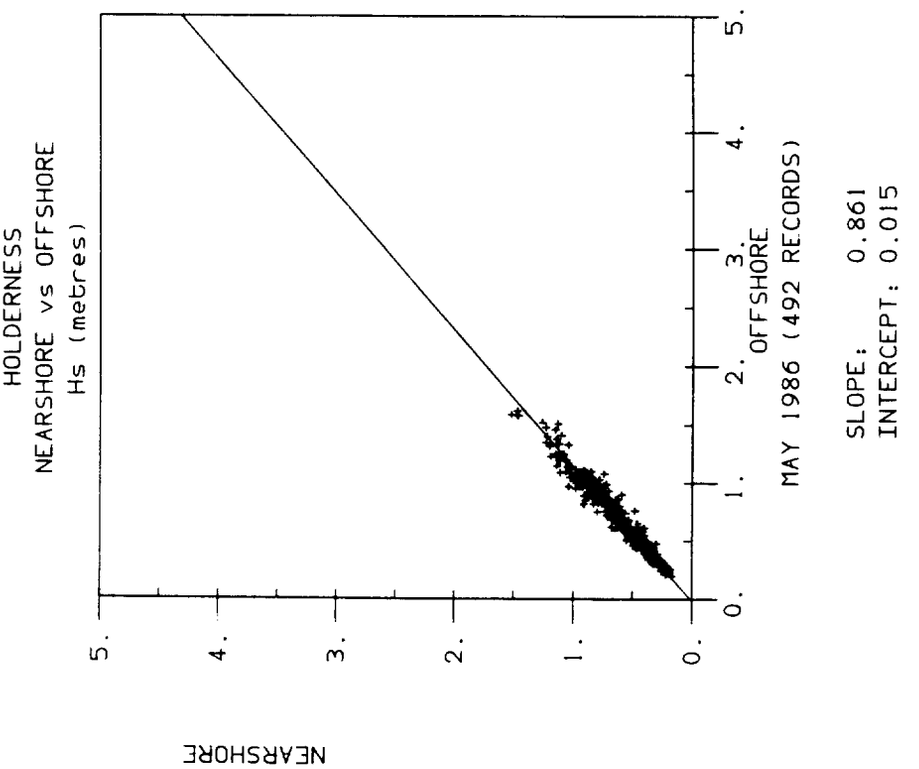

Fig. 15d

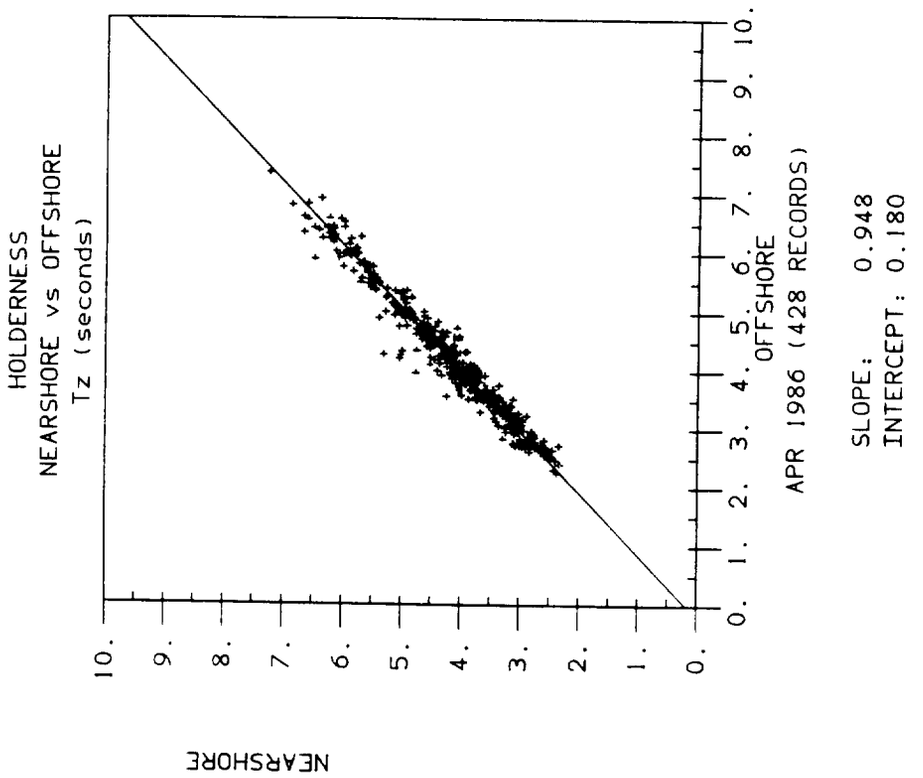

Fig. 16a

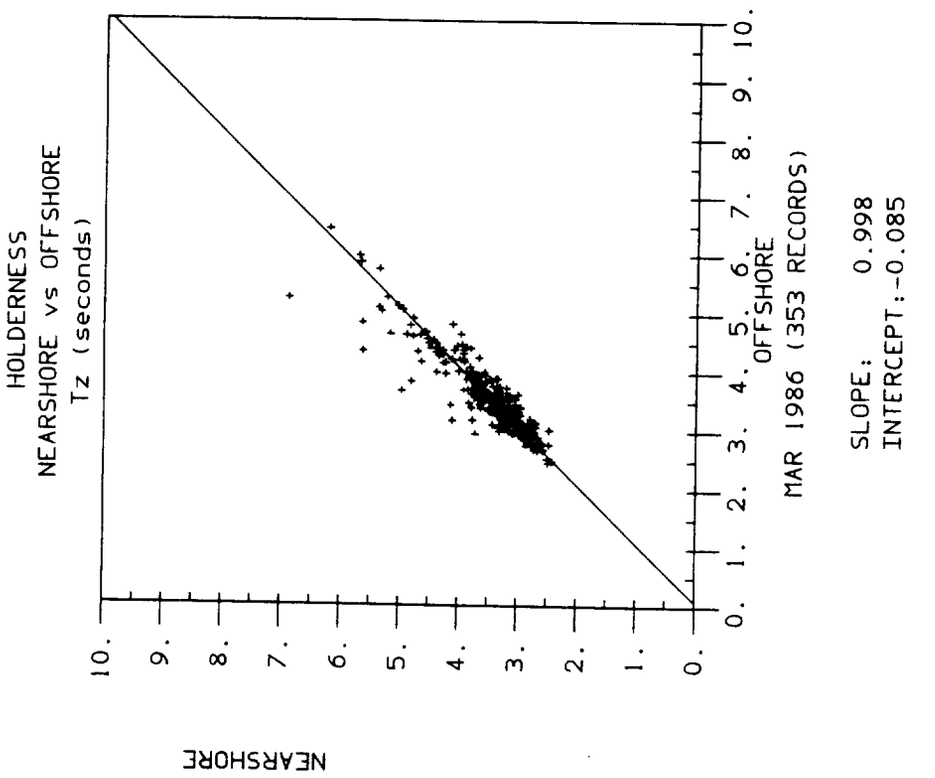

Fig. 16b

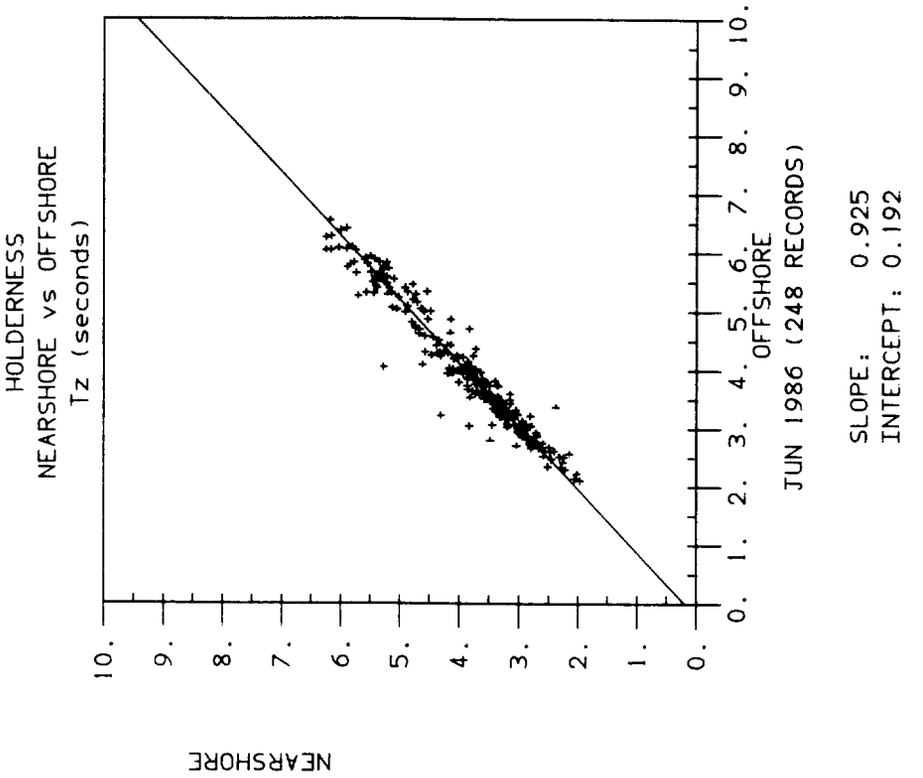

Fig. 16c

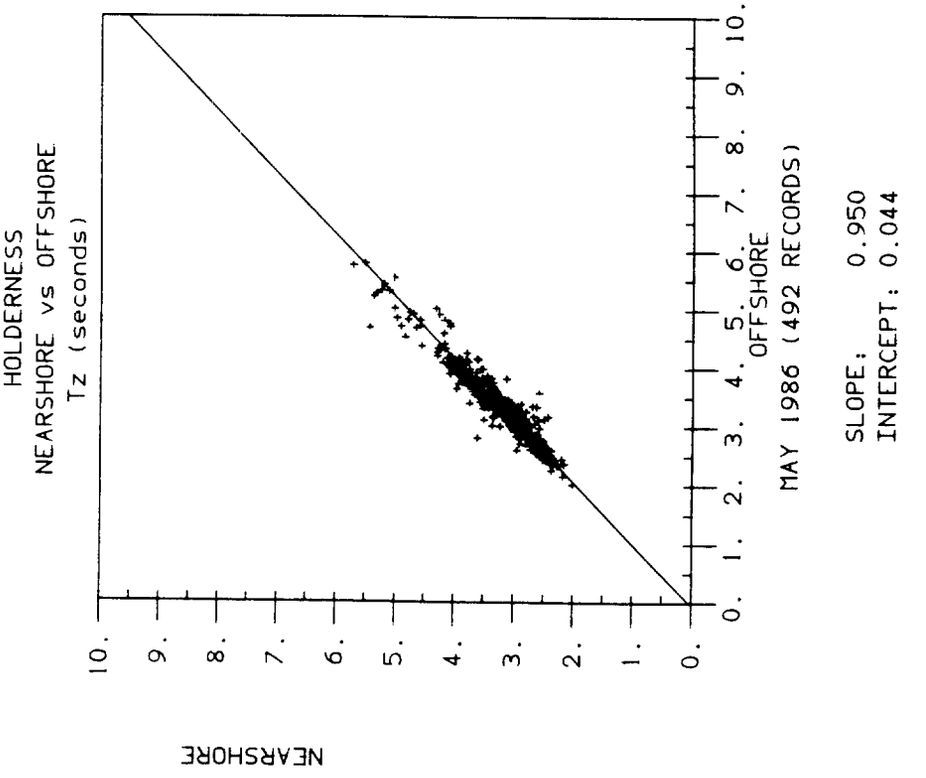

Fig. 16d

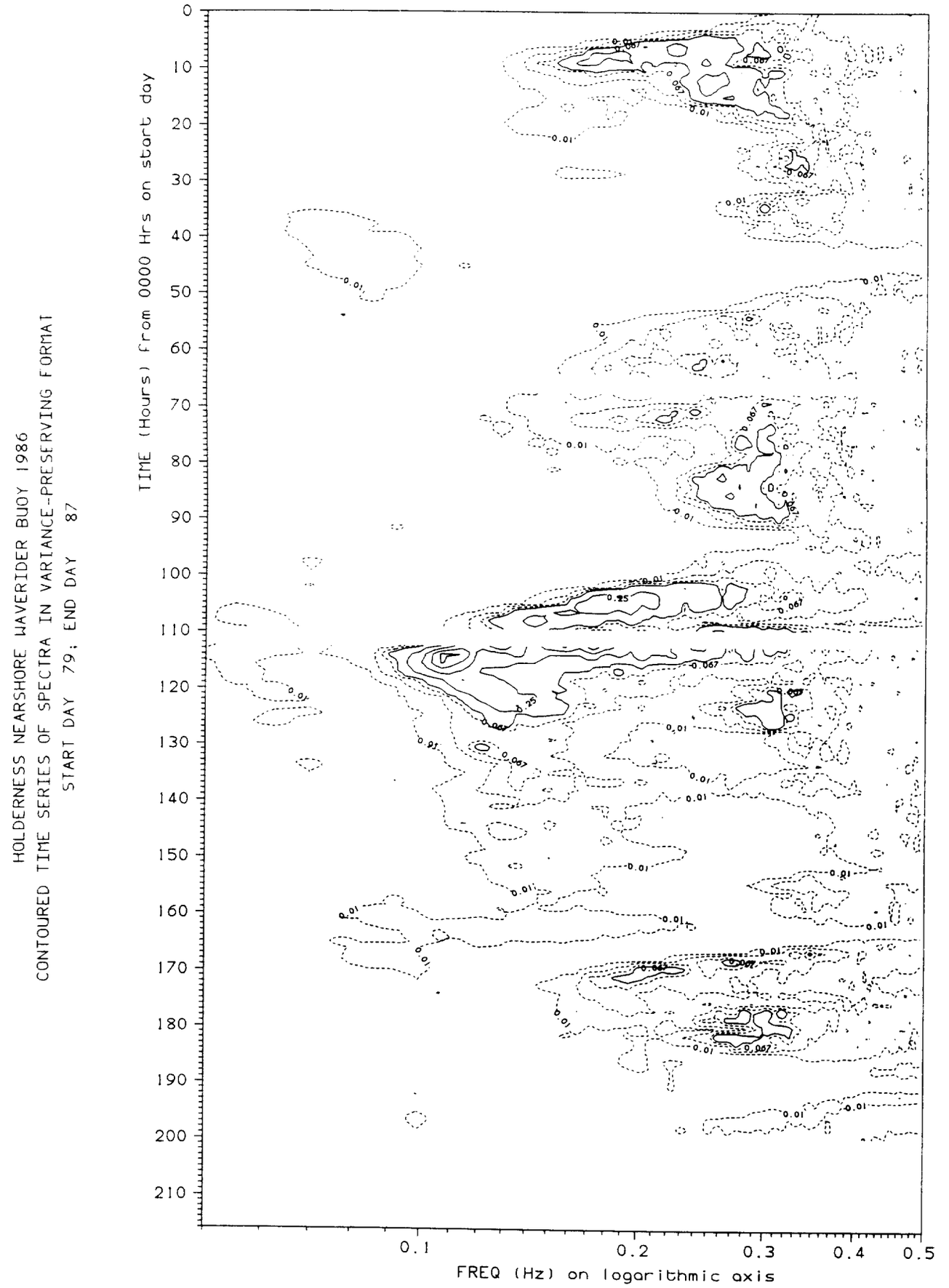
HOLDERNESS NEARSHORE WAVERIDER BUOY 1986
CONTOURED TIME SERIES OF SPECTRA IN VARIANCE-PRESERVING FORMAT
START DAY 79; END DAY 87
TIME (Hours) from 0000 Hrs on start day
0
10
20
30
40
50
60
70
80
90
100
110
120
130
140
150
160
170
180
190
200
210
0.1
0.2
0.3
0.4
0.5
FREQ (Hz) on logarithmic axis

Fig. 17

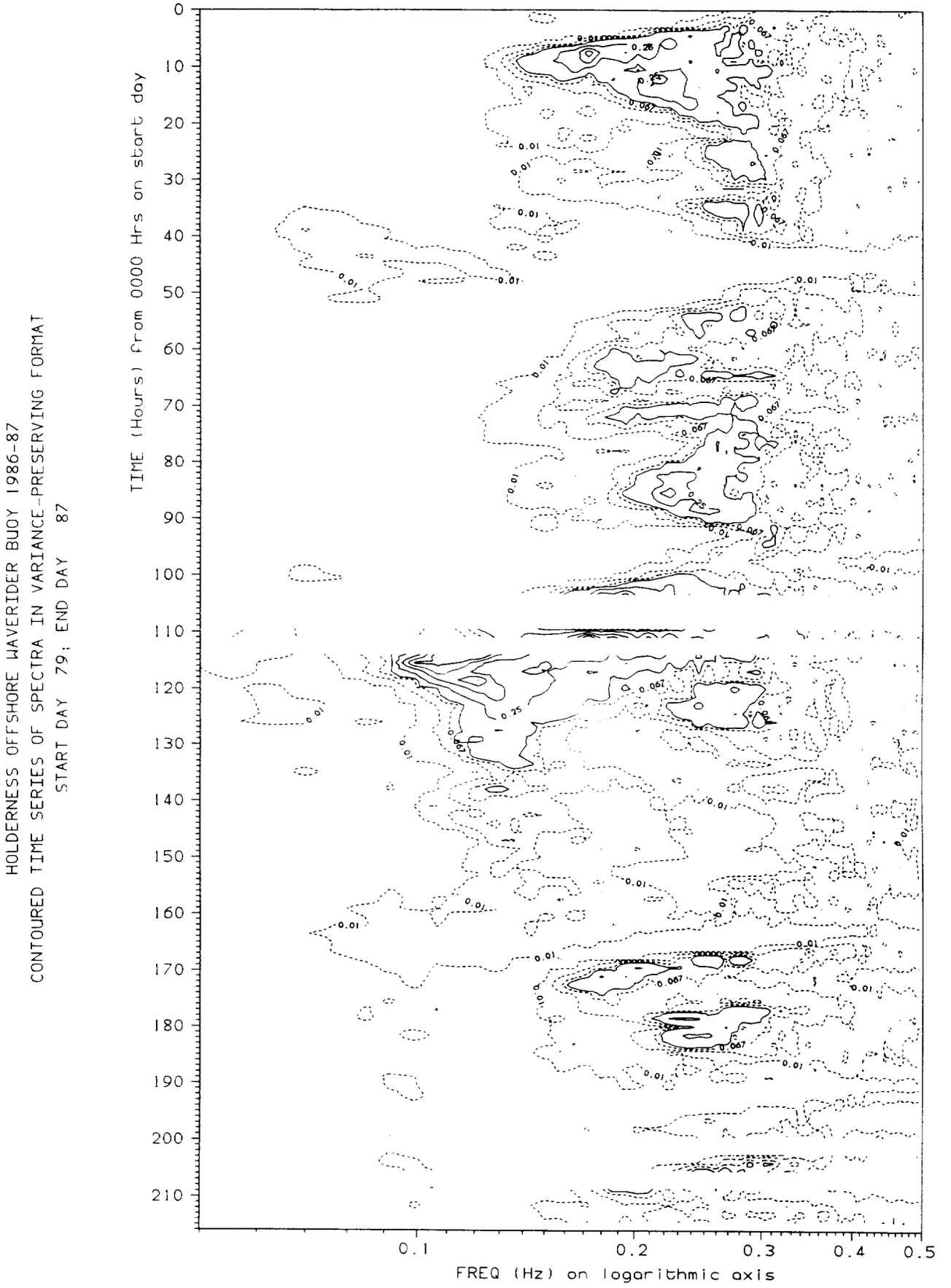
HOLDERNESS OFFSHORE WAVERIDER BUOY 1986-87
CONTOURED TIME SERIES OF SPECTRA IN VARIANCE-PRESERVING FORMAT
START DAY 79; END DAY 87
TIME (Hours) from 0000 Hrs on start day
0
10
20
30
40
50
60
70
80
90
100
110
120
130
140
150
160
170
180
190
200
210
0.1
0.2
0.3
0.4
0.5
FREQ (Hz) on logarithmic axis

Fig. 18

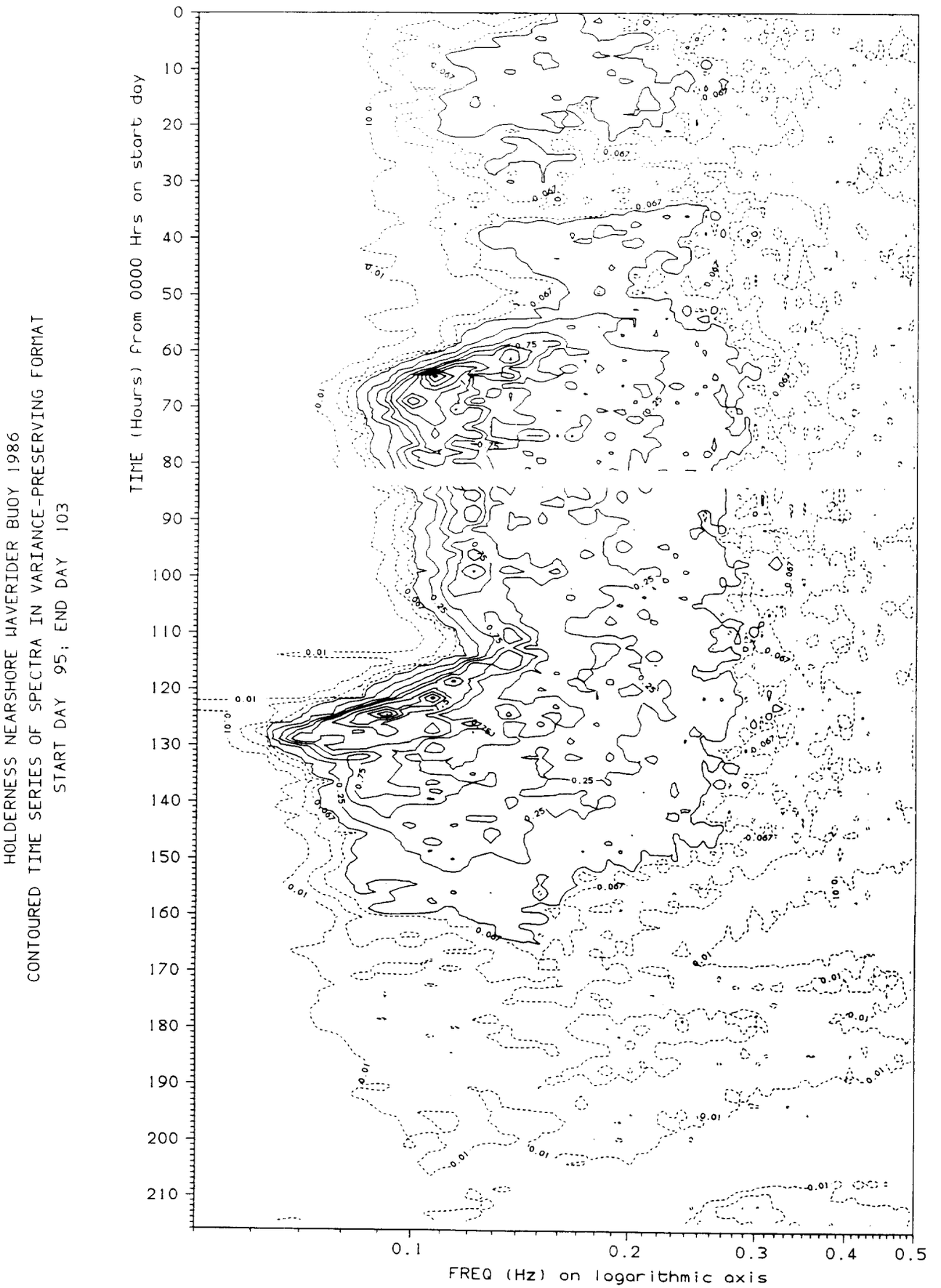
HOLDERNESS NEARSHORE WAVERIDER BUOY 1986
CONTOURED TIME SERIES OF SPECTRA IN VARIANCE-PRESERVING FORMAT
START DAY 95; END DAY 103
TIME (Hours) from 0000 Hrs on start day
FREQ (Hz) on logarithmic axis
0
10
20
30
40
50
60
70
80
90
100
110
120
130
140
150
160
170
180
190
200
210
0.1
0.2
0.3
0.4
0.5

Fig. 19

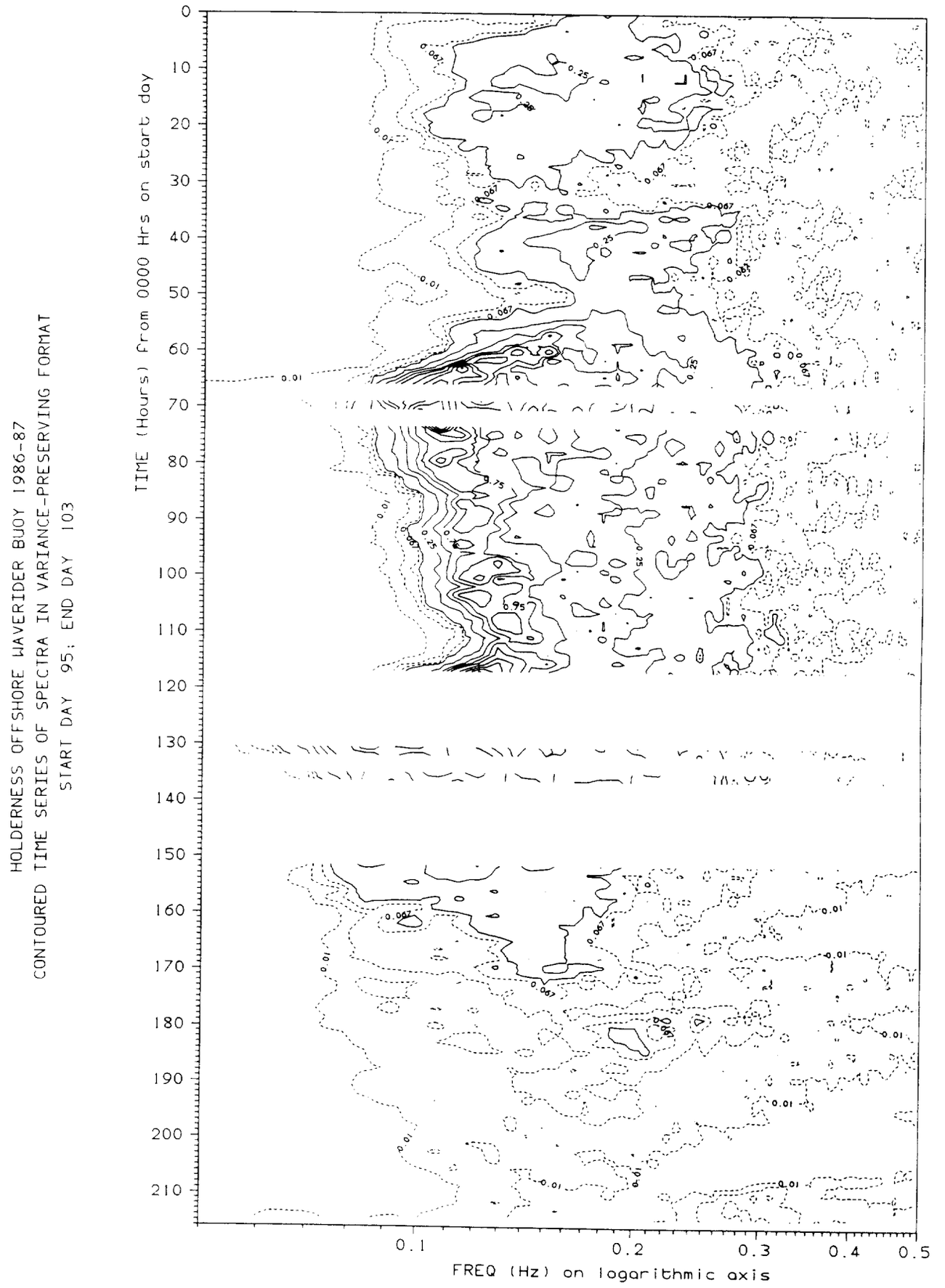
HOLDERNESS OFFSHORE WAVERIDER BUOY 1986-87
CONTOURED TIME SERIES OF SPECTRA IN VARIANCE-PRESERVING FORMAT
START DAY 95; END DAY 103
TIME (Hours) from 0000 Hrs on start day
0
10
20
30
40
50
60
70
80
90
100
110
120
130
140
150
160
170
180
190
200
210
0.1
0.2
0.3
0.4
0.5
FREQ (Hz) on logarithmic axis

Fig. 20

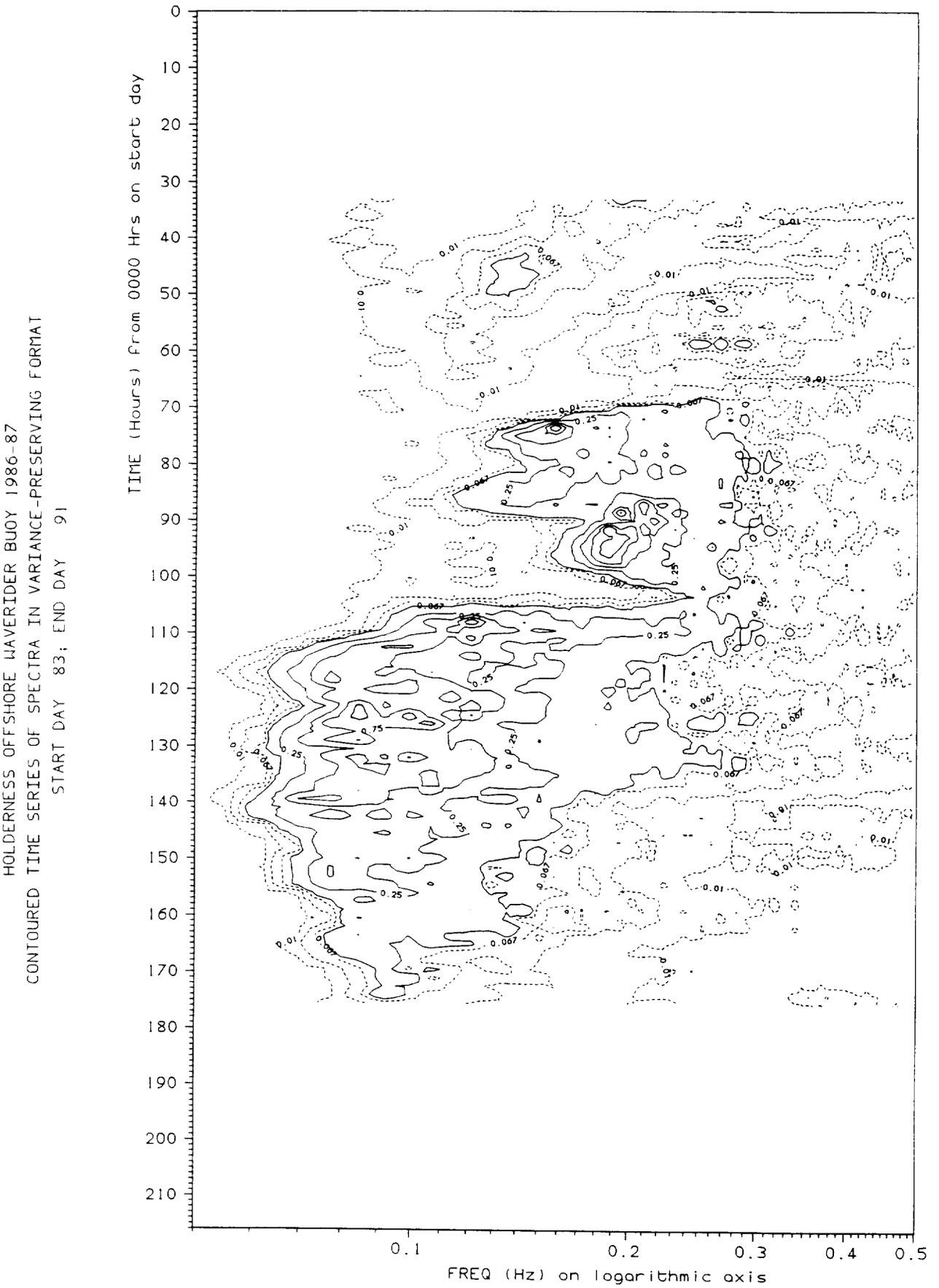
HOLDERNESS OFFSHORE WAVERIDER BUOY 1986-87
CONTOURED TIME SERIES OF SPECTRA IN VARIANCE-PRESERVING FORMAT
START DAY 83; END DAY 91
TIME (Hours) from 0000 Hrs on start day
0
10
20
30
40
50
60
70
80
90
100
110
120
130
140
150
160
170
180
190
200
210
0.1
0.2
0.3
0.4
0.5
FREQ (Hz) on logarithmic axis

Fig. 21

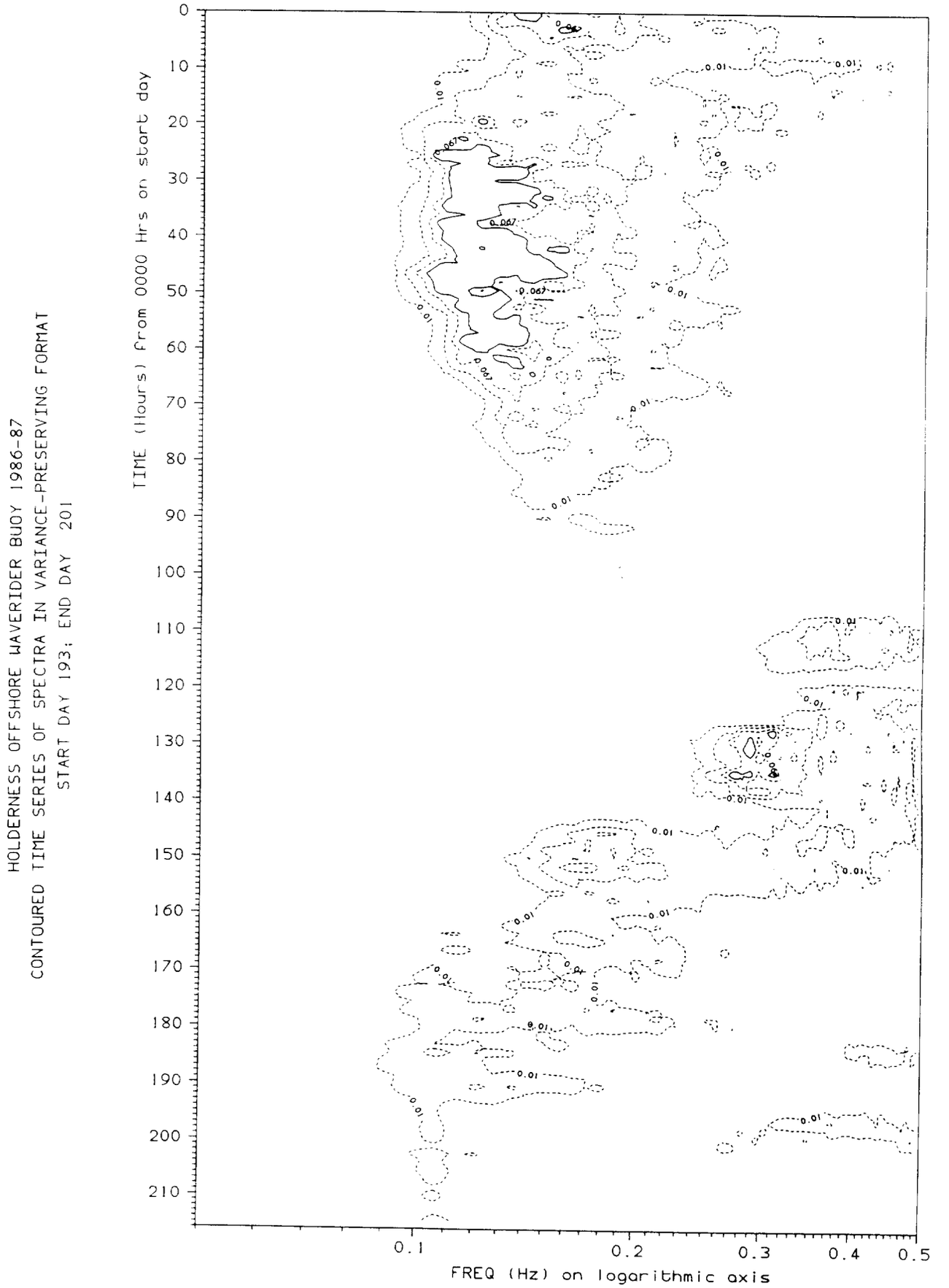
HOLDERNESS OFFSHORE WAVERIDER BUOY 1986-87
CONTOURED TIME SERIES OF SPECTRA IN VARIANCE-PRESERVING FORMAT
START DAY 193; END DAY 201
TIME (Hours) from 0000 Hrs on start day
0
10
20
30
40
50
60
70
80
90
100
110
120
130
140
150
160
170
180
190
200
210
0.1
0.2
0.3
0.4
0.5
FREQ (Hz) on logarithmic axis
0.067
0.047
0.01

Fig. 22

HOLDERNESS NEARSHORE WAVERIDER BUOY 1986
SPECTRA OF TIME SERIES OF HIGH FREQUENCY RECORDS
START DAY: 95

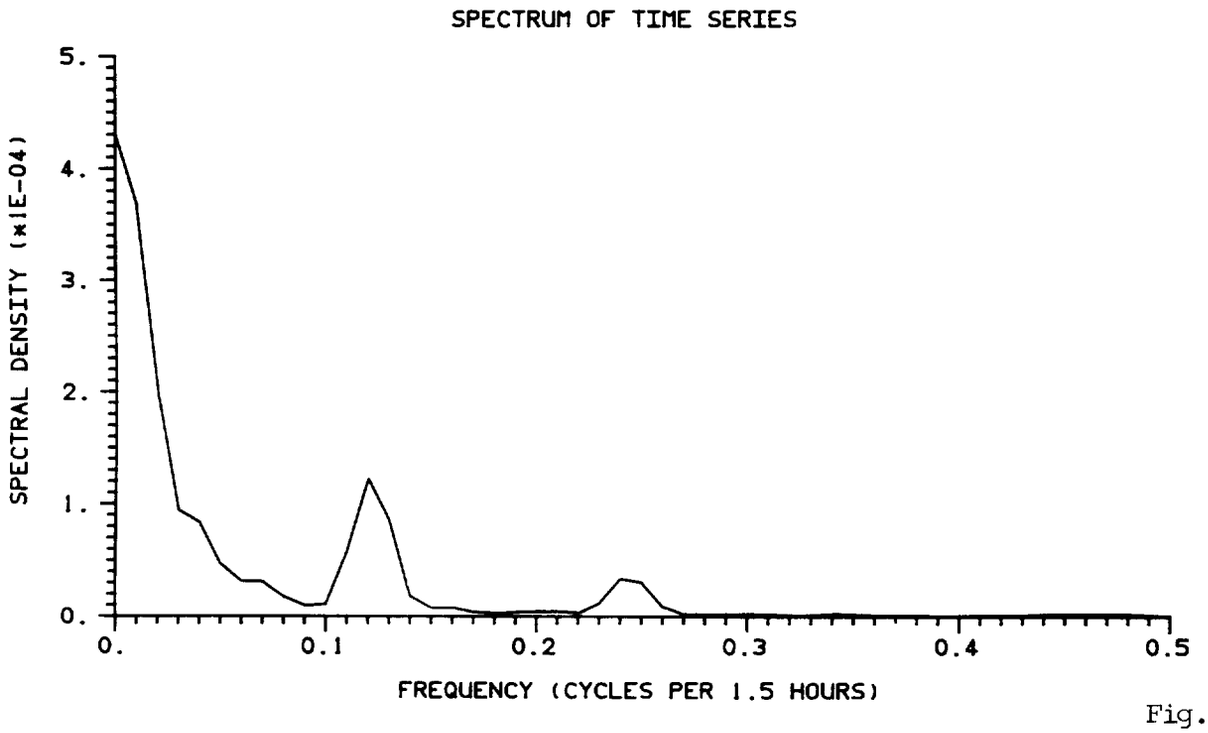

Fig. 23a

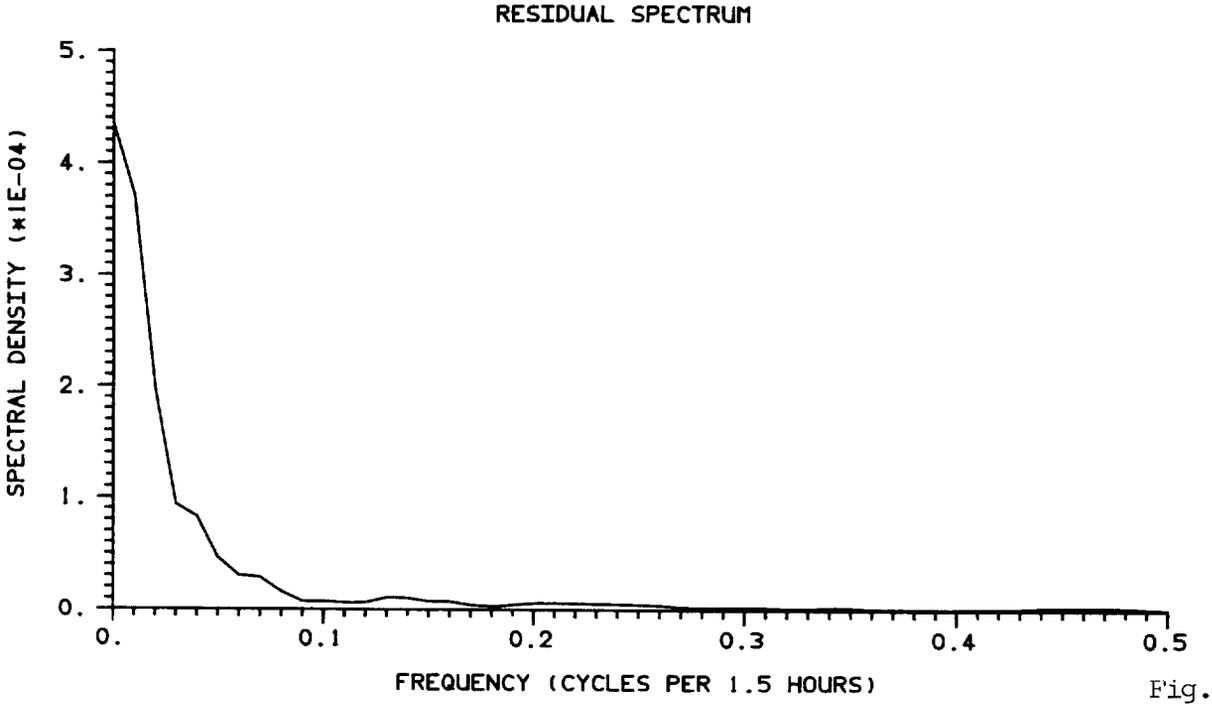

Fig. 23b

HOLDERNESS OFFSHORE WAVERIDER BUOY 1986-87
SPECTRA OF TIME SERIES OF HIGH FREQUENCY RECORDS
START DAY: 95

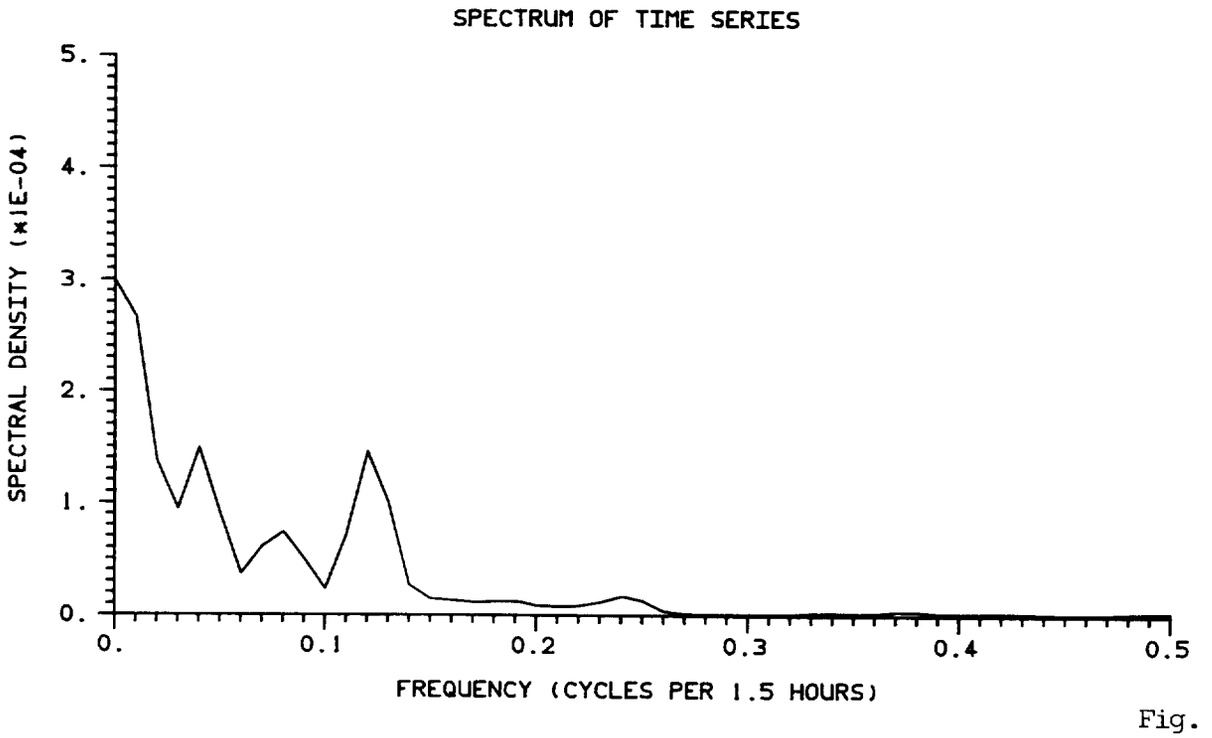

Fig. 24a

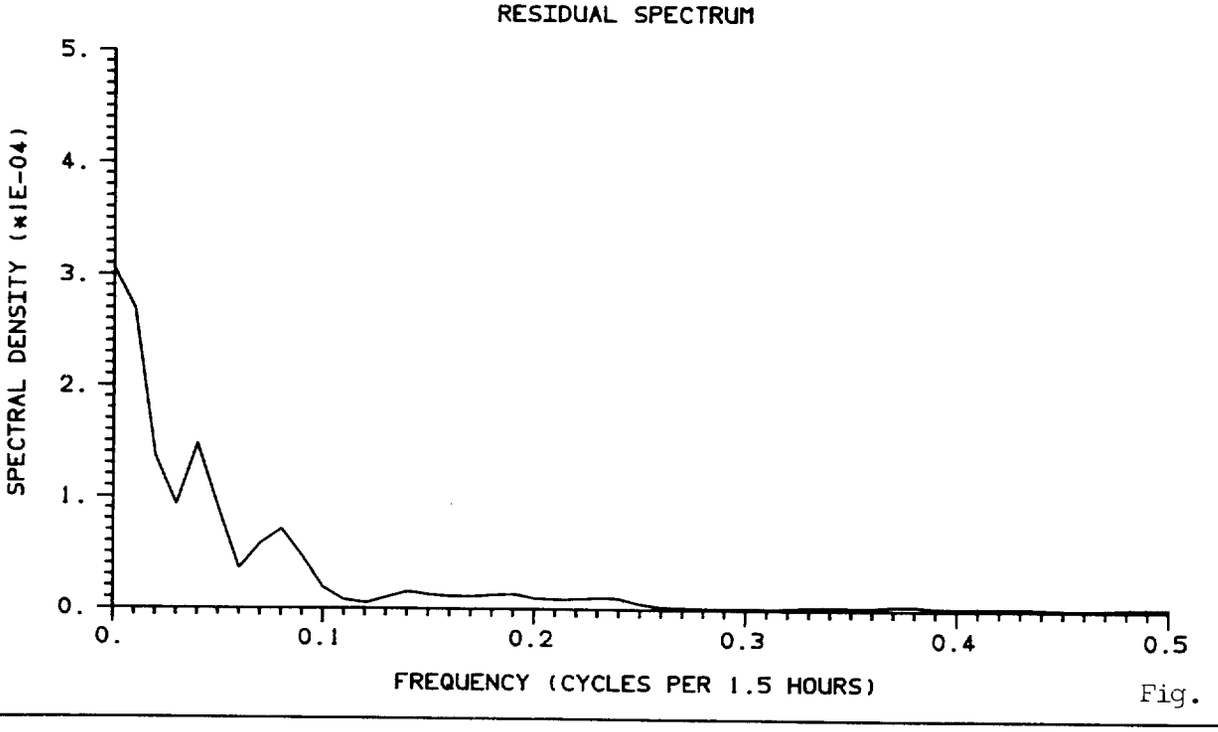

Fig. 24b

HOLDERNESS WAVERIDER BUOYS 1986
CROSS-SPECTRUM OF TIME SERIES AT FREQUENCY 0.41 Hz
START DAY: 95

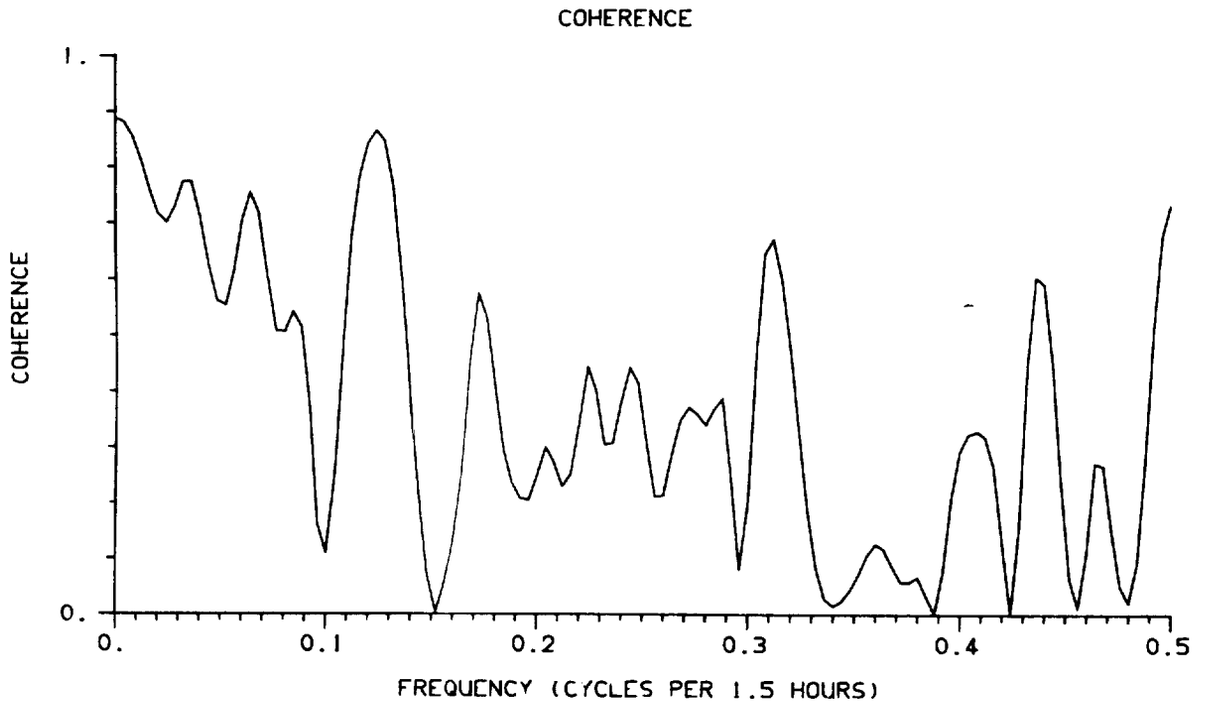

Fig. 25a

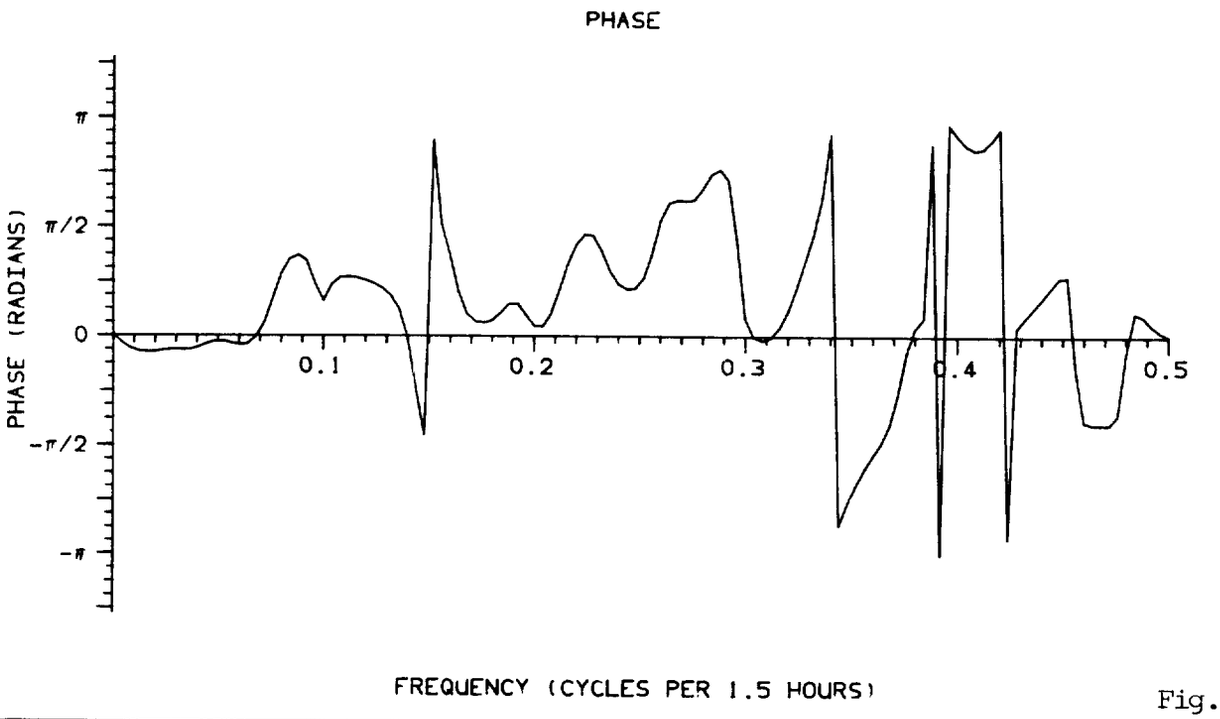

Fig. 25b

HOLDERNESS WAVERIDER BUOYS 1986
CROSS-SPECTRUM OF TIME SERIES AT FREQUENCY 0.41 Hz
START DAY: 95

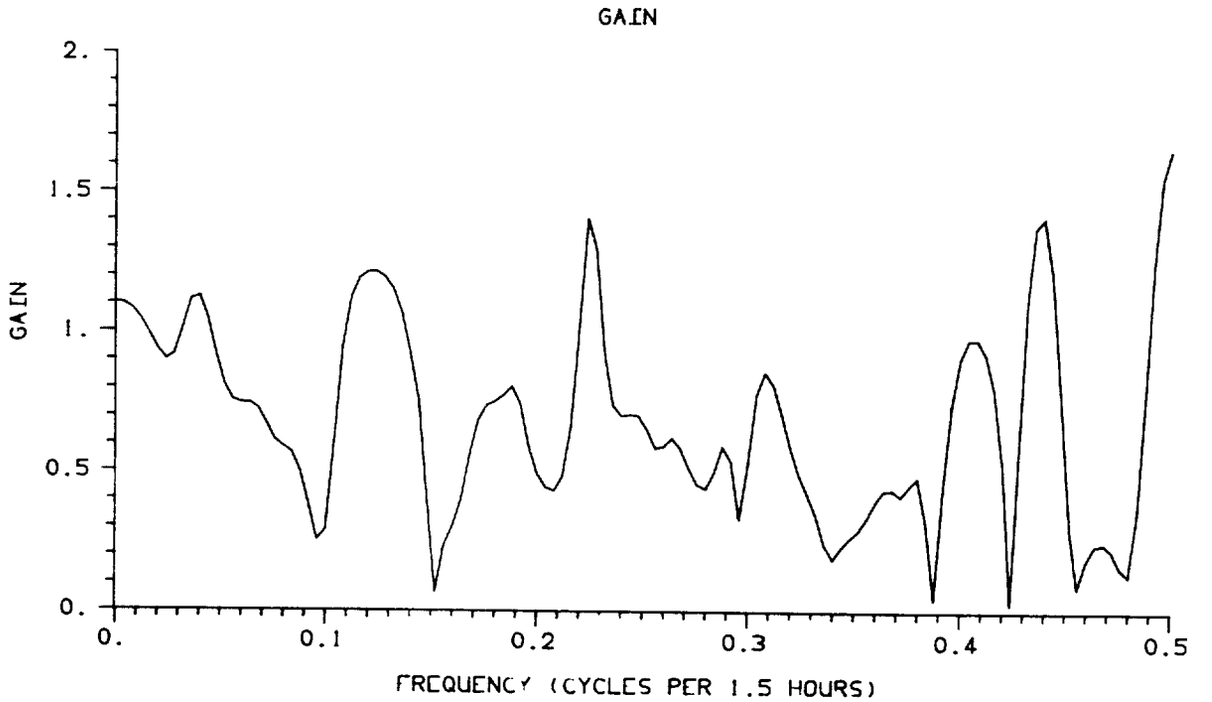

Fig. 25c

HOLDERNESS NEARSHORE WAVERIDER BUOY 1986
CURRENT COMPUTED FROM TIME SERIES OF SPECTRAL DENSITIES
AT FREQUENCY 0.38 Hz, FROM DAY 97 TO DAY 101

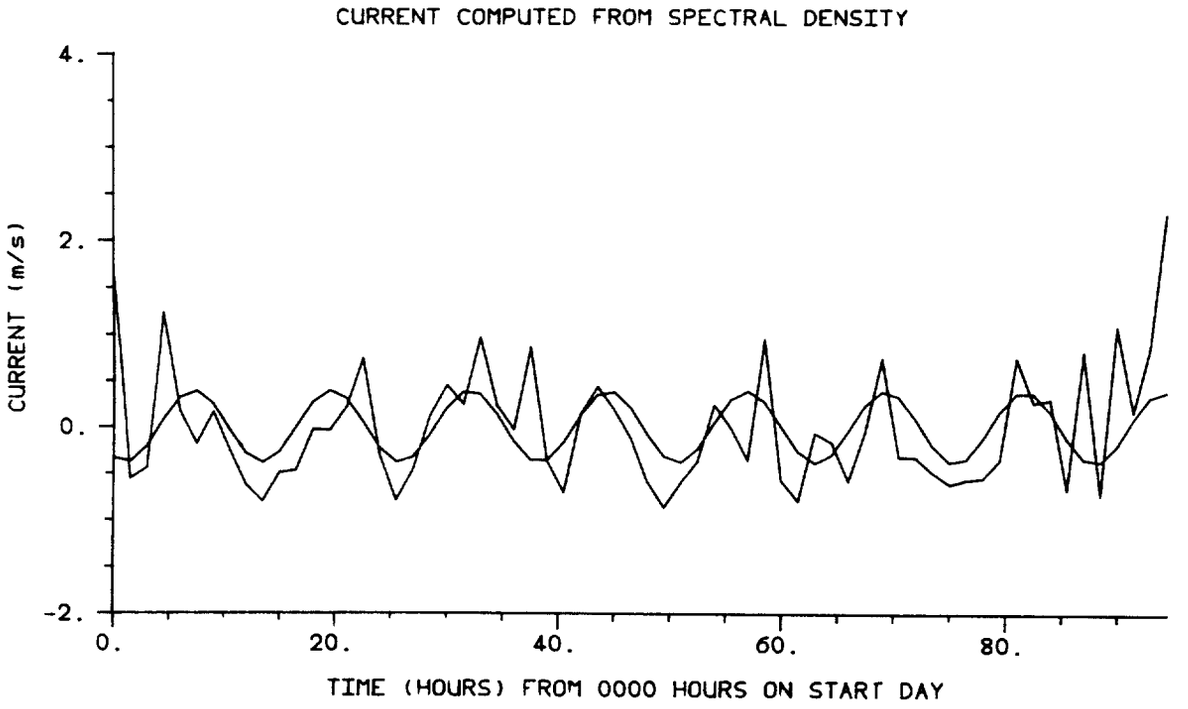

Fig. 26a

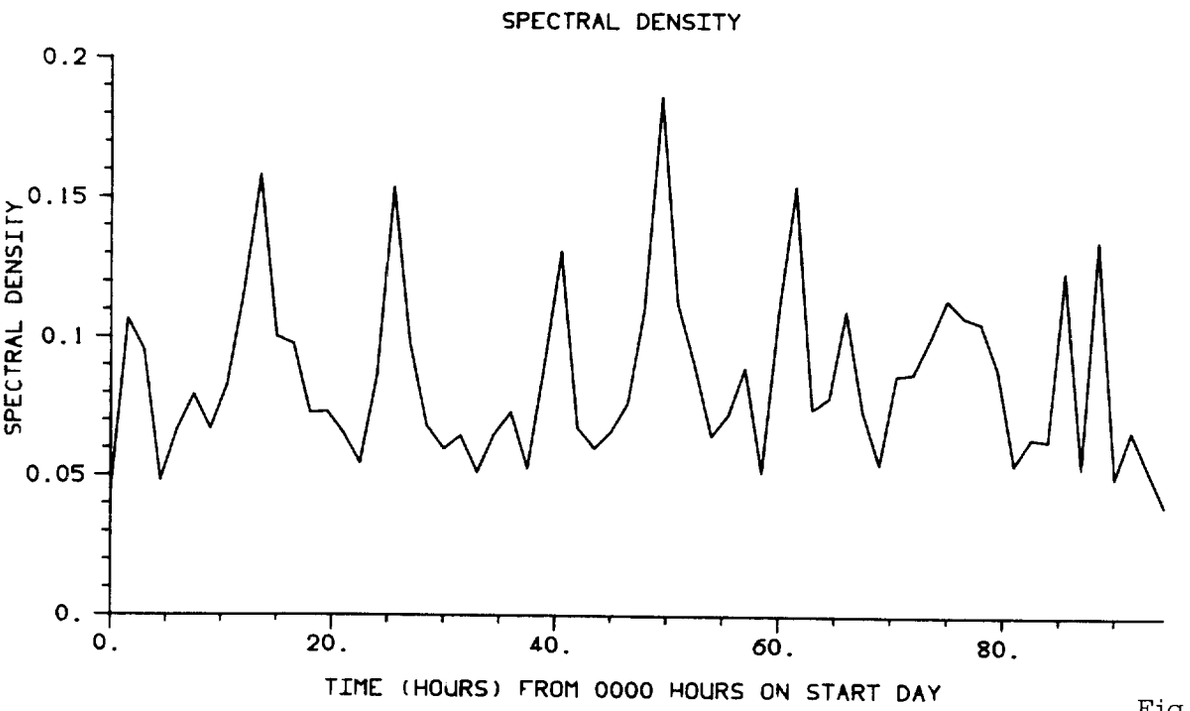

Fig. 26b

HOLDERNESS OFFSHORE WAVERIDER BUOY 1986-87
CURRENT COMPUTED FROM TIME SERIES OF SPECTRAL DENSITIES
AT FREQUENCY 0.38 Hz, FROM DAY 97 TO DAY 99

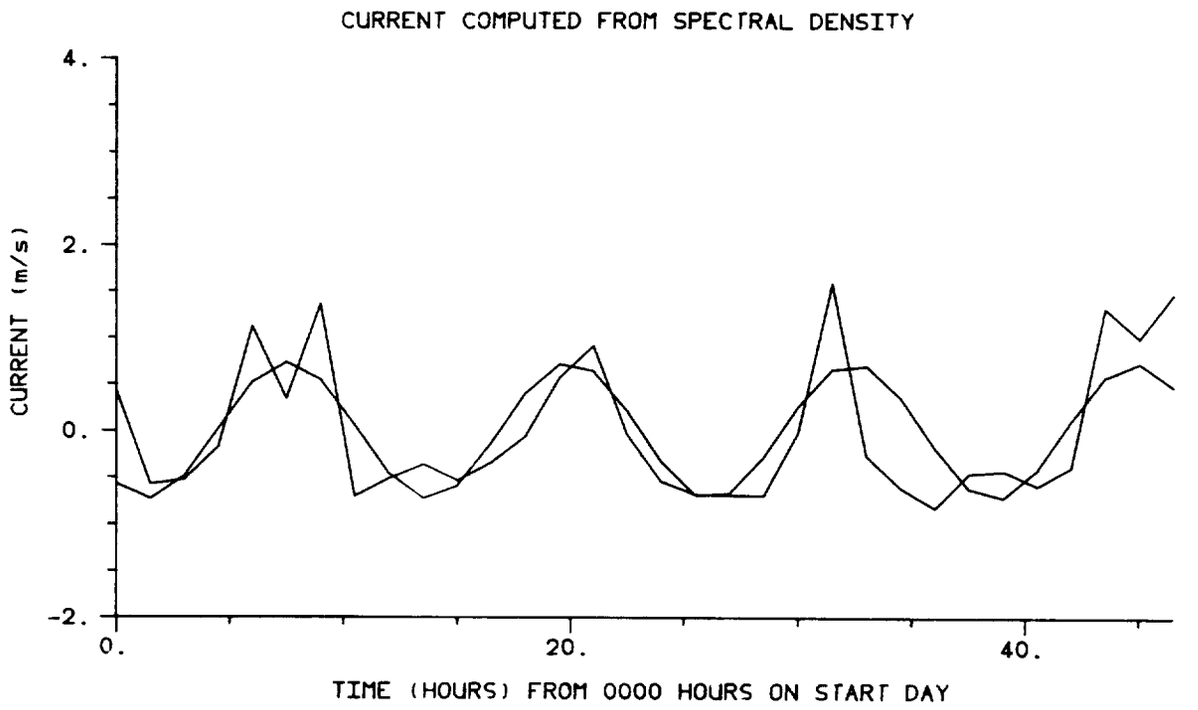

Fig. 26c

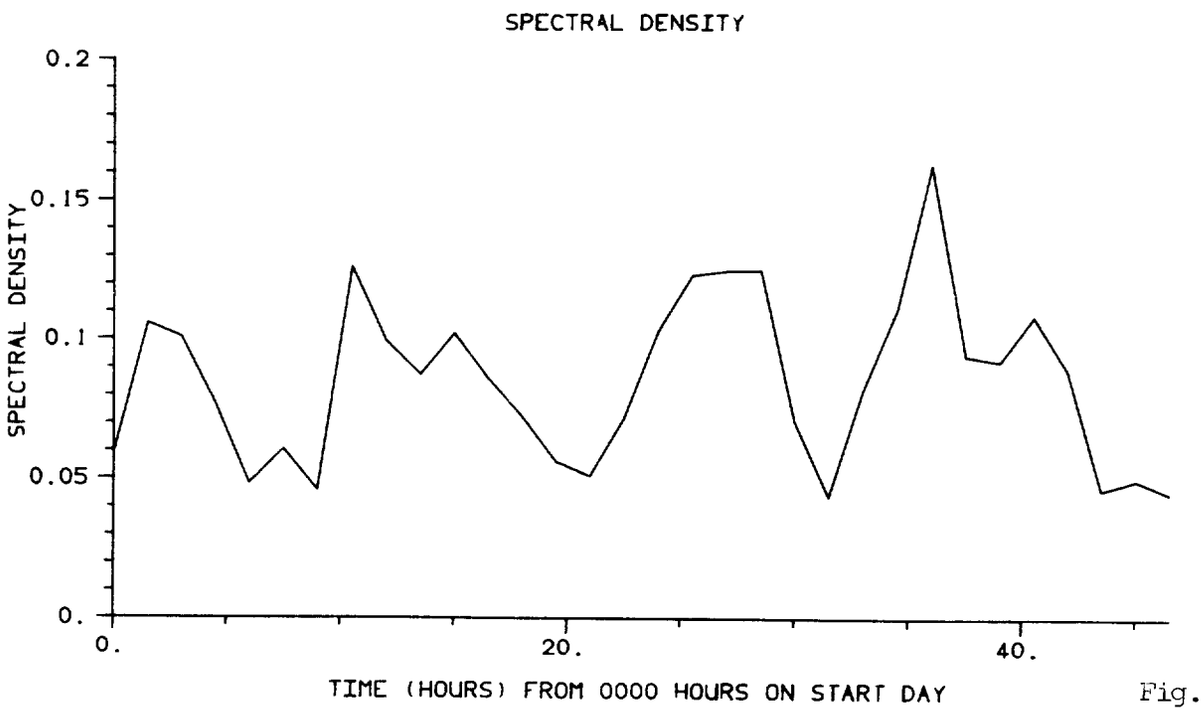

Fig. 26d

HOLDERNESS WAVERIDER BUOYS 1986
Tz SPECTRUM
START DAY: 130

NEARSHORE

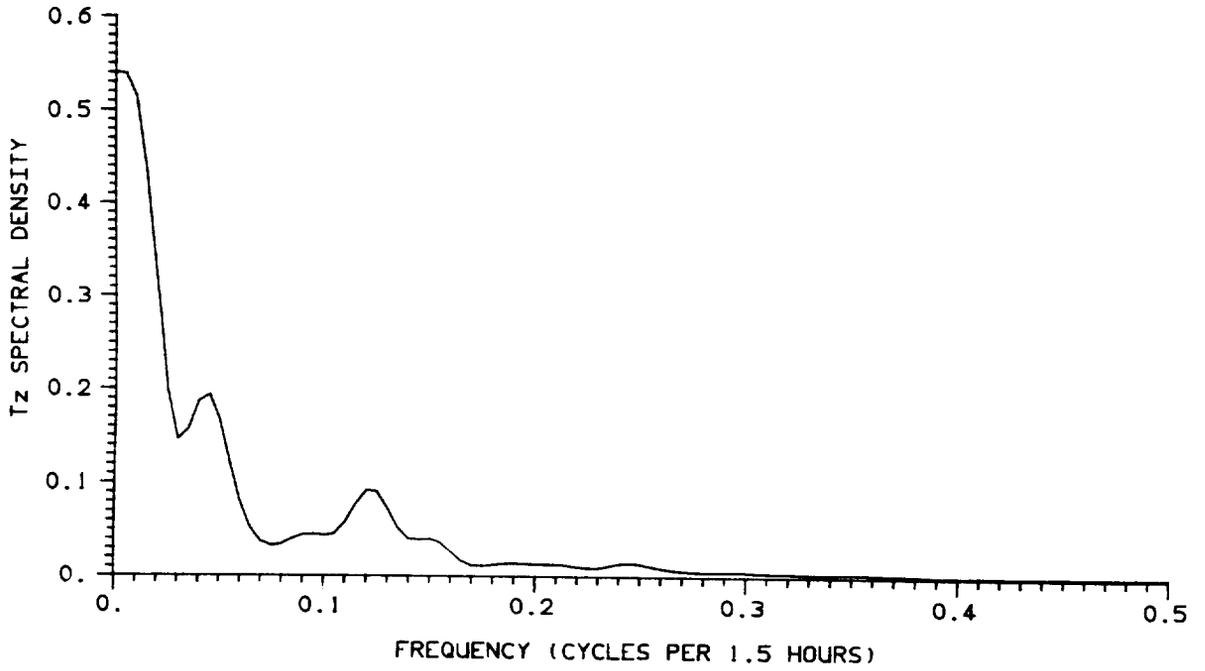

Fig. 27

OFFSHORE

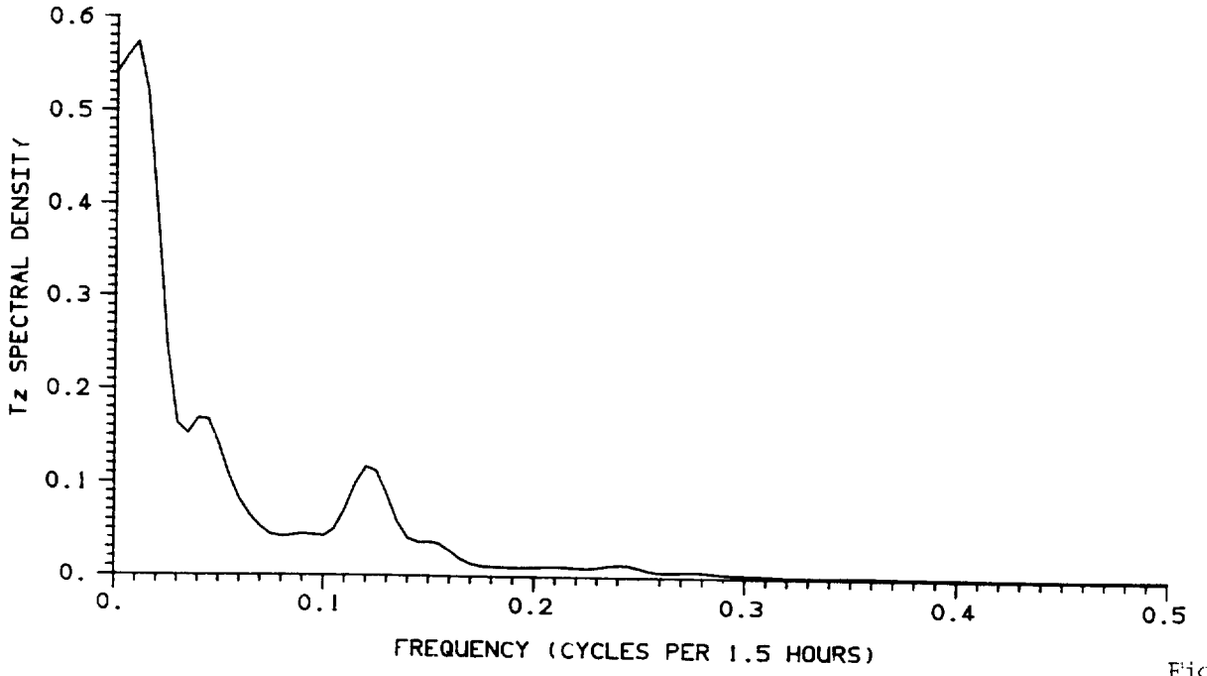

Fig. 28

HOLDERNESS WAVERIDER BUOYS 1986
MEAN RATIO OF (NEARSHORE/OFFSHORE) SPECTRAL DENSITY

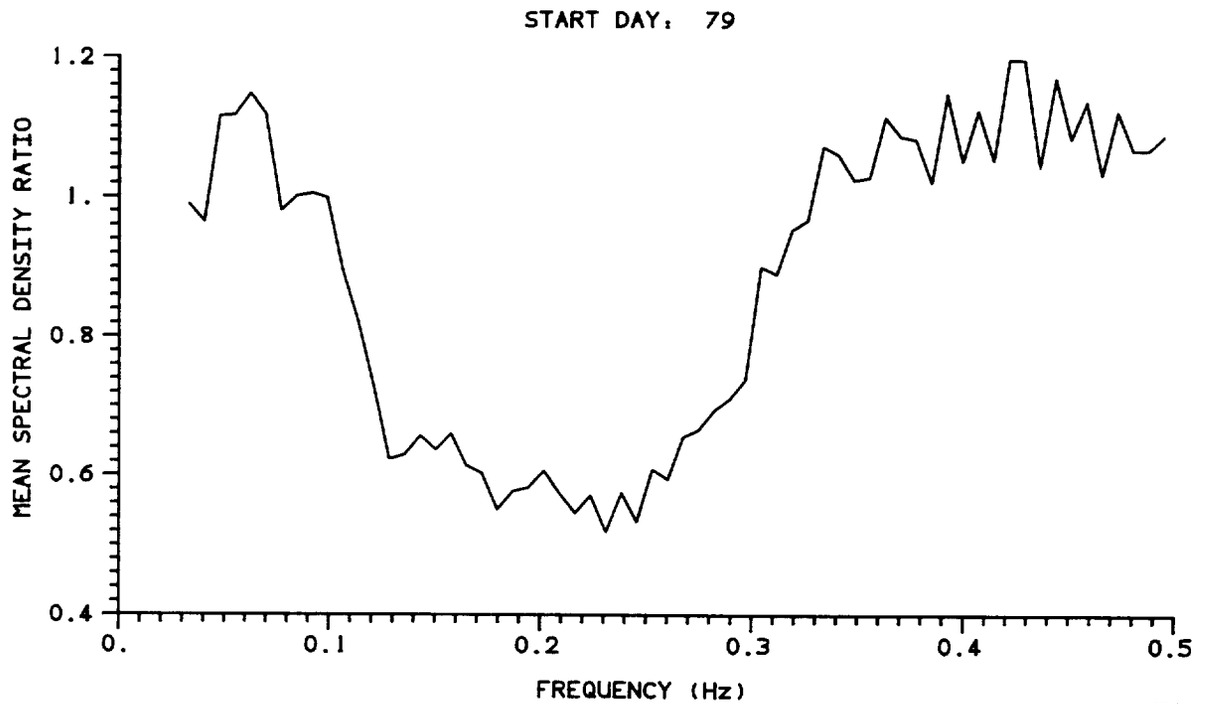

Fig. 29

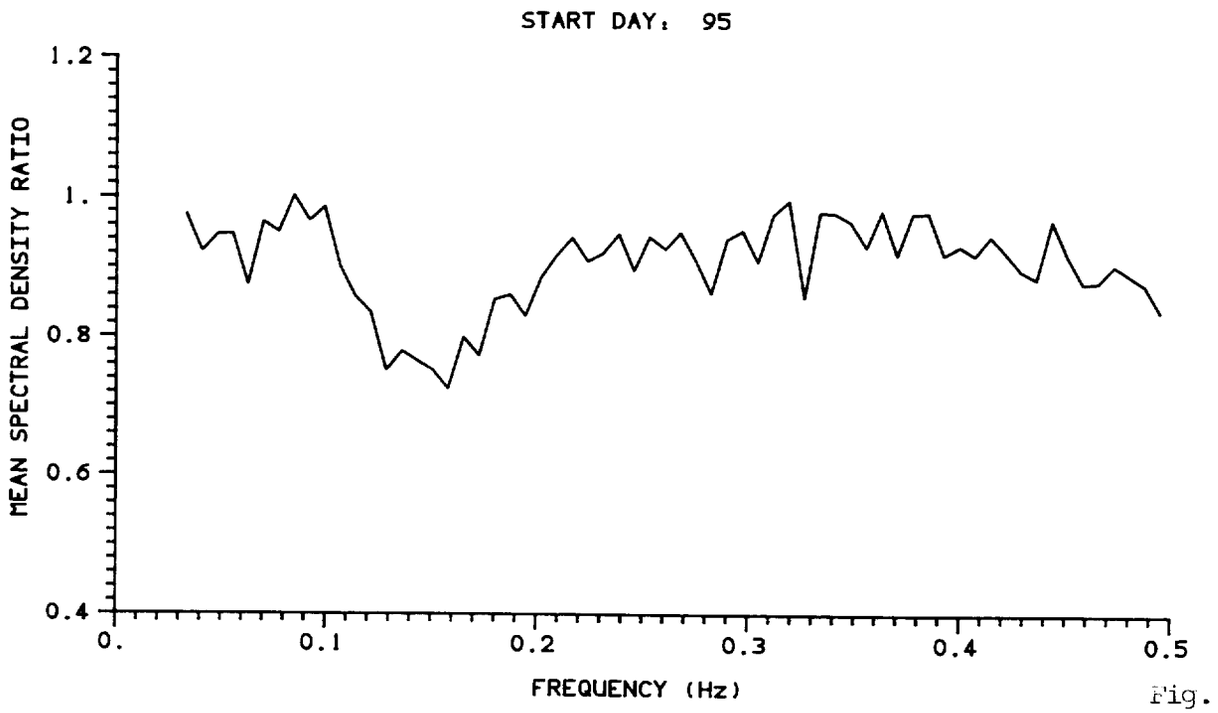

Fig. 30

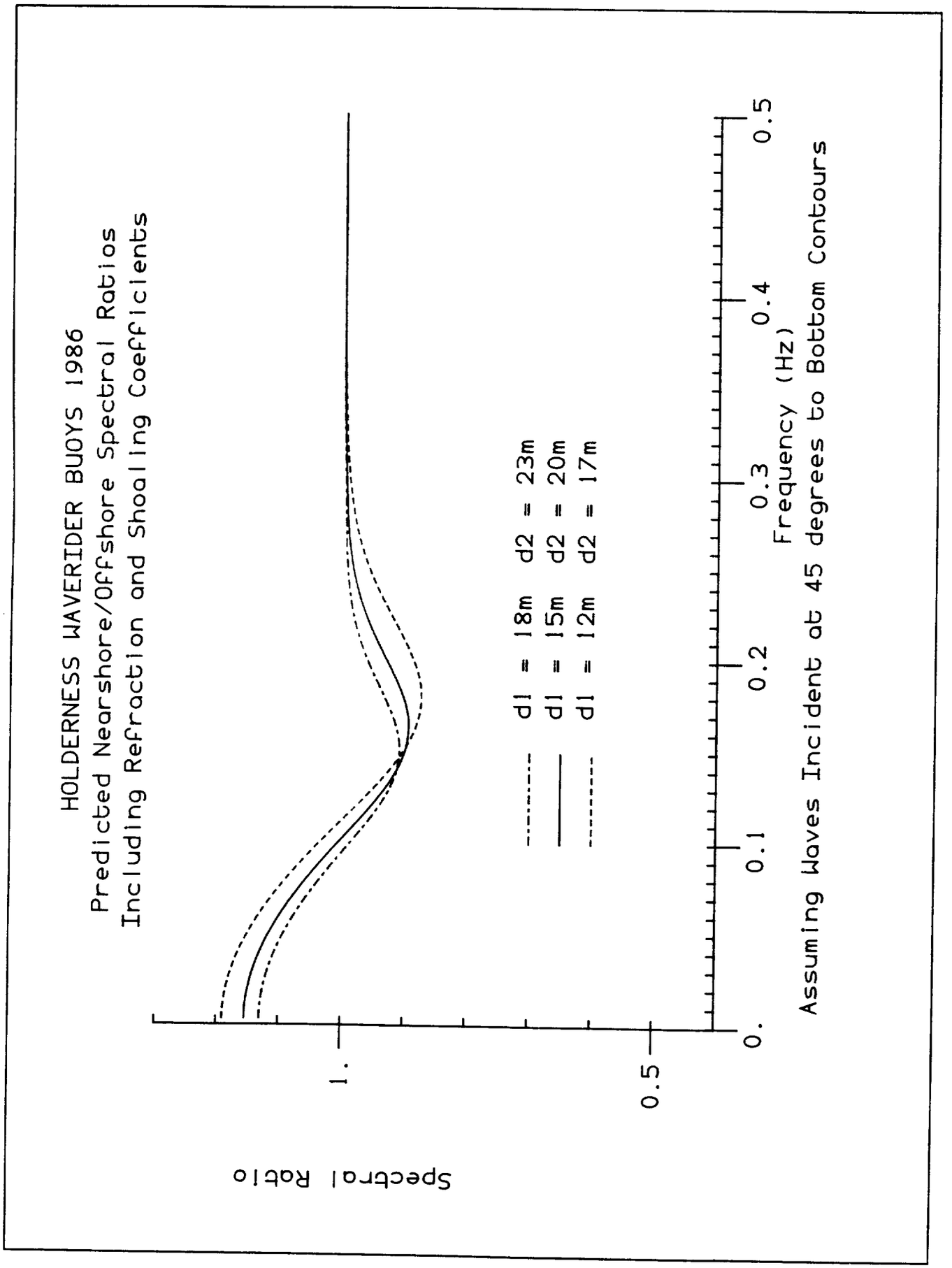
HOLDERNESS WAVERIDER BUOYS 1986
Predicted Nearshore/Offshore Spectral Ratios
Including Refraction and Shoaling Coefficients
Assuming Waves Incident at 45 degrees to Bottom Contours
Spectral Ratio
Frequency (Hz)
1.
0.5
0.
0.1
0.2
0.3
0.4
0.5
d1 = 18m d2 = 23m
d1 = 15m d2 = 20m
d1 = 12m d2 = 17m

Fig. 31

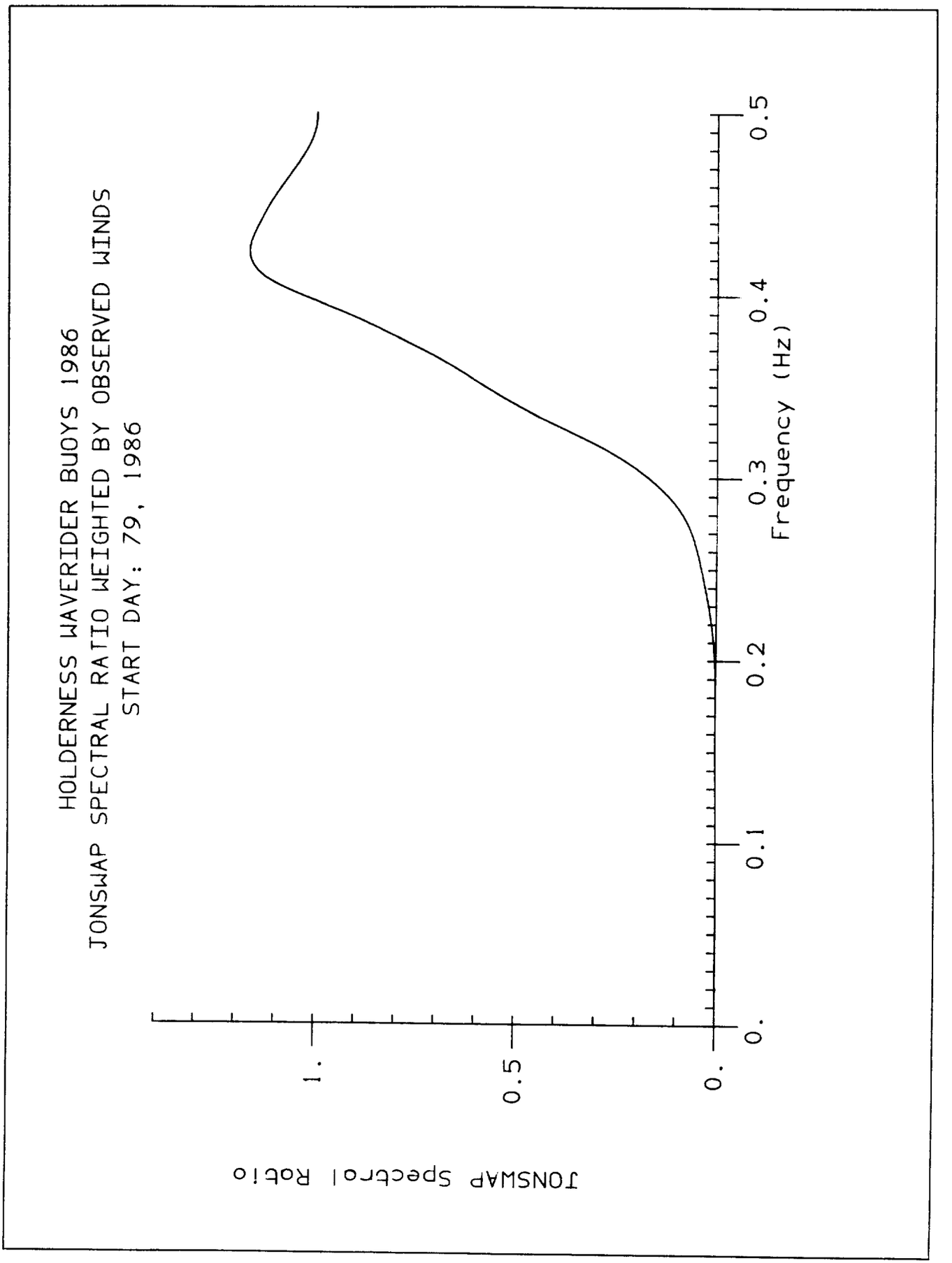
HOLDERNESS WAVERIDER BUOYS 1986
JONSWAP SPECTRAL RATIO WEIGHTED BY OBSERVED WINDS
START DAY: 79, 1986
JONSWAP Spectral Ratio
1.
0.5
0.
0.
0.1
0.2
0.3
0.4
0.5
Frequency (Hz)

Fig. 32

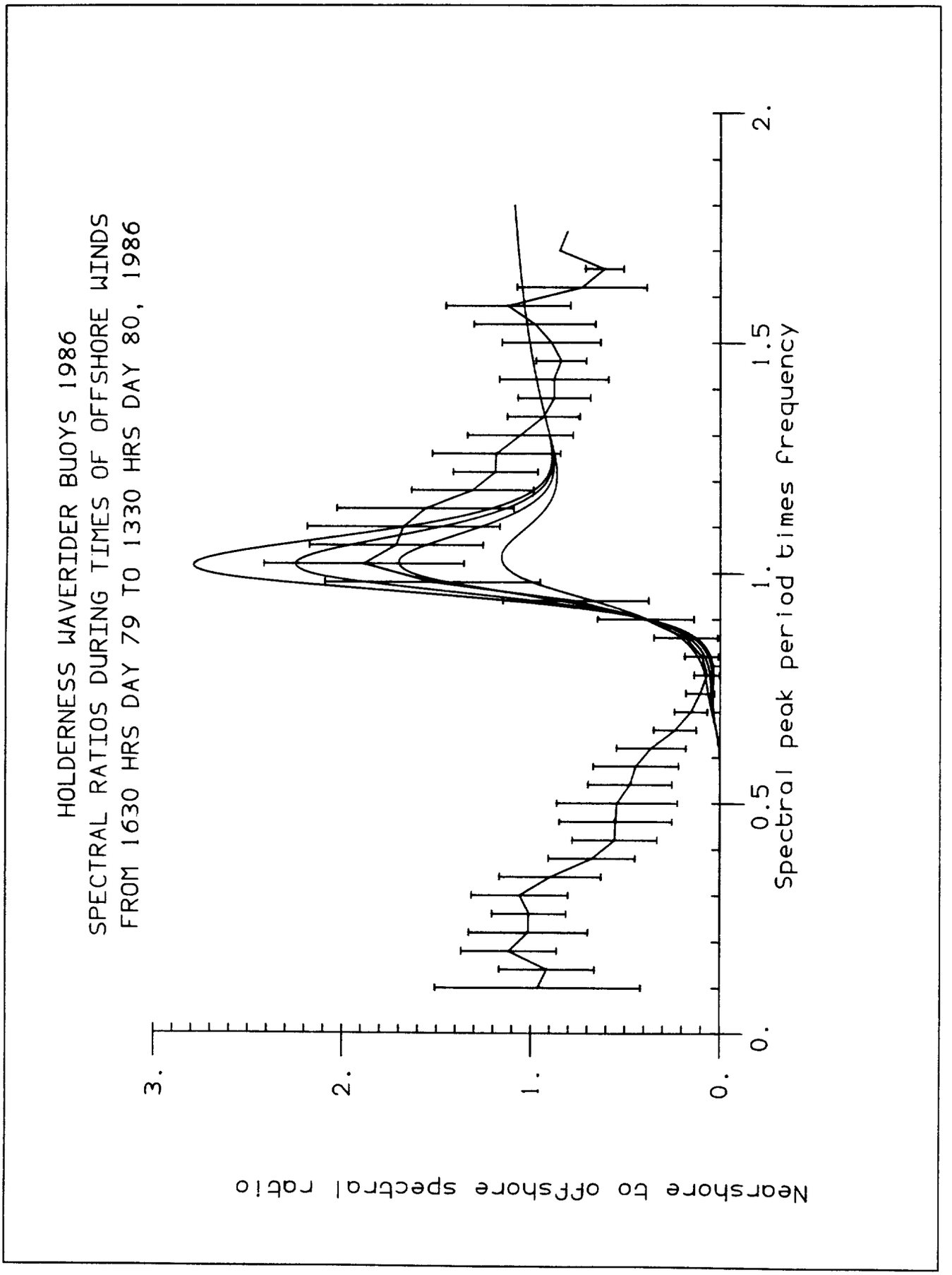
HOLDERNESS WAVERIDER BUOYS 1986
SPECTRAL RATIOS DURING TIMES OF OFFSHORE WINDS
FROM 1630 HRS DAY 79 TO 1330 HRS DAY 80, 1986
Nearshore to offshore spectral ratio
3.
2.
1.
0.
0.
0.5
1.
1.5
2.
Spectral peak period times frequency

Fig. 33